



No. 102 – December 2000

## TELESCOPES AND INSTRUMENTATION

## Successful Installation of the VIRMOS Laser Mask Manufacturing Unit (MMU) at Paranal

G. AVILA<sup>1</sup>, G. CONTI<sup>2</sup>, E. MATTAINI<sup>2</sup>, L. CHIAPPETTI<sup>2</sup>, D. MACCAGNI<sup>2</sup>,  
E. SANT'AMBROGIO<sup>2</sup>, O. LE FÈVRE<sup>3</sup>, G. VETTOLANI<sup>4</sup>, M. SAÏSSE<sup>3</sup>

<sup>1</sup>ESO; <sup>2</sup>CNR – Istituto Fisica Cosmica “G. Occhialini”, Milano;

<sup>3</sup>Laboratoire d’Astrophysique de Marseille, Marseille; <sup>4</sup>CNR – Istituto di Radioastronomia, Bologna

The Mask Manufacturing Unit (MMU), one of the three main components of the VIRMOS project, has been delivered and successfully installed at Paranal Observatory at the beginning of August. The MMU is a laser-based system, which will be used to cut the slit masks for the VIMOS, NIRMOS and FORS2 spectrographs. The unit also manages the selection, storage and insertion of the masks into dedicated cabinets. A batch of masks has been manufactured on Paranal for a test with FORS2. The quality of the masks (position accuracy and roughness of the slits) are fully compliant with the instrument specifications.

### Introduction

A consortium of French-Italian astronomical institutes is building three instruments for the VLT: VIMOS, NIRMOS and the MMU. The whole is the so-called VIRMOS project [1]. VIMOS (Visible Multi-Object Spectrograph) and NIRMOS (Near Infra-Red Multi-Object Spectrograph) are focal reducer and spectrographs with imaging capability

to be used for deep and large field observations. VIMOS is right now in the system test phase at the Observatoire de Haute-Provence and is expected to be delivered to the community in July 2001. NIRMOS is entering the manufacturing phase.

The VIMOS field of view is split in 4 quadrants of  $7 \times 8$  each ( $8 \times 6$  for NIRMOS) and therefore, for each, a slit mask is needed for a Multi-Object Spectroscopy observation. The masks

(up to 15 per quadrant) are inserted during the day in the so-called Instrument Cabinets. Before the observations, the 4 cabinets are installed on the four channels of VIMOS. The Mask Exchanger Unit is a device in the instrument, which allows exchanging the masks remotely according to the observation programme. The MMU is

Figure 1: The laser cutting system as installed in the MMU Laboratory at Paranal. The invar sheet on which the slits will be cut is mounted and clamped on the X – Y translation stage.

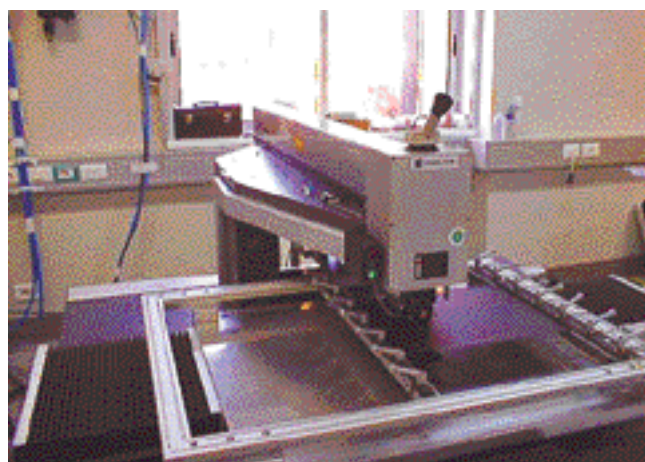


Table 1. Required specifications for the VIRMOS masks. The results after installation in Paranal are included.

Item	Specification	Test results in Paranal
Slit width	300 to 1000 $\mu\text{m}$	100 $\mu\text{m}$
Shape	It shall be feasible to cut slits of arbitrary shapes, with the above-mentioned edge quality and slit width (degradation of 30% acceptable)	Any shape. Radius of curvature: > 2 mm. Same slit width and edge quality as above
Edge quality	< 5 $\mu\text{m}$ peak to peak	1.3 $\pm$ 0.3 $\mu\text{m}$
Absolute positional accuracy with respect to the mask support frame	< 30 $\mu\text{m}$ , including temperature variations between fabrication and operation in VIMOS and NIRMOS	15 $\mu\text{m}$
Speed	> 7 m/h (1.9 mm/s)	6 mm/s

located in a laboratory in the Camp Area. From there the 4 Instrument Cabinets, loaded with the masks, are transported by car to the telescope in suitcases re-arranged for this purpose.

The FORS Consortium has retrofitted in FORS2 a Mask eXchange Unit (MXU), which gives the possibility to place slit masks in the focal plane of the telescope [2]. The multiplex capabilities of the instrument may be increased up to 200 targets per mask. Up to 10 masks (produced by the MMU) can be stored in the unit. The loading of the masks into the MXU is done manually during the day, but the selection and exchange of the masks during the observations is remotely

controlled by the instrument control software.

### Description and Performance of the MMU [3]

Figure 1 shows a picture of the laser-cutting machine. An air pad X – Y translation stage is mounted on the polished surface of a very stable granite table of 2.5 tons. The 0.2 mm thick black coated invar sheets are mounted on the X – Y table and they are flattened with an air clamping system. A 20 W pulsed (1.6 KHz) Nd – YAG ( 1064 nm) laser is mounted on top of the table. An expander and objective lens focus a 40  $\mu\text{m}$  waist spot on the masks. Cutting of

the material occurs under a 16 bar compressed air jet. The laser system (manufactured by the German LPKF company) is also equipped with a double close water circuit for the cooling of the pumping lamp and with an air pressured device for exhausting of the mask debris. The X – Y moving table allows a position absolute accuracy better than 15  $\mu\text{m}$  and can cut slits with a width down to 100  $\mu\text{m}$  (0.17 arcsec on the sky). The shape of the slits can be adapted to the observer needs, the width along the slit may even vary. The minimum radius of curvature of the slits is 2 mm.

The physical size of each VIMOS mask is 305  $\times$  305 mm but the useful area is 244  $\times$  279, which fits the detector field of view (7  $\times$  8 ). Figure 2 shows true to scale the 4 VIMOS quadrants and the location of the masks. The dispersion direction of the spectra on the CCDs is also shown.

Figure 3 gives a typical laser cut VIMOS mask showing, in addition to the slits, the reference marks for high position accuracy on the VIMOS focal plane, the attaching holes for the handling of the masks by the Mask Exchange Unit, the holes for reference stars and the identification code.

The main requirements on the masks for VIMOS and NIRMOS are listed in Table 1. It shows also the results obtained at Paranal after installation. All of them are better than the required values.

The number of slits per mask may be greater than 200 when VIMOS is used in low-resolution mode (R~200). Up to 5 slits can be drilled along the dispersion without spectra overlapping. The high cutting speed of 6 mm/s allows to produce up to 32 “low-resolution” masks (8 fields) in an 8-hour working time.

Since the spectroscopic observations through the masks have to be done at the best observing conditions (targets near the meridian), the direct images of the fields to be taken by VIMOS to prepare the masks have to be recorded at the beginning of the night several weeks before the spectroscopy

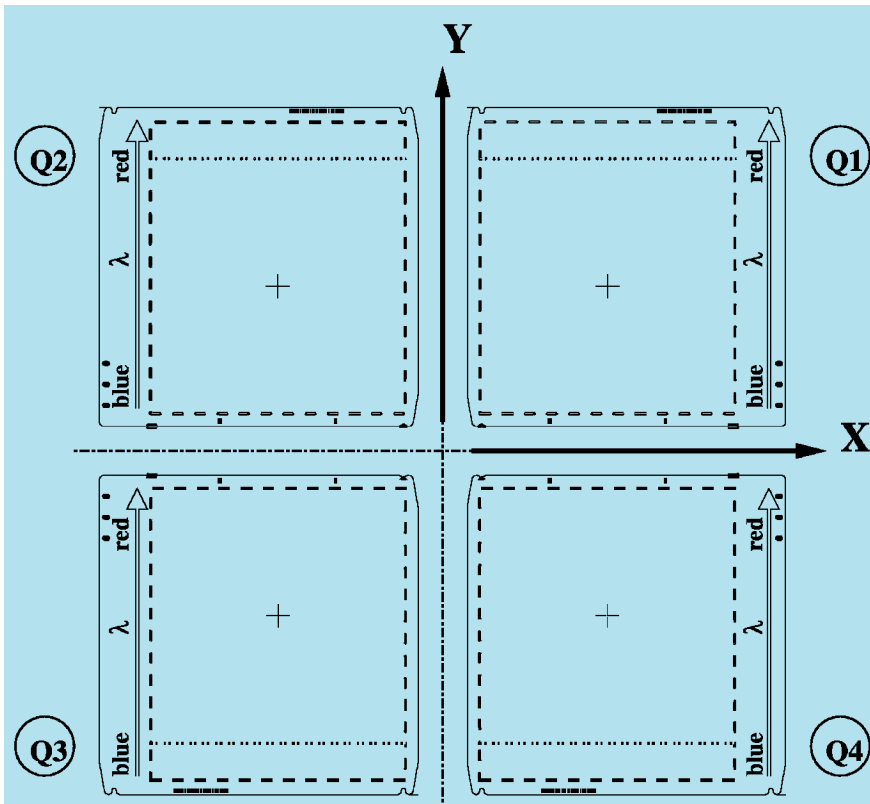


Figure 2: Distribution of the 4 slit masks on the focal plane of the VIMOS quadrants. Each mask is 305  $\times$  305 mm.

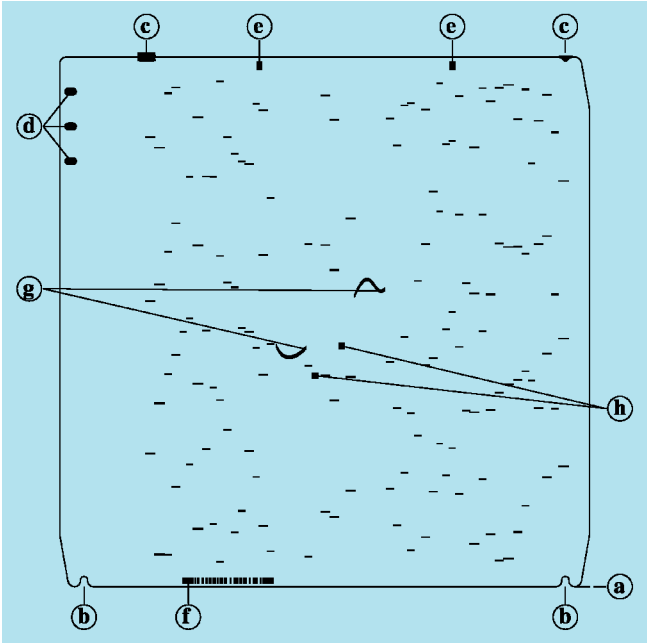


Figure 3: Typical VIMOS mask sample showing examples of straight and curved slits (g), square holes for reference stars (h), mechanical references for high position accuracy on the Nasmyth focal plane of the 4 masks (b, c) and identification code (f).

converted in "gerber" CAD compatible format files. A final conversion is done by the LPKF-owned software to create a file with the cutting commands. Once the masks are made, they are stored in the Storage Cabinet and from there, they are inserted into the cabinets, which are installed into VIMOS (NIRMOS) for the spectroscopy observations.

## Installation and Operation

A room in the General Storage building just in front of the Auxiliary Telescope Hall (ATH) in the Camp Area was built as the MMU Laboratory. All necessary facilities like electricity, water, pressurised air, LAN, telephone and air condition were designed and implemented in time by the Paranal Engineer and Facility departments. Due to the size and weight of the laser table, the front wall of the MMU Laboratory had to be removed for the installation (Figure 4).

Two weeks were necessary to install all the MMU components, interface them and put all the system in operation. Mr. A. Mueller from LPKF spent three days to install, align, operate the laser, and to perform the first maintenance protocol according to the Contract. On August 2 the first VIMOS mask was successfully produced in Paranal.

In the following days, the protocol to prepare the FORS-2 masks for the MXU was completed mainly by A. M. Aguayo and W. Hummel. All the necessary masks for the test run with FORS 2 were produced.

The MMU, after additional check-ups and minor failures during this installation period, is now in operation and ready to manufacture the observation masks for FORS2 visitor observers as of November 2000 and early next year for VIMOS commissioning.

We want to thank the Paranal Engineering and Facilities Departments

run. Also, masks for a large number of fields must be available to optimise and adapt to the scientific programme, the optimal target position with respect to the meridian and the required exposure times. For this purpose, a hardware and software system called Mask Handling System has been implemented to control the identification, classification and flow of the masks. The cutting machine engraves a bar code at the bottom of the masks (Figure 3, (f)) for the identifications.

A Storage Cabinet was built to store the manufactured masks (Figure 5) before they are inserted in the Instrument Cabinets (the boxes that contain the 15 masks to be placed on the VIMOS quadrants during the observations). Up to 400 masks may be stored (100 per VIMOS quadrant). A bar code laser system is used to keep track of the masks in the Storage Cabinet. Finally, the so-called Instrument Cabinet Robot (Figure 6), is a device to insert semi-

automatically, in a known order, the masks into the Instrument Cabinets. Once loaded, the Instrument Cabinets are transported from the MMU Laboratory to the telescope and mounted into VIMOS (NIRMOS).

Three main software packages were built for the MMU. The Mask Handling Software provides a Graphical User Interface for all masks handling functions excluding the manufacturing. It records the storage order of the masks in the Storage Cabinet, interfaces the Instrument/VLT software and acts as front end for the LPKF file converter software. The Cut Manager Software is a GUI for the handling of mask files and is a front end of the LPKF cutting software.

The mask preparation begins with the preparation of a file by the observer from direct images taken with VIMOS (NIRMOS) with the positions (in mm) of the slits. The files are sent to a PC in the MMU Laboratory where they are



Figure 4: Moving the 2.5-ton Laser Table inside the MMU Laboratory. The wall had to be removed for this purpose.



Figure 5: The VIMOS Storage Cabinet. 400 masks may be stored (100 per VIMOS quadrant).

led by P. Gray and J. Eschwey for their work in preparation to and during the commissioning of the MMU. Special thanks go to P. Sansgasset, P. Robert, U. Kaberger, E. Bugueño, M. Tapia, G. Gillet and P. Mardones.

### References

- [1] Le Fèvre et al.: 2000, in *Optical and IR Telescope Instrumentation and Detectors*. Proc. SPIE **4008**, 546.
- [2] H. Schink et al.: 2000, in *Optical and IR Telescope Instrumentation and Detectors*. Proc. SPIE **4008**, 175.
- [3] Conti, G. et al.: 2000, *Astronomy & Astrophysics*, submitted.

Email address: gavila@eso.org

Figure 6: The Instrument Cabinet Robot. The four Instrument Cabinets corresponding to the four channels of VIMOS (or NIRMOS) are inserted in the stand.



# First Astronomical Light with TIMMI2, ESO's 2nd-Generation Thermal Infrared Multimode Instrument at the La Silla 3.6-m Telescope

H.U. KÄUFL<sup>1</sup>, N. AGEORGES<sup>1</sup>, E. DIETZSCH<sup>5</sup>, J. HRON<sup>4</sup>, H. RELKE<sup>2</sup>, D. SCHOLZ<sup>3</sup>, A. SILBER<sup>1</sup>, M. SPERL<sup>4</sup>, M. STERZIK<sup>1</sup>, R. WAGNER<sup>2</sup>, U. WEILENMANN<sup>1</sup>

<sup>1</sup>ESO, Garching bei München, Germany

<sup>2</sup>Astrophysikalisches Institut und Universitäts-Sternwarte Jena, Germany

<sup>3</sup>Physikalisch Technische Fakultät der Friedrich-Schiller-Universität, Technische Betriebseinheit, Jena, Germany

<sup>4</sup>Institut für Astronomie der Universität Wien, Austria

<sup>5</sup>Leipziger Straße 100, Jena, Germany

## Introduction

We report the first astronomical tests of TIMMI2 between October 6 and 11, 2000. A short overview of the project history and the project context is given. This is followed by a basic description of the instrument and its modes as well as a report on the achieved and projected sensitivities. A more in depth technical description including first operational experiences will be given in one of the upcoming issues of *The Messenger*. As to the scientific interest of TIMMI2, readers are referred to, e.g., Käufel 1993.

## The TIMMI2 Project

In 1992, when ESO commissioned the original TIMMI instrument, visiting astronomers could use a modern competitive instrument featuring imaging and low-resolution spectroscopy in the wavelength region from  $\approx 5 \mu\text{m}$  to  $\approx 17.5 \mu\text{m}$  (cf. Käufel et al. 1992, 1994a, 1994b). Back in 1992, to the best of our knowledge, TIMMI was the only such instrument available as a common user instrument at any observatory. TIMMI was built under contract for ESO by the *Service d'Astrophysique*, Saclay,

France (PI Pierre-Olivier Lagage). TIMMI, featuring a  $64 \times 64$  gallium doped silicon array and mostly germanium refractive optics inside a solid-nitrogen/liquid-helium dewar, was in constant use until its decommissioning in 1999 (cf. Stecklum et al. 1999). By then, the development of detectors had progressed so rapidly, that the instrument no longer appeared competitive.

In fact, in 1993 ESO joined a consortium of French institutes to develop, based on the array used e.g. in TIMMI, a next-generation device (cf. e.g. Lucas et al. 1994). Already the format of this device ( $128 \times 192$  pixel) suggested that it would be desirable to build a new camera, rather than trying to use the new device in the existing set-up. Even larger arrays were announced by US suppliers. To that end ESO had developed some basic ideas for the optics of a next-generation instrument for the La Silla 3.6-m telescope (cf. Käufel & Delabre, 1994).

As a result of the *La Silla 2000 questionnaire* (see Anderson 1994) in *The Messenger* 78, ESO received a proposal from the *Astrophysikalisches Institut und Sternwarte* of the *Friedrich-Schiller-Universität* (FSU) in Jena,

Germany, to build TIMMI2. This proposal, reflecting ESO's optical concept, was based on a modern cryostat cooled by a Closed Cycle Expansion Cooler Machine and was also featuring a polarimetric option (not available in TIMMI). Personnel cost and capital investments could largely be covered by funds raised by the Institute in Jena. The PI in Jena was Hans-Georg Reimann. After some negotiations, a *Memorandum of Understanding* was signed and the work began in early 1996. The design sketch of ESO (see above) was first transformed into a FEM<sup>1</sup> certified conceptual design, both for the optics and mechanics, by the company Jena-Optronik GmbH. Based on this work, the final design and the detail design of the instrument were done at the physics department of the FSU. To the extent that this was feasible, all mechanical parts were manufactured in the workshops of the FSU. In the course of the project, the group at the FSU could enlist a team from the *Sternwarte der Universität Wien* for

<sup>1</sup>A representative mechanical design for the optical bench was made and its flexure was modelled with the finite element method.

support, especially with the data-flow aspects of TIMMI2. Because of a concatenation of detrimental influences, most notably delays in the delivery of the detector and the associated electronics, the original schedule could not be kept. The instrument could be shipped only end of April 2000 from Jena to La Silla. During the extended assembly and commissioning phase in May, the TIMMI2 team took a short break to visit the upper Elqui valley. On the way back, a serious car accident occurred. The PI, Hans-Georg Reimann was killed and other members of the team were more or less seriously injured (cf. *The Messenger* No. 100).

Work on the project was resumed in July, and in early August the full functionality of the instrument was established on the observing floor of the 3.6-m telescope. End of September, the team reconvened and the instrument could be interfaced for the very first time with the telescope.

While TIMMI2 was under development, the 3.6-m telescope underwent fundamental improvements and an extensive upgrade. In a first stage, the image quality was substantially improved (S. Guisard et al. 1997). It should be noted that for an instrument working at  $\geq 5 \mu\text{m}$  at a 4-m-class telescope, the performance in terms of S/N is basically proportional to the Strehl ratio. Equally beneficial for the performance of TIMMI2 was the decision to change the telescope control system (TCS) to VLT standards. This involved a complete rebuilding of the by then more than 20-year-old hardware of the f35 chopping secondary/adaptor (cf. Moorwood & van Dijsseldonk 1985). TIMMI2 can now be set up to execute in a semiautomatic way complicated exposure sequences (chopping, nodding, mosaic scans, etc.). Such sequences may be essential for observing moderately extended objects (e.g. Käufel 1995a,b).

## TIMMI2 Technical Description

### Optics

TIMMI2, like its predecessor TIMMI, or many other ESO instruments (e.g. SOFI, EFOSC, FORS) is a focal reducer with a collimated beam at the intermediate pupil. An aperture wheel allows for the selection of various field masks or slits. Behind the intermediate pupil a lens/grism wheel (3 grism and  $\approx 25$  filter positions) is located. It is followed by an objective wheel. TIMMI2 is equipped with a Raytheon  $240 \times 320$  arsenic doped silicon blocked impurity band (BIB) array detector (cf. Estrada et al. 1998). The device has its peak quantum efficiency at  $\approx 10 \mu\text{m}$  and can be operated over an extended range ( $\approx 2 \mu\text{m} \leq \leq 28$

$\mu\text{m}$ ). With this format, Nyquist sampling of the diffraction pattern of the telescope at  $\approx 8 \mu\text{m}$  (i.e. a pixel scale of 0.3 arcsec/pix) results in a field-of-view of  $72 \times 96 \text{ arcsec}^2$  compared to  $19 \times 19 \text{ arcsec}^2$  for TIMMI.

Thus the focal length of the collimator and consequently the size of the intermediate pupil had to be increased correspondingly. TIMMI2 is equipped with a spherical mirror ( $f = 350 \text{ mm}$ , used in an off-axis configuration) which gives a beam diameter at the pupil stop of 10 mm. As the total length of the cryogenic optical train in the dewar is of the order of  $2.5 \times f_{\text{collimator}}$ , i.e.  $\approx 900 \text{ mm}$ , a double fold of the optical path was chosen. Therefore, between collimator and pupil stop, the optical axis passes a folding mirror which has some power to compensate the astigmatism introduced from the off-axis operation of the spherical mirror. This arrangement is extremely simple and robust while generally w.r.t. optical quality superior to the use of e.g. an off-axis parabola.

The lens wheel has 8 positions:

- Ge-lens ( $f = 143 \text{ mm}$ ) for imaging with 0.2 arcsec/pixel at  $\approx 10 \mu\text{m}$
- Ge-lens ( $f = 95.5 \text{ mm}$ ) for imaging with 0.3 arcsec/pixel at  $\approx 10 \mu\text{m}$
- CdTe-lens ( $f = 143 \text{ mm}$ ) for imaging with 0.2 arcsec/pixel at  $\approx 20 \mu\text{m}$

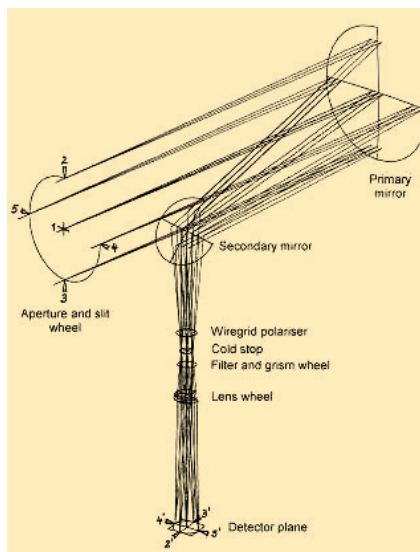


Figure 2: Schematics of the TIMMI2 Optics. Primary mirror: off-axis spherical mirror; secondary mirror: folding mirror.



Figure 1: Hans-Georg Reimann shortly before the accident during the re-assembly of TIMMI2 on the 3.6-m telescope observing floor.

- Si-lens ( $f = 89.5 \text{ mm}$ ) for imaging with 0.3 arcsec/pixel at  $\approx 3\text{--}5 \mu\text{m}$
- Ge-lens ( $f = 63.6 \text{ mm}$ ) for spectroscopy with 0.45 arcsec/pixel at  $\approx 10 \mu\text{m}$  including the order sorting filter
- CdTe-lens ( $f = 47.8 \text{ mm}$ ) for spectroscopy with 0.6 arcsec/pixel at  $\approx 20 \mu\text{m}$  including the order sorting filter
- the other positions are reserved for technical/alignment purposes.

All lenses used here are simple meniscus lenses and give basically for all configurations a theoretical image quality better than 0.5 arcsec. For more details on the optical design see Reimann et al. 1998 and 2000 or Dietzsch & Reimann, 1998.

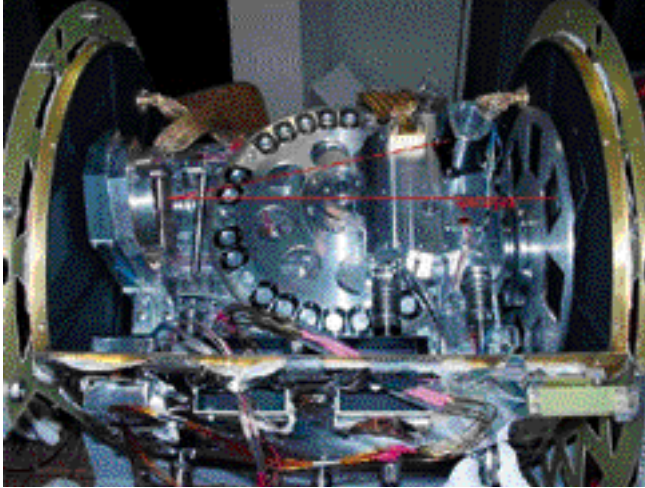
The tests at the telescope have confirmed the theoretical image quality, i.e. TIMMI2 is for all practical purposes either diffraction- or seeing-limited.

TIMMI2 can be used in polarimetric mode. A, in principle, continuously rotating analyser can be inserted between the internal folding mirror and the cold pupil spot.

### Cryostat

The TIMMI2 cryostat is extremely simple: it consists of two short ISO-standard stainless-steel tubes welded together under right angles. To the extent this was feasible, standard ISO-norm parts were used. To achieve good vacuum and cryogenic performance, all inner surfaces were polished and gold plated. The optical bench consists of a light-weighted aluminium structure supported (and thermally insulated) by a fibre-glass structure. The optical bench is enclosed by a radiation shield. Cooling of the instrument is achieved with a commercial 2-stage Gifford-McMahon Closed Cycle Cooler (supplied by Sumitomo Heavy Industries). The goal of the cryogenic design was to have all surfaces and components within the radiation shield cooled well enough that the instrument remains for all practical purposes (including medium-resolution

Figure 3: Close view from the top of the TIMMI2 cold optical bench (baffles and shields partially re-moved). Left and right in the picture the fibre-glass support structure and the solid parts of the radiation shield can be seen. To guide the eye, the optical path, starting on the right at the aperture/slit-wheel leading to the collimator and from there to the folding mirror is indicated. The folding mirror sends the light through the (encapsulated) polariser unit to the filter wheel, cold stop and lens wheel, then to the detector unit which is mounted to the back of the bench. The distance aperture/slit wheel to collimator is  $\approx 350$  mm. Three drive shafts are clearly visible, from left to right: filter-wheel, polariser movement and polariser insertion.



spectroscopy or L-band imaging) limited by the external background radiation (for details on the calculation of background noise limited operation see e.g. Käufel et al. 1991)<sup>2</sup>. Typical temperatures are 70 K for the radiation shield, 40 K for the optical bench, 34 K for the lens wheel and  $\approx 8$  K for the detector array. Temperatures are monitored with several PT-100 sensors for  $T \geq 30$  K and 2 Si-diodes for the detector area. The detector temperature is actively controlled with a commercial PID-controller.

Cooling down to operating conditions and starting with evacuation takes typically 48 hours. Several strong heaters are mounted to the cold bench to allow for baking during evacuation ( $T \leq 50^\circ\text{C}$ ) and to speed-up the warming-up at the end of operation. In case of *target-of-opportunity* observations, additional filters can be added to the filter wheel with a minimum intervention.

For motorising the 5 cryogenic functions, all bearings and gears were designed and assembled according to the principles also in use in other ESO infrared instruments (ISAAC, SOFI). As a thermal IR instrument is less critical with respect to light-tightness of the shields/baffles than a near-IR instrument, the motors of TIMMI2 are located outside the vacuum vessel. For the drive shafts, ferro-fluidics sealed penetrations are used. The penetrations at the radiation shield use an auxiliary bearing which ensures adequate light tightness and heat-sinking of the drive shafts.

<sup>2</sup>Readers not entirely familiar with this type of infrared instrumentation are reminded that the number of thermally emitted photons from telescope, atmosphere and dewar entrance window exceed by orders of magnitude those collected from the astronomical source: e.g. while a 1 Jy source at  $10\ \mu\text{m}$  will generate of the order of  $10^7$  photo-electrons, the background generates of the order of  $10^{10}$  photo-electrons per pixel(!) per second.

### Telescope Interface and Calibration

TIMMI2 is interfaced to the f35 adapter with a special interface plate allowing for pupil alignment. Integrated into this plate is a wheel with 12 positions allowing the insertion of a sky simulator, a flat-field source and spectral calibrators (plastic sheets with narrow spectral features).

### Electronics

The TIMMI2 hardware is controlled via an Ethernet-IEEE488-bus interface. It is largely based on commercial electronics. The motor positions are monitored by means of inductive sensors which may be complemented by micro-switches in the near future.

All functions (including the vacuum pumps and the closed-cycle cooler) can be controlled either by computer from a password-protected dialog box in the user-interface or directly using the corresponding front panel switches. For general routine operation, comput-

er control is preferred as it appears safer; hand-operation, however, is essential as it is the only means to handle non-standard or error situations.

The detector is read out with a commercial electronics system (IR-Observer<sup>TM</sup>) from Wallace Instruments. It generates all clocks and voltages for readout and chopping. The system is interfaced to a LINUX-PC.

### Computer System and Data Flow

As mentioned above, in the thermal IR, detectors work under extremely high flux conditions which force – to avoid saturation – rapid readout of the detectors. In the case of the Raytheon  $240 \times 320$  device in use in TIMMI2, 16 Analogue-to-Digital Converters work in parallel and generate of the order of 30 Mbyte per second. Storage and distribution of data at this rate is considered undesirable. Therefore, an automatic preprocessing pipeline has been developed. The scope of this pipeline is in a first processing step to simply co-add the data and in a second step to apply shift-and-add and cosmetic correction to the data while performing a simple consistency check (monitoring of average signal and variance). The scope and architecture are described in Relke et al. 2000. The ultimate goal is to provide one frame conforming to the ESO-DICB standards per target-instrumental mode configuration, or, in other words, e.g. in imaging, the output of TIMMI2 shall be equivalent to a dark, bias, flat-field and bad-pixel corrected CCD-image. At this stage of the project, however, it was not yet feasible to try the preprocessing pipeline.

### First Results

The first commissioning was limited to 5 nights. After mechanical mounting, within hours, the first images could be obtained. Various electronic and software problems, however, did not allow to achieve acceptable performance from the beginning. Because of the

Figure 4: The TIMMI2-adapter assembly on its way to the telescope. While TIMMI2 could be hand-carried conveniently to the telescope, TIMMI2 needs a fork-lift and other special tools. The metal hoses lead to the closed-cycle cooler expansion machine attached to the top of the vacuum vessel. The TIMMI2 cryostat is interfaced to the recycled f/35 adapter by means of a special alignment plate which holds also a wheel with calibration targets.



residual risk associated with mounting of the TIMMI2 adaptor package with a mass of  $\approx 400$  kg, it was decided to use the engineering rather than the science-grade array for the first test. Another risk was that due to potential problems with the cable twist between the Closed Cycle Cooler Compressor and the instrument, the cooling machine could stall, which in turn could result in some contamination problems associated with the induced warming-up. Fortunately, none of these problems occurred and the results of the tests can be summarised as follows:

- The instrument mounting procedure is safe and the interruption of the cooling machine can be limited to  $\approx 60$  minutes; this in turn implies that the instrument is in stable operating conditions within 3 hours after mounting.
- The instrument works safely at least up to zenith distances  $\geq 60^\circ$ ; the technical position South, telescope horizontal, can also be reached without any operational problems.
- The flexure between the guide probe CCD and the TIMMI2 optics is less than 1 arcsec up to 2 airmasses.
- The internal camera background and detector dark-current is negligible for all scientific instrument modes.
- The image quality is  $\leq 0.8$  arcsec for  $\leq 13 \mu\text{m}$  and strictly diffraction limited for longer wavelengths.
- The instrument sensitivity is within expectations.<sup>3</sup>
- The optics does not produce any significant ghosts.
- The basic functionality of the user-interface could be established.

## Improvements and Outlook

While the instrument configuration as tested gave already acceptable results, the TIMMI2 team will try, before the arrival of the first visiting astronomers in mid-January 2001, to implement a variety of improvements, both to boost performance and to make TIMMI2 more robust:

- The mechanics of the polarisation will be slightly modified to reduce mechanical friction.
- The inductive position sensors will be modified.
- The distance between Dewar entrance window and telescope focus will be increased.
- The signal preamplifiers in the read-out electronics will be modified.

<sup>3</sup>E.g., at  $\approx 12 \mu\text{m}$  with a  $1\text{-}\mu\text{m}$  bandwidth filter, the limiting flux for point sources is  $\approx 40$  mJy,  $10^{-10}$  in 1 hour (elapsed time, including all overhead). The performance of TIMMI2 as it was tested is competitive with all other instruments existing, but TIMMI2 has by far the largest field of view. Nevertheless, the TIMMI2 performance is a factor of 4 worse than the theoretical limit (BLIP performance, see e.g. Käufel et al. 1991). We are very confident that we can do a factor of 2 better (see section **Outlook** below), and the implementation of the relevant improvements hopefully will have taken place before this article goes into print.

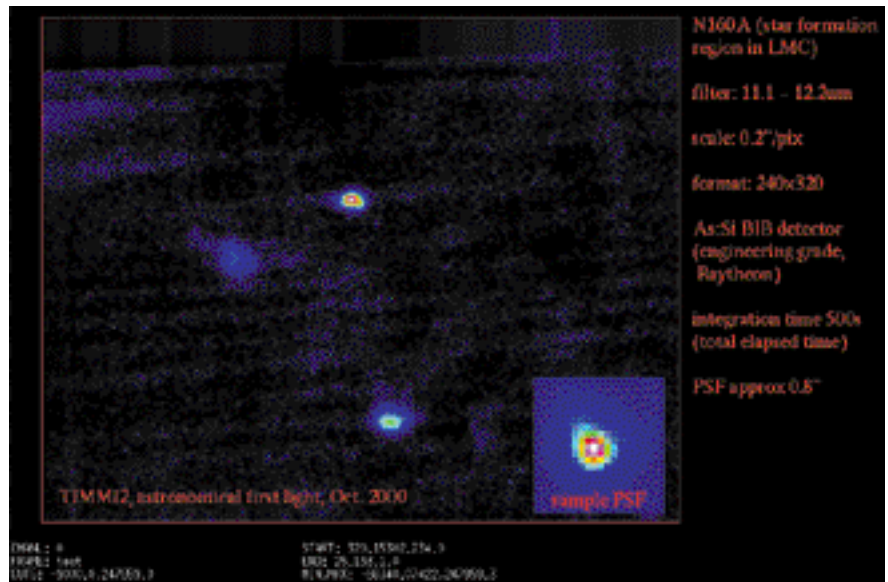


Figure 5: Image of the LMC star-formation region N160A. This was one of the first integrations on a scientifically interesting target with TIMMI2. The residual stripiness is due to grounding problems. While in principle this could be easily removed by Fourier filtering of the data, the cause is understood and the ground-loop problem will be solved while this article goes into print. The insert shows at a magnified scale a typical point-spread-function.

- The engineering grade array will be replaced with the science grade detector. At this point the detector will be carefully aligned with the instrument axis and the instrument orientation in turn with the celestial co-ordinates.

During operation the following problems occurred, which will be solved largely in the near future:

- Problems associated with the too high impedance of transient filters on the detector board in the cryostat will be resolved by modifying the filters as appropriate.
- Line frequency pick-up problems will be solved by opto-insulation of the chopping secondary interface; moreover the grounding scheme of the detector board will be re-examined.
- Saturation problems in the Q-band will temporarily be relieved by adding a neutral density filter until the final filters become available.
- The vibrations introduced from the Closed Cycle Cooler expansion machine produce some second-order artefacts. The immediate cure will be to reduce the CCC-head support resonance frequency by two, and in the coming months, the CCC-head will be supported independently on the telescope rotator.

With the above-mentioned improvements implemented, TIMMI2 has the potential to be the most sensitive and advanced instrument of its kind. Particularly in view of the rapid development of this project, future observers are invited to consult the TIMMI2 web page<sup>4</sup>.

<sup>4</sup><http://www.ls.eso.org/lasilla/Telescopes/360cat/timmi/index.html>

## Some Special Remarks

The first commissioning of TIMMI2 was originally foreseen earlier this year. During the preparation phase, part of the TIMMI2 team set out for what was planned to be a weekend trip to the upper Elqui Valley. On Saturday, May 27, in the late afternoon, they suffered a serious car accident (cf. *The Messenger* 100, p. 56). The PI of TIMMI2, Hans-Georg Reimann from the University of Jena, was killed in the accident. While the team is reasonably satisfied with the successful installation of the instrument, they are all sad that Hans-Georg is no longer with them. To the whole team he had become a very close and good friend. Without his initiative, the project would never have had its kick-off meeting, and the smooth execution of the project was rooted in his equally optimistic and inspiring personality combined with his solid knowledge in the field of astronomy and its associated technologies.

## Acknowledgements

In 1996, the Phase-A Study and the pre-design (by Jena-Optronik GmbH, Jena/Germany) of TIMMI2 was funded by the *Thüringer Ministerium für Wissenschaft, Forschung und Kultur* as Project B503-95025. Subsequently, from January 1997 through December 2000, funding of the manufacturing, assembly, and testing of the complete device came from the *Bundesministerium für Bildung und Forschung, Verbundforschung Astrophysik*, under grant Nr. 05 3JN204. The contribution of the *Institut für Astronomie der Universität Wien* was funded by the Austrian *Ministry of Science and Transport* and

by the *Österreichische Nationalbank, Jubiläumsfonds-Projekt Nummer 6876*.

For the progress of the work, the skilful support by our colleagues at the ESO duty stations Garching, La Silla and Santiago and at the *Friedrich-Schiller-Universität, Jena*, was of great help in all phases. Special thanks go to the staff of the machine shop of the Physics Department of the *Friedrich-Schiller-Universität* who actually manufactured the majority of the mechanical parts from raw materials, and to the *Astro-Taller* on La Silla.

## References

E. Dietzsch and H.-G. Reimann, 1998; TIMMI2: A Combined Astronomical MIR Camera, Spectrometer and Polarimeter for ESO; Proceedings SPIE Vol. **3482**, pp. 151–160.  
 A.D. Estrada, G. Doingo, J.D. Garnett, A.W. Hoffman, N.A. Lum, P.J. Love, S.L. Solomon, J.E. Venzon, G.R. Chapman, C. McCreight, M. McKelvey, R. McMuray, J. Estrada, S. Zins, R. McHugh, and R. Johnson, 1998; Si: As IBC IR focal plane arrays for ground-based and space-based astronomy; Proceedings of SPIE conference 3354 Infrared Astronomical Instrumentation, Kona 1998, pp. 99–108.  
 S. Guisard, U. Weilenmann, A. van Dijksseldonk, H.U. Käufel, and J. Roucher, 1997; Image Quality of the 3.6m Telescope (part

VI): Now Diffraction Limited at 10 Microns at the f/35 Focus; *The Messenger* **90**, 9–11.  
 H.U. Käufel, P. Bouchet, A. van Dijksseldonk and U. Weilenmann, 1991; A Sky-Noise Measurement and its Implication for Ground-Based Infrared Astronomy in the 10- $\mu$ m Atmospheric Window; *Experimental Astronomy* **2**, 115–122.  
 H.U. Käufel, R. Jouan, P.O. Lagage, P. Masse, P. Mestreau and A. Tarrus, 1992; TIMMI at the 3.6m Telescope; *The Messenger* **70**, 67–70.  
 H.U. Käufel, 1993; Ground-Based Astronomy in the 10 and 20 $\mu$ m Atmospheric Windows at ESO – Scientific Potential at Present and in the Future; *The Messenger* **73**, 8–12.  
 H.U. Käufel and B. Delabre, 1994; Improved Design and Prototyping for a 10/20 $\mu$ m Camera/Spectrometer for ESO's VLT, in proc. of *Instrumentation in Astronomy VIII*; SPIE Vol 2198, p. 1036–1047.  
 H.U. Käufel, R. Jouan, P.O. Lagage, P. Masse, P. Mestreau, A. Tarrus, 1994a; TIMMI, ESO's new 10 $\mu$ m Camera/Spectrometer; *Infrared Phys. Technol.* **35**, 203–210.  
 H.U. Käufel, 1994b; N-Band Long-Slit Grism Spectroscopy with TIMMI at the 3.6m Telescope; *The Messenger* **78**, 4–7.  
 P.O. Lagage, R. Jouan, P. Masse, P. Mestreau, A. Tarrus, H.U. Käufel; 1993, TIMMI: a 10  $\mu$ m Camera for the ESO 3.6m telescope; in proc. SPIE vol. 1946, p. 655–666, *Infrared Detectors and Instrumentation*, A.M. Fowler (ed.).  
 H.U. Käufel, 1995a; Acquisition, cleaning and calibrating of ground based thermal IR

data; in proc. of the ESO/ST-ECF workshop on *Calibrating and understanding NST and ESO instruments*, ESO, ed. P. Benvenuti p. 99–104.  
 H.U. Käufel, 1995b; Observing extended objects with chopping restrictions on 8m class telescopes in the thermal infrared; in proc. of the ESO/ST-ECF workshop on *Calibrating and understanding HST and ESO instruments*, ESO, ed. P. Benvenuti p. 159–164.  
 C. Lucas, P. Pantiguy, D. Alloin, C. Cesarsky, P.O. Lagage, H.U. Käufel, J.L. Monin, 1994; New 8-13 $\mu$ m Si:Ga/DRO Hybrid Arrays for Very Large Telescopes; Proc. of *Infrared astronomy with arrays: the next generation*, p. 425–428, ed. I. McLean, Kluwer.  
 A. Moorwood and A. van Dijksseldonk, 1985; New Infrared Photometer and F/35 Chopping Secondary at the 3.6m Telescope; *The Messenger* **39**, p. 1.  
 H.G. Reimann, U. Weinert and S. Wagner, 1998; "TIMMI2, a new IR-Multimode Instrument for ESO", Proc. SPIE Conf. **3354**, p. 865. (See also [http://cdsads.ustrasb.fr/cgi-bin/nph-bib\\_query?bibcode=1998SPIE.3354..865R&db\\_key=](http://cdsads.ustrasb.fr/cgi-bin/nph-bib_query?bibcode=1998SPIE.3354..865R&db_key=))  
 H. Relke, M. Sperl, J. Hron, H.U. Käufel, H. Linz, H.G. Reimann, R. Wagner: 2000. Proc. SPIE Vol. 4009, p. 440–448, *Advanced Telescope and Instrumentation Control Software*, Hilton Lewis, Ed.  
 B. Stecklum, H.U. Käufel, A. Richichi, 1999; The lunar occultation of CW Leo – a great finale for TIMMI, 1999 *The Messenger* **95**, 25–27.

Email address: [hukaufel@eso.org](mailto:hukaufel@eso.org)

# Exploring the Lyman Forest at $z = 2$ with UVES

S. CRISTIANI, S. D'ODORICO, T.-S. KIM, ESO

## 1. The Signature of Neutral HI in the High-Redshift Universe

The Lyman- resonance line of neutral hydrogen provides a sensitive probe to study the cosmological distri-

bution of the baryonic matter and the conditions in the intergalactic medium (IGM) over a wide range of redshifts, up to  $z \sim 6$ . Observations of the "forest" of Lyman- absorptions along the lines of sight to quasars, the most luminous ob-

jects known, reveal a wealth of structures, ranging from fluctuations of the diffuse IGM to the interstellar medium in protogalactic objects. The properties of the Lyman- forest at different redshifts constrain the cosmological parameters, such as the density of baryons and the density parameter  $\Omega_b$ , and are the key to issues like the formation of galaxies and large-scale structure, the origin and properties of the ionising radiation background. In particular, it was early recognised by Gunn & Peterson (1965) that, to avoid producing a very large HI opacity at wavelengths just below that of the quasar's Lyman- emission line, a strong photoionisation by the metagalactic UV background is necessary, which at high redshift is produced by the first generation of stars, which also enrich the IGM with metals (also observed in the form of absorptions).

Unlike most of the other astronomical objects, Lyman- absorbing "clouds"

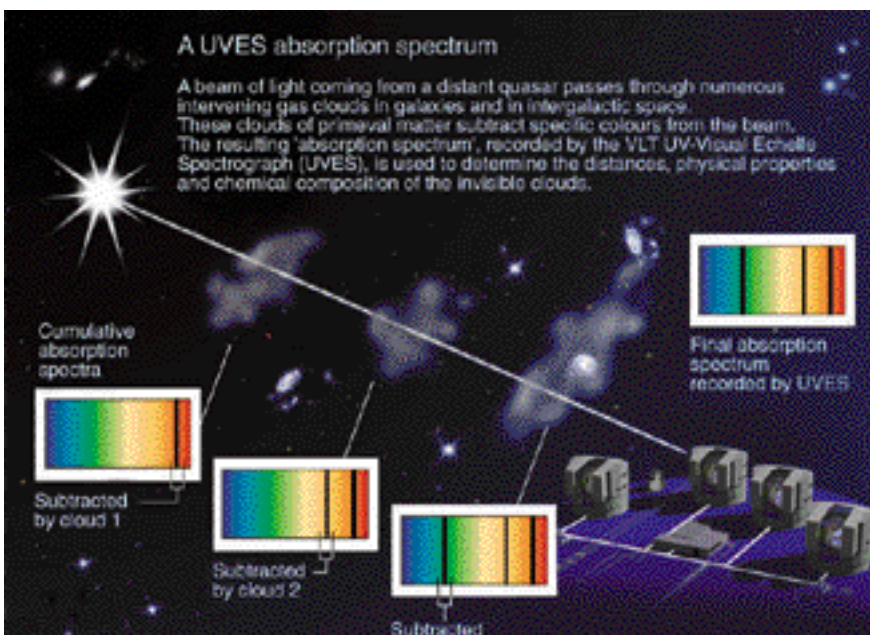


Figure 1: An artistic view (thanks to Ed Janssen) of how absorbing "clouds" distributed in the Universe leave their imprint in the spectrum of a distant, background quasar, which acts as a light beacon.

were first discovered at great distances ( $z \geq 2$ ) due to cosmological redshift and the near-UV atmospheric absorption. Only in relatively recent times and with the advent of the Hubble Space Telescope (HST) has it been possible to gain a limited (in sensitivity and resolution) access to the ultraviolet and study nearby examples. The epoch corresponding to redshifts between 1.5 and 2.5 is one of the most interesting, characterised by an intense universal star formation, though one of the most difficult to study because the “signatures” of luminous matter at these redshifts (both stars and emitting gas) fall mainly in the less accessible IR region. The key resonance absorption lines like Lyman- lie at these redshifts in the UV region where, before UVES, no efficient high-resolution spectrograph was in operation at very large telescopes.

## 2. A First Look at the IGM at $z = 2$ with the New Echelle Spectrograph at the VLT, UVES

UVES (Dekker et al. 2000) is the two-arm echelle spectrograph, mounted on one of the Nasmyth platforms of the Kueyen telescope (UT2) of the VLT. In the instrument design phase it was decided to go for a two-arm configuration (UV-Blue and Visual-Red channels, to be operated in parallel with a dichroic beam splitter) to optimise the efficiency especially in the extreme UV (close to the atmospheric cut-off) and in the Near-Infrared (where IR array-based instruments start to become competitive with CCD-based ones). CCD devices, gratings and coatings of optical materials for a variety of reasons cannot be manufactured with a flat, maximised efficiency curve over the 300–1100 nm range. By splitting the range in two, remarkable gains can be achieved at the extreme wavelengths. The current efficiency curve of UVES is shown in Figure 2. The efficiencies below 400 nm and above 800 nm are considerably higher than in the powerful echelle spectrograph HIRES which has been successfully in operation for a few years now at Keck.

This advantage immediately offers the possibility of obtaining new results. The observations of the Lyman alpha forest in the spectra of quasars at  $z = 1.5$ – $2$  is a good example of the pay-off of the higher UV efficiency. Already during commissioning and science verification, QSOs at redshift around 2 were extensively observed and the data are now available from the ESO archive. The analysis on the forest (Kim, Cristiani & D’Odorico 2000) gives the first detailed information on the IGM in this redshift range.

To illustrate the extraordinary possibilities offered by UVES in terms of sensitivity and resolution, a small portion of

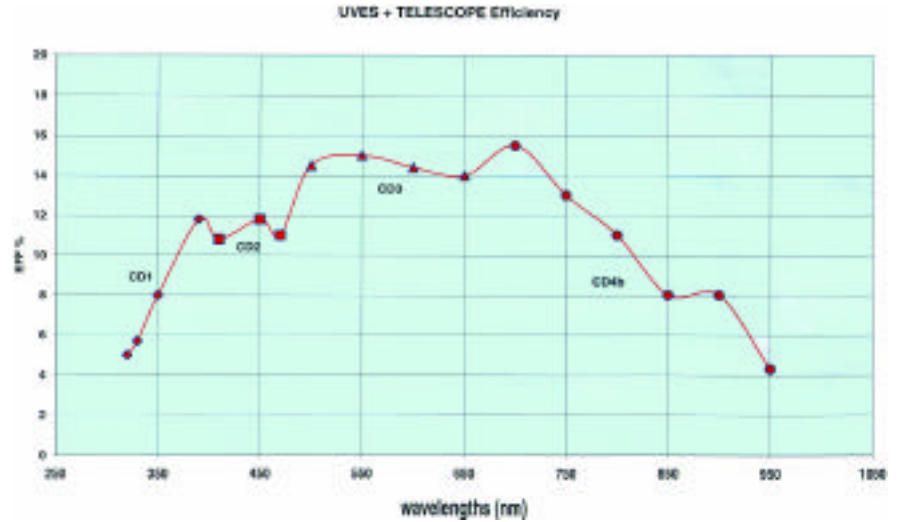


Figure 2: The overall detection efficiency of UVES including the three reflections in the telescope. No atmospheric absorption and no slit losses. The values have been derived from observations of spectrophotometric standards. The overall range is covered by two UVES exposures in dichroic mode. The different symbols correspond to the spectral ranges covered by the 4 different cross-disperser gratings (CD). The Blue arm of the spectrograph was used till 470 nm. Status as of November 2000, after the installation of the final CD4.

the spectrum of the QSO HE 0515-44 is shown in Figure 3, in the range 310–326 nm.

The data have been reduced with the UVES pipeline (Ballester et al. 2000) and analysed with the package VPFIT (Carswell et al.: <http://www.ast.cam.ac.uk/~rfc/vpfit.html>). Voigt profiles are fitted to the absorption lines (isolated and in groups) to derive the redshifts  $z$ , the Doppler parameters  $b$ , and the column densities  $N$ .

## 3. The Evolutionary Properties of the Lyman Forest

### 3.1 The opacity of the IGM and the number density of Lyman- $\alpha$ lines

Figure 4 shows the Lyman-forest normalised spectra of two QSOs: the

high- $z$  Q0000-263 with an emission redshift  $z_{em} = 4.127$  and the HDF-S QSO, J2233-606, with an emission redshift  $z_{em} = 2.238$ . The resolution of the two echelle spectra has been degraded to cover the full range between the Lyman- and Lyman- emissions. It is impressive to see how fast the number of absorptions (and the average opacity) increases with increasing redshift. The HI opacity,  $\tau_{HI}$ , can be defined as  $f = f_c \exp^{-\tau_{HI}}$ , where  $f$  is the observed flux at a wavelength and  $f_c$  is the unabsorbed continuum level. We can compute then the effective opacity  $\tau_{eff}$  as  $\exp^{-\tau_{eff}} = \langle \exp^{-\tau} \rangle$ , where  $\langle \rangle$  indicates the mean value averaged over .

The new UVES results, together with data from the literature, show that the evolution of the effective opacity follows pretty well an exponential law from  $z =$

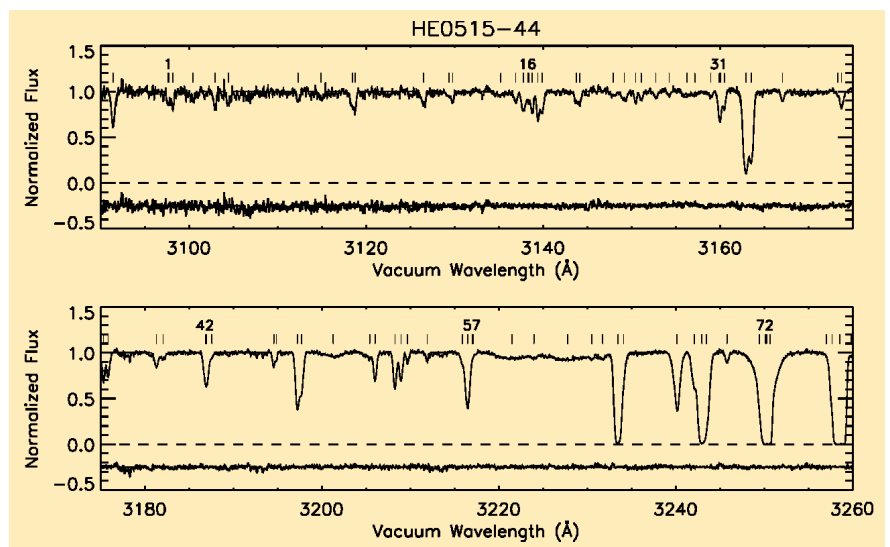


Figure 3: The spectrum of HE0515-44 superposed with the Voigt profile fitted spectrum. The residuals (the differences between the observed and the fitted flux) shown in the bottom part of each panel are shifted by  $-0.25$ .

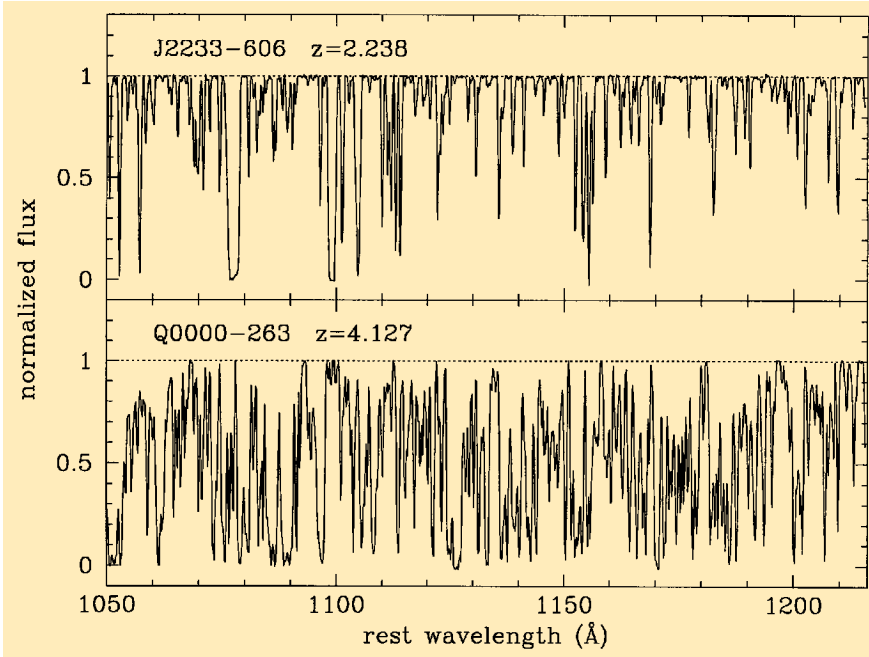


Figure 4: Comparison between the Lyman- $\alpha$  forest of two QSOs: J2233-606 with an  $z_{em} = 2.238$  and Q0000-263 with an  $z_{em} = 4.127$ . The exponential increase of the number of lines with increasing redshift is apparent.

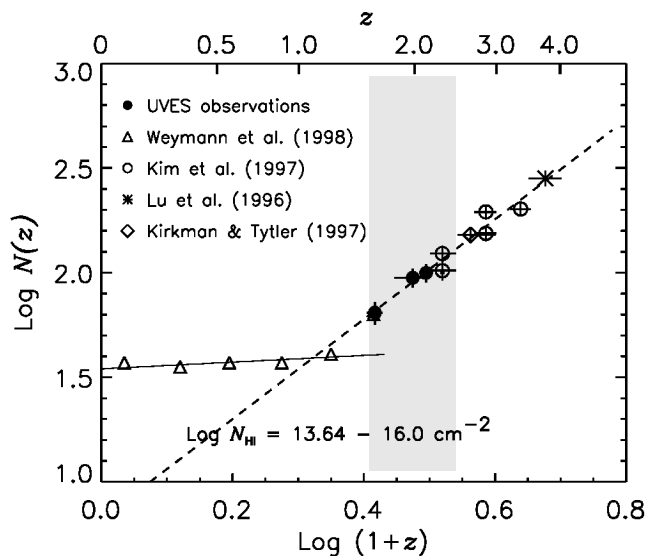
1.6 up to  $z \sim 5$ :  $\bar{\tau}_{eff}(z) = 0.0034 \pm 0.0009 (1+z)^{3.35 \pm 0.17}$ .

The number density of lines per unit redshift is defined as  $\bar{N}(z) = \bar{n}_0(1+z)$ , where  $\bar{n}_0$  is the local comoving number density of the forest. For a non-evolving population,  $\bar{n}_0 = 1$  and  $0.5$  for  $q_0 = 0$  and  $0.5$ , respectively. Figure 5 shows the number density evolution of the Lyman- $\alpha$  forest in the interval  $N_{HI} = 10^{13.64-16} \text{ cm}^{-2}$ . This range has been chosen to allow a comparison with the HST sample at  $z < 1.5$  of Weymann et al. (1998), for which a threshold in equivalent width of  $0.24 \text{ \AA}$  was adopted. The long-dashed line is the maximum-likelihood fit to the UVES and the HIRES data at  $z > 1.5$ :  $dN/dz = (6.7 \pm 3.8) (1+z)^{2.38 \pm 0.15}$ . Interestingly, the HST data point at  $\langle z \rangle = 1.6$  (the open triangle at the boundary of the shaded area), which has been measured in the line-of-sight to the QSO UM 18 and suggested to be an outlier, is now in excellent agreement with the extrapolated fit from higher  $z$ . The UVES observations imply that the turn-off in the evolution does occur at  $z \sim 1.2$ , not at  $z \sim 1.7$  as previously suggested. Down to  $z \sim 1.5$ , the number density of the forest evolves as at higher  $z$ .

The evolution of the  $\bar{N}(z)$  is governed by two main factors: the Hubble expansion and the metagalactic UV background. At high redshift, the expansion, which tends to increase the ionisation of the matter (the rate of recombination is quadratically dependent on the density), and the UV background, increasing or non-decreasing with decreasing redshift, work in the same direction and cause a steep evolution of the number of lines with  $z$ . At low redshift, the UV background starts to de-

crease with decreasing redshift, due to the reduced number of ionising sources, and this effect counteracts the Hubble expansion. As a result, the evolution of the number of lines slows down. Up to date, numerical simulations have been remarkably successful in reproducing the observed evolution (see, for example Davé et al. 2000, Machacek et al. 2000), leaving little doubt about the general interpretation of the phenomenon. However, the same simulations predicted the break in the  $dN/dz$  power law at a redshift  $z \sim$

Figure 5: The number density evolution of the Ly $\alpha$  forest. The column density range  $N_{HI} = 10^{13.64-16} \text{ cm}^{-2}$  has been chosen to allow the comparison with the HST data of Weymann et al. (1998), which are shown as open triangles. The filled symbols are derived from HE 0515-44 at  $\langle z \rangle = 1.61$ , from J2233-606 at  $\langle z \rangle = 1.98$  and from HE 2217-2818 at  $\langle z \rangle = 2.13$ . The open circles, the star, and the diamond are taken from the HIRES data at similar resolutions by Kim et al. (1997), Lu et al. (1996), and Kirkman & Tytler (1997), respectively. The horizontal error bars represent the  $z$  interval over which the number density was estimated. The vertical error bars represent the Poisson  $1\sigma$  error. The shaded area is the  $z$  range where UVES is extremely sensitive. The long-dashed line is the maximum likelihood fit to the UVES and the HIRES data at  $z > 1.5$ . The UVES observations indicate that the slope of the number density evolution of the Ly $\alpha$  forest at  $z > 2.4$  continues at least down to  $z \sim 1.5$  and that a change occurs at  $z \sim 1.2$ .



1.8 that now appears too high. This suggests that the UV background implemented in the simulations is not the correct one: it was thought that at low redshift QSOs are the main source of ionising photons, and, since their space density drops below  $z \sim 2$ , so does the UV background. However, galaxies can produce a conspicuous ionising flux too, perhaps more significant than it was thought, as shown by recent measurements by Steidel et al. (2000). The galaxy contribution, then, can keep the UV background relatively high until at  $z \sim 1$  the global star formation rate in the Universe quickly decreases, determining the qualitative change in the number density of lines.

### 3.2 The temperature of the IGM

If the Lyman- $\alpha$  forest is in thermal equilibrium with the metagalactic UV background, the line width of the absorption lines, described by the  $b$  parameter of the Voigt profile, is directly related to the gas temperature of the absorbing medium determined by the balance between adiabatic cooling and photoheating:  $b = \sqrt{2kT/m_{ion}}$ . In practice, additional sources of broadening exist, such as the differential Hubble flow across the absorbers, peculiar motions, Jeans smoothing. However, a lower limit to the line widths exists, set by the temperature of the gas. Hence we can measure this cutoff and get the temperature of the IGM. The situation is slightly more complex because for a photoionised gas, there is a temperature-density relation, i.e. the equation of state:  $T = T_0 (1 + \delta_b)^{\tau-1}$ , where  $T$  is the gas temperature,  $T_0$  is the gas temperature at the mean gas density,  $\delta_b$  is the

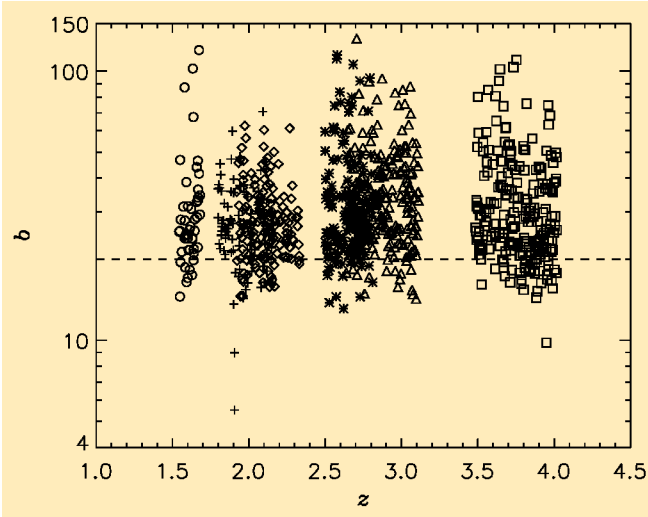
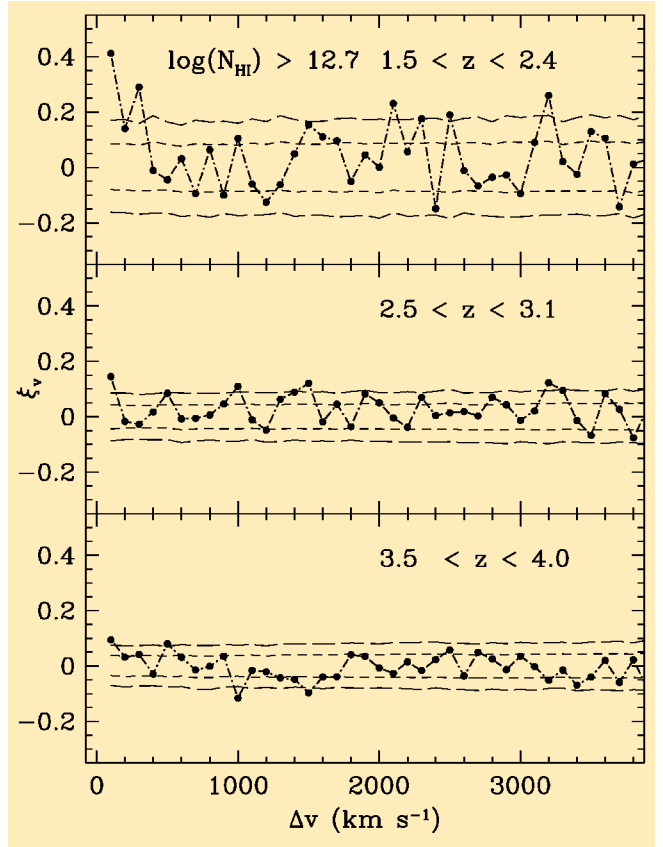


Figure 6: The  $b$  distribution of the Ly $\alpha$  forest as a function of  $z$ . The horizontal dashed line indicates a 20 km/sec  $b_c$  value. The circles, the pluses, the diamonds, the stars, the triangles and the squares are from HE0515–44, J2233–606, HE2217–2818, HS1946+7658, Q0302–003 and Q0000–263, respectively. There is an indication of increasing  $b_c$  with decreasing  $z$  at  $z \sim 3.7$ . At lower  $z$ ,  $b_c$  is not clearly defined.

Figure 7: Evolution of the two-point correlation function with redshift for Ly $\alpha$  lines with column densities above  $N_{\text{HI}} = 10^{12.7} \text{ cm}^{-2}$ . The short-dashed and long-dashed lines represent the  $1\sigma$  and  $2\sigma$  confidence limits for a Poissonian process.



baryon overdensity,  $(\rho_b - \bar{\rho}_b)/\bar{\rho}_b$  and  $\tau$  is a constant which depends on the ionisation history (Hui & Gnedin, 1997). The equation of state translates into a lower cut-off  $b_c(N_{\text{HI}})$  in the  $N_{\text{HI}}-b$  distribution.

In Figure 6, the  $b$  distribution of the Ly forest as a function of  $z$  is shown. The cut-off Doppler ( $b$ ) parameter seems to be approximately constant with  $b_c \sim 18 \text{ km s}^{-1}$  at  $1.5 < z < 4$ , corresponding to a reference temperature of  $2 \cdot 10^4 \text{ K}$ . Two possible features are observed: a systematic increase of the  $b$  values from  $z \sim 4$  to  $z \sim 3.5$  – due to the HeII reionisation? (Schaye et al. 2000) and a region of higher-than-average Doppler widths at  $2.2 < z < 2.4$  that will be further discussed in the last subsection.

### 3.3 The clustering properties of the Lyman forest

The Lyman- forest contains information on the large-scale distribution of the matter and the simplest way to study it is to compute the two-point velocity correlation function,  $(\xi_v)$ . The correlation function compares the observed number of pairs ( $N_{\text{obs}}$ ) and the expected number of pairs ( $N_{\text{exp}}$ ) from a random distribution in a given velocity bin ( $v$ ):  $(\xi_v) = N_{\text{obs}}(v)/N_{\text{exp}}(v) - 1$ , where  $v = c(z_2 - z_1)/[1 + (z_2 + z_1)/2]$ ,  $z_1$  and  $z_2$  are the redshifts of two lines and  $c$  is the speed of light (Cristiani et al. 1997; Kim et al. 1997).

Studies of the correlation function of the Ly forest have generally led to conflicting results even at similar  $z$ . Some studies find a lack of clustering (Sargent et al. 1980 at  $1.7 < z < 3.3$ ; Rauch et al. 1992 at  $z \sim 3$ ; Williger et al. 1994 at  $z \sim 4$ ), while others find clustering at scales  $v \sim 350 \text{ km s}^{-1}$  (Cristiani et al. 1995, 1997 at  $z \sim 3$ ; Hu et al. 1995 at  $z \sim 2.8$ ; Kulkarni et al. 1996 at  $z \sim 1.9$ ; Lu et al. 1996 at  $z \sim 3.7$ ). Figure 7 shows the velocity correlation strength at  $v < 4000 \text{ km s}^{-1}$ . Clustering is clearly detected at low redshift: at  $1.5 < z < 2.4$  in the  $100 \text{ km s}^{-1}$  bin we measure  $\xi_v = 0.4 \pm 0.1$  for lines with  $\log N_{\text{HI}} \geq 12.7 \text{ cm}^{-2}$ . The amplitude of the correlation at  $100 \text{ km s}^{-1}$  decreases significantly with increasing redshift from  $0.4 \pm 0.1$  at  $1.5 < z < 2.4$ , to  $0.14 \pm 0.06$  at  $2.5 < z < 3.1$  and  $0.09 \pm 0.07$  at  $3.5 < z < 4.0$ . A pattern of this type is predicted by the models of hierarchical formation of structures, in the

interpretation, however, it should not be forgotten that a given column density corresponds to different overdensities at the various redshifts. In particular an absorber at  $z = 2$  is dynamically analogous to an absorber that has column density several times higher at  $z = 3$ .

### 3.4 Voids and protoclusters

Voids, i.e. regions with a significant underdensity of absorption lines, are occasionally observed in QSO spectra (Dobrzycki & Bechtold 1991, Cristiani et al. 1997). The typical sizes observed so far are of the order of few tens comoving Mpc. Figure 8 shows two voids (of 54 and 43 Mpc) observed in the spectrum of the object HE2217-2818. The joint probability of finding two voids with a size larger than 40 comoving Mpc in a random distribution of lines at  $z \sim 2$  is of the order of  $2 \times 10^{-4}$ . A third void of 61 Mpc is observed in the spec-

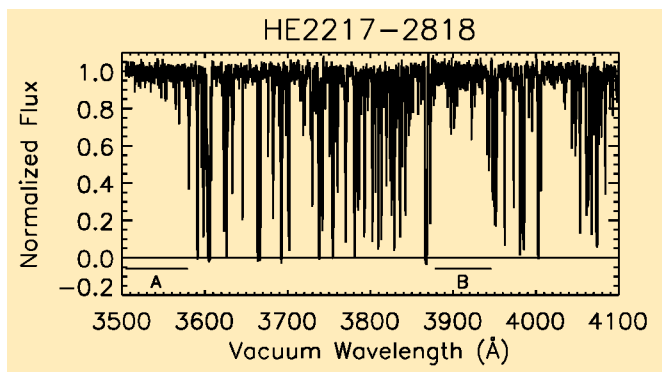


Figure 8: The spectrum of HE2217–2818 with two voids regions. The voids are indicated as A at  $z = 1.912$  and B at  $z = 2.218$ .

trum of HE0515-44. There are different ways to produce a void in the forest: a large fluctuation in the gas density of the absorbers, an enhanced UV ionising radiation from nearby QSOs, feedback from forming galaxies or AGN heating the proto-cluster gas. In particular Theuns et al. (2000) have shown how a typical quasar sight-line intersects one protocluster per unit redshift. It is interesting to note that the void B in the spectrum of HE2217-2818 corresponds to a region of above-than-average Doppler parameter (see above), indicating that the gas in the void has been heated. To give a definitive answer about the nature of these voids, deep imaging and follow-up spectroscopy are needed, in order to identify possible AGN and/or galaxies at the redshift of the voids. This is a challenging programme but well within the possibilities of the VLT.

#### 4. Acknowledgements

We are indebted to all people involved in the conception, construction

and commissioning of UVES and UT2 for the quality of the data used in this paper, obtained in the first weeks of operation of the instrument.

#### References

- Ballester P., Modigliani A., Boitquin O., Cristiani S., Hanuschik R., Kaufer A., Wolf S., 2000, *The Messenger*, **101**, 31.  
 Cristiani, S., D'Odorico, S., Fontana, A., Giallongo, E., Savaglio, S., 1995, *MNRAS*, **273**, 1016  
 Cristiani, S., D'Odorico, S., D'Odorico, V., Fontana, A., Giallongo, E., Savaglio, S., 1997, *MNRAS*, **285**, 209.  
 Davé R., Hernquist L., Katz N., Weinberg D.H., 1999, *ApJ* **511**, 521.  
 Dekker, H., D'Odorico S., Kaufer A., Delabre B., Kotzowski H., 2000, *SPIE Proceedings 4008*, 534.  
 Dobrzycki A., Bechtold J., 1991, *ApJ* **377**, L69.  
 Gunn J.E., Peterson B.A., 1965, *ApJ*, **142**, 1633.  
 Hu, E. M., Kim, T.-S., Cowie, L. L., Songaila, A., Rauch, M., 1995, *AJ*, **110**, 1526.  
 Hui L., Gnedin N. Y., 1997, *MNRAS*, **292**, 27.  
 Kim, T.-S., Hu, E.M., Cowie, L.L., Songaila, A., 1997, *AJ*, **114**, 1.

- Kim T.-S., Cristiani S., D'Odorico S., 2000, *A&A* submitted.  
 Kirkman, D., Tytler, D., 1997, *AJ*, **484**, 672.  
 Kulkarni, V. P., Huang, K., Green, R. F., Bechtold, J., Welty, D.E., York, D.G., 1996, *MNRAS*, **279**, 197.  
 Lu, L., Sargent, W.L.W., Womble, D.S., Takada-Hidai, M., 1996, *ApJ*, **472**, 509.  
 Machacek M.E., Bryan G.L., Meiksin A., Anninos P., Thayer D., Norman M., Zhang Y., 2000, *ApJ* **532**, 118.  
 Rauch, M., Carswell, R.F., Chaffee, F.H., Foltz, C. B., Webb, J. K., Weymann, R. J., Bechtold, J., Green, R. F., 1992, *ApJ*, **390**, 387.  
 Sargent, W. L. W., Young, P. J., Bokserberg A. Tytler, D., 1980, *ApJS*, **42**, 41.  
 Schaye J., Theuns T., Rauch M., Efstathiou G., Sargent W.L.W., 2000, *MNRAS*, **318**, 817.  
 Steidel C.C., Pettini M., Adelberger K.L. astro-ph/0008283.  
 Theuns T., Mo H.J., Schaye J., astro-ph/0006065.  
 Weymann, R.J., et al., 1998, *ApJ*, **506**, 1.  
 Williger, G.M., Baldwin, J.A., Carswell, R.F., Cooke, A.J., Hazard, C., Irwin, M.J., McMahon, R.G., Storrie-Lombardi, L.J., 1994, *ApJ*, **428**, 574.

Email address: scristia@eso.org



## The La Silla New Page

### 2p2 Team News

H. JONES

#### Personnel Movements

In September we welcomed new team member Lisa Germany from Australia. Lisa is a new ESO Fellow and has interests in supernovae and their use in cosmological distance determinations.

September, however, was also a month for departures when we said goodbye to long-time team member James Brewer. James was a pivotal member of the 2p2 Team since his arrival at ESO in 1996. He has returned to Canada to take up a position at the University of British Columbia, in Vancouver, Canada. We wish him all the best under northern skies.

At the start of November, Rene Mendez formally took charge as Team Leader, replacing Patrick François, who will continue working with the team into early 2001.

#### First Stage of BOB-P2PP Software Installation at the ESO/MPG 2.2-m

The first commissioning period for the Broker for Observation Block (BOB) software at the ESO/MPG 2.2-m took place during October 7 to 16. This software will allow the 2.2-m to be controlled through observation blocks

(OBs) in the same way as the VLT, 3.6-m and NTT telescopes. Thanks to the hard efforts of Tatiana Paz, Cristian Urrutia and Eduardo Robledo (of the La Silla Software and Communications Team), the several months of software writing in the lead-up to its first-test at the telescope paid off. During the October test nights it was possible to move the telescope around the sky and execute sequences of short test exposures, using OBs.

Much work is needed to refine and test the code in the coming months, particularly in the way it communicates between the telescope, CCD controller and image acquisition software. Thus, part of the challenge lies in coordinating the separate tasks of these systems, which may be called upon many times during a single sequence.

Additional technical time in November and December will be used to complete the development and testing. In the meantime, a new Instrument Package containing WFI-specific templates for use in P2PP is undergoing revision and testing.

#### Sub-Arcsecond Images with the Wide-Field Imager

On the night of October 19–20, the Wide-Field Imager (WFI) was produc-

ing 20-minute B-band exposures of 0.6 arcsec seeing. This impressive result demonstrates the significant gains that the recent work of Alain Gilliotte and Gerardo Ihle on the 2.2-m image quality have made. In the past, the 2.2-m has exhibited occasional astigmatism under certain pointing conditions (2p2 Team Report, *The Messenger* No. 100). However, recent improvements to the fixed points on which the M1 mirror sits by the opto-mechanical teams on La Silla, have diminished these effects. However, careful focus control is essential to take full advantage of these improvements.

On the same night, the WFI delivered 1.2-arcsec images at an airmass of 1.8, and closely followed the seeing measured by the DIMM seeing monitor.

#### Telescope Information

Remember to consult the 2p2 Team Web pages when you require any information about the ESO 1.52-m, Danish 1.54-m or ESO/MPG 2.2-m telescopes. These are regularly updated with recent news postings and information for new observers. They can be visited at <http://www.ls.eso.org/lasilla/Telescopes/2p2/>.

# A Study of the Activity of G and K Giants Through Their Precise Radial Velocity; Breaking the 10-m/sec Accuracy with FEROS

J. SETIAWAN<sup>1</sup>, L. PASQUINI<sup>2</sup>, L. DA SILVA<sup>3</sup>, A. HATZES<sup>4</sup>, O. VON DER LÜHE<sup>1</sup>, A. KAUFER<sup>2</sup>, L. GIRARDI<sup>5</sup>, R. DE LA REZA<sup>3</sup>, J.R. DE MEDEIROS<sup>6</sup>

<sup>1</sup>Kiepenheuer-Institut für Sonnenphysik, Freiburg (Breisgau), Germany; <sup>2</sup>European Southern Observatory  
<sup>3</sup>Observatorio Nacional, Rio de Janeiro, Brazil; <sup>4</sup>Thüringer Landessternwarte Tautenburg, Tautenburg, Germany  
<sup>5</sup>Dipartimento di Astronomia, Università di Padova, Padova, Italy  
<sup>6</sup>Universidade Federal do Rio Grande do Norte, Natal, Brazil

## 1. Scientific Background

Asteroseismology is an indispensable tool that uses the properties of stellar oscillations to probe the internal structure of stars. This can provide a direct test of stellar structure and evolution theory. Precise stellar radial velocity (RV) measurements made in recent years have not only discovered the first extra-solar planets, but have also uncovered new classes of low-amplitude variable stars. One such is represented by the K giant stars which exhibit RV variations with amplitudes in the range of 50–300 m/s (Walker et al. 1989, Hatzes & Cochran 1993, 1994 ab). This variability is multi-periodic and occurring on two time-scales: less than 10 days and several hundreds of days.

In the most detailed study of a K giant star, Merline (1996) found 10 pulsation modes with periods ranging from 2–10 days in Arcturus. These modes were equally spaced in frequency, the characteristic signature of p-mode oscillations analogous to the solar 5-minute oscillations. The relatively large number of modes that may exist in giant stars means that these objects may be amenable to asteroseismic techniques. Asteroseismology is one of the next milestones in astrophysics, and presently there are relatively few classes of stars on which these techniques can be applied, so it is important when more such objects are discovered.

Asteroseismology can be used to derive such fundamental stellar parameters as mass and radius. This is particularly useful for giant stars as these occupy a region of the H–R diagram where it is difficult to obtain accurate stellar parameters. Furthermore, the evolutionary tracks of main-sequence stars in the spectral range A–G, all converge on the giant branch, so it is impossible to establish the nature of the progenitor star only from these theoretical tracks. Asteroseismology may play a key role in understanding the stellar properties, structure, and evolution of

giant stars and their progenitors. In particular, when combining accurate distances (e.g. from HIPPARCOS), the spectroscopic determination of the chemical composition and gravity along with the oscillation spectrum, the stellar evolutionary models will be required to fit all these observations. This could provide an unprecedented test bench for the theories of the stellar evolution. Before this can be done, however, one must derive the full oscillation spectrum (periods and amplitudes) for a significant number of giant stars.

Although the short-period variations in giants can only arise from radial and non-radial pulsation, the nature of the long-period RV variations is still open to debate. Possibilities include planetary companions, rotational modulation by surface structure, or non-radial pulsation. Each of these hypotheses has a high astrophysical impact, and there are strong arguments to support each of them.

When surface structures, such as active regions and spots, move on the vis-

ible stellar surface (as a result of stellar rotation), they will also induce variability in the core of deep lines, as the Ca II H and K, which are formed in the chromosphere (see e.g. Pasquini et al. 1988, Pasquini 1992). Since FEROS allows the simultaneous recording of the most relevant chromospheric lines, it will be possible to test directly from our spectra the rotational modulation hypothesis. In Figure 1, Ca II K line spectra of one target star taken at different epochs are over-imposed: no evidence for strong variability in the line core is detected.

The expected rotational periods for some giants are consistent with the observed periods and some evidence for equivalent-width variations of activity indicators accompanying the RV variations have been found in two K giants (Larson et al. 1993; Lambert 1987). If the RV variations were caused by surface inhomogeneities, then these would be large enough to be resolved by future ground-based interferometry. These stars will thus make excellent

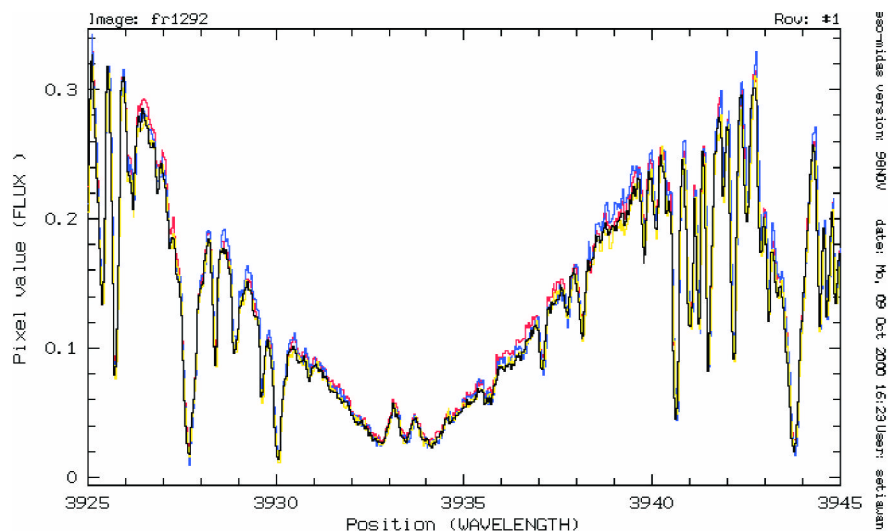


Figure 1: Ca II K line observations of one of the target stars. Observations taken in different nights are overlapped. In case of rotational modulation induced by surface inhomogeneities, the chromospheric core of this line will show detectable variations.

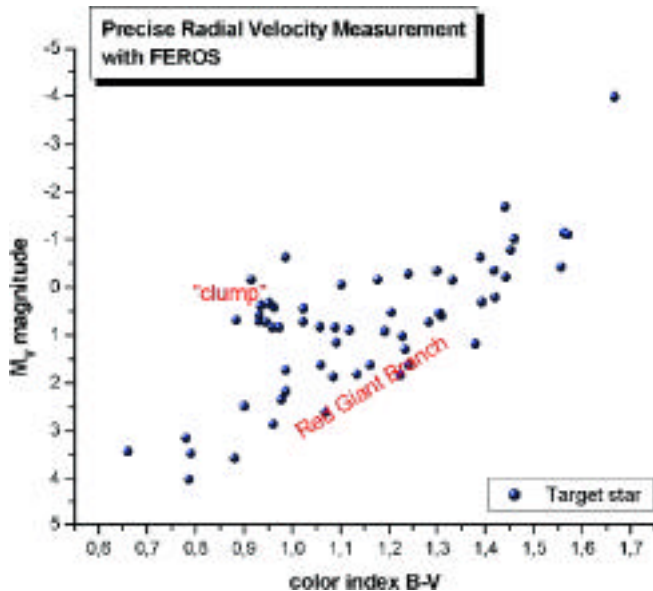


Figure 2: H-R diagram for the 63 stars observed so far for our precise radial velocity survey with FEROS. The sample well covers the Red Giant Branch and the “clump” region.

targets for VLTI observations (von der Lühse et al. 1996).

The non-radial g-mode oscillations seem unlikely, since these are not expected to propagate through the deep outer convection zone in these stars, but nature is always full of surprises. Alternatively, these long-period variations may represent more exotic pulsations such as toroidal modes. The planet hypothesis is supported by these periods being long lived (for more than 12 years) and coherent. In the case of the star Aldebaran, the long-period RV variations were not accompanied by line-profile variations (Hatzes & Cochran 1998). Although these seem to exclude rotations and pulsations, conclusive evidence in support of the planetary hypothesis has proved elusive.

## 2. Observations

K giant RV variability is still a largely unexplored area. Not only is the nature of the long-period variations unknown, but a knowledge of the characteristics of the short-period (p-mode) oscillations as a function of a giant’s position in the H-R diagram is also lacking.

For these reasons, in ESO Period 64 (October 1999 – April 2000), we started an unprecedented survey of precise radial-velocity measurements as a European-Brazilian collaboration aimed at obtaining a sample of about 100 G-K giants and subgiants along the whole upper part of the HR-diagram (see Fig. 2). We opted for using the FEROS spectrograph (Kaufer et al. 1999), at the 1.52-m telescope, because:

(1) its large spectral coverage allowed the observer to record simultaneously fundamental lines like the H and K of CaII, suitable for investigating rotationally induced modulations (cf. Section 1);

(2) its high efficiency permitted the acquisition of data on a large sample of stars in one night, and finally,

(3) the radial velocity accuracy of 23 m/s, which was shown during the commissioning period (Kaufer et al. 1999) was at a level adequate for the study of giant variability. We also were confident that the FEROS performances could be improved with a targeted strategy and by upgrading the software and the data analysis.

As part of the ESO time on FEROS we obtained in Periods 64 and 65 a total of 5 full and 6 half nights. An additional 12 half nights were allocated as part of the Brazilian time. Early in our programme, after surveying only 27 stars, we had indications that 80% of our target objects showed variations on the time-scales of a few to hundreds of days. This is consistent with the results of earlier, more limited surveys. Variability in G and K giants may indeed be ubiquitous. In Period 65 we could enlarge the sample which now consists of 63 stars covering a large fraction of the upper HR-diagram. The H-R diagram of the observed stars is shown in Figure 2. From this figure it is clear that the sample spans the whole Red Giant Branch as well as the region of the “clump”. The targets were selected on the basis of accurate HIPPARCOS parallaxes in order to ensure a reliable determination of the basic stellar parameters. The high resolution and high S/N ratio of the FEROS spectra will also allow the spectroscopic determination of effective temperatures, gravities and metallicities. With such an extensive data base it will be possible to investigate the dependence of the radial velocity variability on a wide variety of stellar parameters, including the estimated stellar mass and evolutionary status. This is important for calibrating theoretical evolutionary tracks.

While the scientific results of this survey will require many more observations and their full analyses, in this *Messenger* contribution we mostly concentrate on the data-analysis process in order to demonstrate the capabilities of FEROS.

We believe that our results (8.3-m/sec RV accuracy) are so encouraging that they open a new possible use of the FEROS spectrograph as a planet hunter with an RV accuracy ap-

proaching that of other, state-of-art techniques. We will outline our methodology in the data reduction and provide some tips for the potential users.

## 3. Pushing the FEROS Capabilities

Although not conceived explicitly for very accurate radial-velocity measurements (original requirements were set to an accuracy of 50 m/sec), FEROS has been equipped with a double-fibre system, where the second fibre can be used either for recording the sky or for obtaining simultaneous calibration spectra to the science exposure (see Fig. 3, which shows a part of a frame containing the stellar and simultaneous calibration spectra), following the technique pioneered by the Geneva group with ELODIE and CORALIE (Baranne et al. 1996).

By using a simple cross-correlation (Kaufer et al., 1999, see also FEROS user manual) in the commissioning time, it was shown that FEROS could obtain a radial-velocity accuracy of 23 m/sec by observing every night the G star HD10700 (Tau Cet), an object which has been demonstrated to have a radial velocity constant to better than 5 m/s (Butler et al. 1996).

A “constant” star is extremely useful to estimate the long-term accuracy of FEROS and to provide a standard for optimising the radial velocity analysis. Demonstrating a lack of RV variability in a standard star would make us more confident of our results on variable stars in the programme. For this pur-

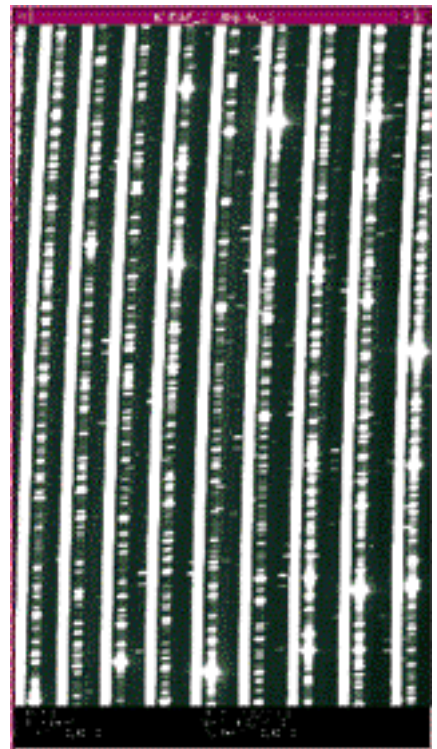


Figure 3: Portion of a FEROS frame showing the stellar spectrum and the simultaneous calibration Th-A spectrum.

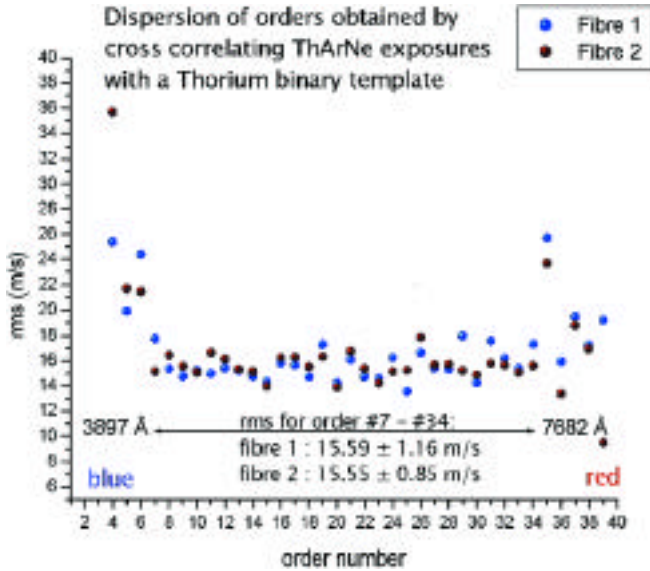


Figure 4: Determining the orders to be used for computing the precise radial velocity by cross-correlating Th-A spectra from each fibre with the numerical Thorium template.

pose one or two observations of HD10700 were acquired on each night of our programme.

The analysis of the data is in principle straightforward and consists of the following steps:

(1) Wavelength calibration with 2-fibre (“double”) Th-A exposures. Wavelength solutions are constructed using two 25-second exposures of a Th-A hollow cathode lamp in the “object-sky” mode.

(2) Spectral extraction. The extraction procedure has been implemented in the FEROS reduction pipeline integrated in MIDAS version 98 and 99. Several extraction options are available.

(3) Removing the blaze function. This is done by the FEROS package using Flat Fields (i.e. observations of spectrophotometric standards are not required).

(4) Rebinning of the spectra. The spectra are rebinned order by order rather than using the merged spectrum normally produced by the FEROS on-line reduction pipeline.

(5) Order-by-order cross-correlation of the object spectrum with an appropriate stellar numerical mask.

(6) Order-by-order cross-correlation of the calibration spectrum, which is called the “simultaneous Th-A”, with a numerical template. This template is based on a Th-A atlas that has been modified for our own purpose. The modification takes into consideration the spectrograph resolution and line blending, and is therefore instrument-dependent. The whole Th-A spectrum needs to be subdivided in small portions and each portion of the mask is “cleaned” by analysing the correspondent cross-correlation function.

(7) Radial-velocity calculation by subtracting the cross-correlations of the stellar and calibration spectra and ap-

plying some additional zero-point offset corrections.

Moreover, it is important to have the wavelength rebinning done with a step fine enough to avoid any spurious effects. In our case we use a rebinning step of 0.03 Angstrom. After spectra rebinning, cross-correlations with the appropriate numerical masks (steps 5 and 6) are performed by using the TACOS package, developed by the Geneva observatory.

The required numerical masks have been prepared for FEROS by modifying existing masks kindly provided by the Geneva observatory. The stellar mask is based on a K giant spectrum.

In order to evaluate the FEROS intrinsic capabilities, the La Silla 2.2-m team kindly acquired a series of 10 Th-A spectra with the calibration lamp illuminating the two fibres; these spectra were cross-correlated with the Th-A template mask, to investigate the behaviour of the instrument. We need in fact to evaluate within which limits the separation between the two fibres can be considered constant.

A total of 50 Th-A exposures were acquired for this purpose. The result is shown in Figure 5, where the shift: fibre 1-fibre 2 cross-correlation is shown. The results are extremely encouraging and indicate that the two fibres “follow” each other with an accuracy of

better than 2.5 m/sec. This indicates that the spectrograph can deliver excellent RV performances.

In order to determine the optimal spectral range to be used for computing the radial velocity, we checked the dispersion of each order by cross-correlating the double Th-A (fibre 1 and fibre 2) with the Th-A mask prepared for FEROS and the results are shown in Figure 4. Orders 7 to 34 may be suitable for computing of accurate radial velocities (note that the order numbering used in this work is the extraction order number, not the real echelle order number).

We mention that since the binary template for the stars was originally prepared for the ELODIE spectrograph, it covers only the wavelength range from 3600–6997 Angstrom corresponding to the FEROS orders 7 to 31. A more extended mask covering also orders 31–34 will be prepared, and the addition of this signal may improve the final RV accuracy.

We mention that since the binary template for the stars was originally prepared for the ELODIE spectrograph, it covers only the wavelength range from 3600–6997 Angstrom corresponding to the FEROS orders 7 to 31. A more extended mask covering also orders 31–34 will be prepared, and the addition of this signal may improve the final RV accuracy.

#### 4. Computing the Radial Velocity

To get the radial velocity variations, we compute the difference of the cross-correlations of the two fibres order by order. In addition, for each order a zero-point offset is finally applied, considering the velocity difference between the two fibres in the double Th-A exposures. The results found so far are shown in the Figure 6 where the radial-velocity measurements of Tau Cet are shown: in 245 days spanning our observations, the rms around the constant radial velocity is 8.3 m/sec.

This puts FEROS as a full member of the select family of spectrographs capable of obtaining an accuracy below 10 m/s, a regime capable of detecting extra-solar planets.

This is quite remarkable, considering that these performances are more than

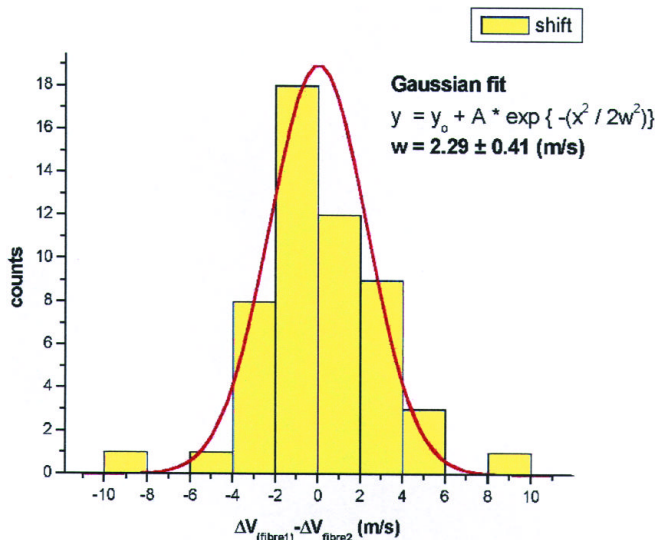


Figure 5: Determining the FEROS calibration stability by checking the shifts between fibre 1 and fibre 2. 50 Th-A exposures have been taken for this purpose; the results indicate an RMS of 2.3 m/sec.

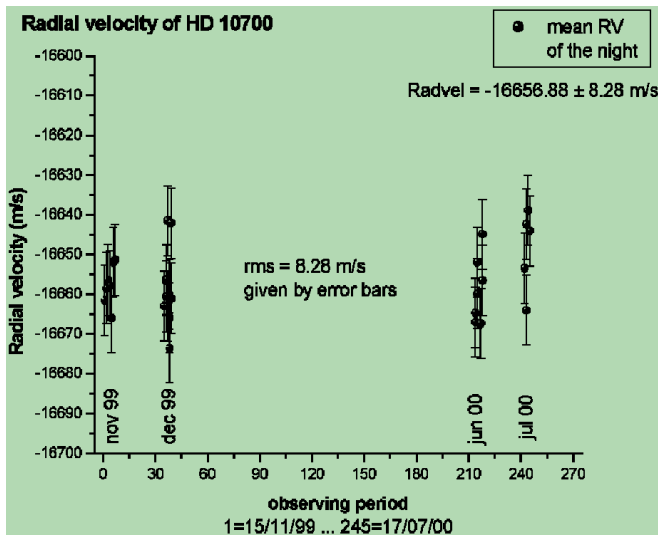


Figure 6: Radial velocity of HD10700 (Tau Ceti) taken for determining the long-term accuracy of FEROS. After monitoring the radial velocity of this constant star for almost one year (245 days), we obtain an rms of 8.28 m/s of constancy.

5 times better than the original specifications of the instrument. But mostly considering that, thanks to its impressive efficiency and large spectral coverage, FEROS is already a quite unique high-resolution spectrograph.

On the technical side, such a good performance is somewhat unexpected since FEROS fibres are not equipped with a light scrambler, and one could imagine that the spectrograph pupil could suffer from small shifts or variable asymmetries in the light distribution. In addition, FEROS is equipped with an image slicer. While this device will help in scrambling the light, and therefore in mitigating the problem above, the light is divided into two parts (half moons), which will have a slightly different wavelength solution. In principle, if the relative illumination of the slices changes slightly from one observation to the next (remember that 8 m/sec corresponds to  $\sim 1/300$  of pixel), this will be enough to introduce additional noise in the precise radial velocity measurements.

So far, in addition to HD10700, another star has been reduced: the K1 III giant HD18322, and the result is very promising: as shown in Figure 7 the peak-to-peak radial-velocity variations are of  $\sim 200$  m/sec and they are consistent with a 40-day period (which is also shown in the same figure). We stress that due to the small number of points the 40-day period we detect may be an alias of another period. More sampling is needed to determine the period accurately.

## 5. Some Tips for Potential Users

The real process, of course, is in practice a bit more complex than described in the previous section, and we would like to give to the potential users

commands “COMPUTE/PREC” and “COMP/BARY” for this purpose, but these will be checked against more accurate methods. This step should be done carefully in order to improve the results. It is also relevant to note that the FEROS pipeline computes the barycentric correction reading the stellar right ascension and declination from the 1.52-m telescope headers and it takes the UT at the beginning of the observations. In our experience, at this accuracy the 1.52-m telescope stellar co-ordinates (contained in the frame FITS headers) may not be accurate enough; also the UT should be computed for the middle of the exposure.

3. The real geographic co-ordinates of the 1.52-m telescope should be used when computing barycentric correction.

We have not developed a full automatic procedure yet, which is supposed to enable computing the radial velocity shortly after the MIDAS pipeline reduction and directly linked to the cross-correlation process using TACOS.

Also, we found that in some observations, one or two of the selected orders depart strongly on the expected solution and they need to be discarded. This operation is at the moment performed manually, and we need to build an algorithm to select the good orders automatically.

of FEROS a number of tips on the handling of the data.

1. When rebinning the wavelength within the FEROS pipeline DRS, if the command “REBIN/FEROS” is used, this will apply the barycentric correction also to the simultaneous Th-A spectrum. This should be corrected with the next MIDAS release.

2. The FEROS spectra are automatically corrected for barycentric correction. We use the MIDAS

We are also conscious that these performances could be improved; there may be effects which we did not take into consideration enough so far; among them we can foresee:

(i) Being interested in giants, our stellar mask spectrum is taken from a K giant template, while Tau Ceti (HD 10700) is a G dwarf. An ad-hoc mask for this star might already improve the results.

(ii) With the help from the Geneva observatory we will try to extend the star template to the red-part regions. This may enable us to gain more information from the spectra.

(iii) FEROS is not equipped with an exposure meter, therefore we can not accurately determine the median time of our observations (in terms of acquired photons); our observations are rather short (a few minutes), but this effect could become relevant in long observations, poor guiding and/or cloudy nights.

(iv) In our first observations we only took two double Th-A exposures every night. Several Th-A observations in the middle of the observing run would be required to monitor any possible shifts during the night and to provide additional calibrations for the offset determining in the radial velocity computation.

## 6. Acknowledgement

We acknowledge the strong support and help by Didier Queloz, Dominique Naef and Francesco Kienzle in sharing their time, experience and the TACOS. We also thank Emanuela Pompei, Rolando Vega and Arturo Torrejon for their assistance during the observing runs. The presence of J.S. at ESO was supported by the ESO DGDF2000 programme.

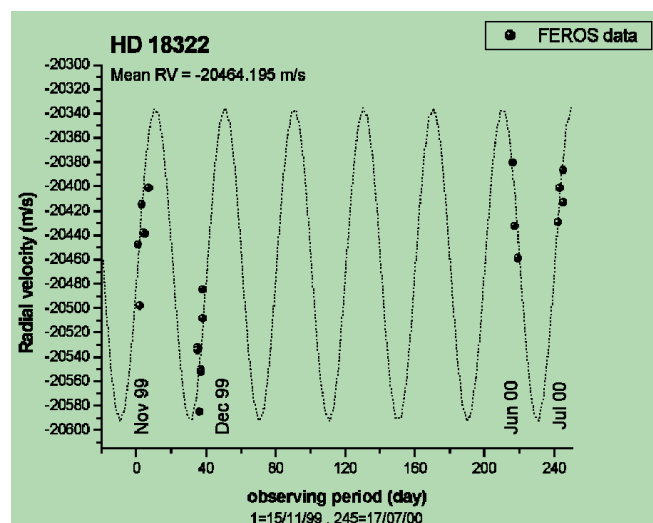


Figure 7: Results of the radial velocity measurements of HD18322. Although there are still many data points missing (no observing runs between December 1999 and June 2000), we are able to show the variability of the star, which is consistent with a periodicity of about 40 days and a peak-to-peak variation of about 200 m/s.

## References

- Baranne, A., et al., 1996, *A&A Suppl Ser* **119**, 1.
- Butler, R.P., et al. 1996, *PASP* **108**, 500.
- Hatzes, A.P. & Cochran, W.D. 1993, *ApJ* **413**, 339.
- Hatzes, A.P. & Cochran, W.D. 1994a, *ApJ* **422**, 366.
- Hatzes, A.P. & Cochran, W.D. 1994b, *ApJ* **432**, 763.
- Hatzes, A.P. & Cochran, W.D. 1998, *MNRAS* **293**, 469.
- Kaufer, A., et al. 1999, *The Messenger* **95**, 8.
- Larson, A. et al. 1993, *PASP* **105**, 825.
- Lambert, D.L. 1987, *ApJS* **65**, 255.
- Merline, W.J. 1996, ASP Conf. Ser. **135**, p. 208.
- Pasquini, L., Pallavicini, R. Pakull, M. 1988, *A&A* **191**, 266.
- Pasquini, L. 1992, *A&A* **266**, 347.
- von der Lühe, O., Solanki, S., Reinheimer, Th. 1996, in IAU Symp. 176, *Stellar Surface Structure* 147–163. Walker, G.A.H., Yang, S., Campbell, B., and Irwin, A.W. 1989, *ApJL* **343**, L21.

# Crowded Field Photometry with the VLT: the Case of the Peculiar Globular Cluster NGC 6712

F. PARESCE<sup>1</sup>, G. DE MARCHI<sup>2</sup>, G. ANDREUZZI<sup>3</sup>, R. BUONANNO<sup>3</sup>, F. FERRARO<sup>4</sup>,  
B. PALTRINIERI<sup>3</sup>, L. PULONE<sup>3</sup>

<sup>1</sup>European Southern Observatory, Garching, Germany

<sup>2</sup>European Space Agency, STScI, Baltimore, USA

<sup>3</sup>Osservatorio Astronomico di Roma, Rome, Italy

<sup>4</sup>Osservatorio Astronomico di Bologna, Bologna, Italy

## 1. Introduction

The Hubble Space Telescope opened up the exciting possibility of carrying out very deep, high-precision stellar photometry in very crowded fields such as those routinely encountered in the core of dense stellar clusters and galaxies. This capability has allowed, for example, the reliable detection of stars all the way down to the bottom of the main sequence (MS) at the centre of nearby globular clusters (GC) six or seven magnitudes below the turn-off (TO) and well into the brown dwarf substellar region of nearby star-forming regions and of resolving the evolved stellar populations in nearby dwarf galaxies. Enormous progress in our understanding of the age, distance, star formation rates, and mass functions of a large sample of stellar populations has been a direct result of the last ten years of HST.

The advent of the VLT with wide-field optical and IR cameras such as FORS and ISAAC present us with a golden opportunity to push further our quest for good quality photometry of faint sources in crowded fields. The potential of very good and stable seeing coupled with the huge collecting area of an 8-m diameter telescope with wide field and broad spectral coverage detectors certainly rivals and even surpasses, in principle, even the exceptional HST capability in this endeavour. In order to test these capabilities in practice, our group proposed to study in depth a particularly interesting example of a crowded stellar environment namely the GC NGC 6712.

We report here the preliminary results of our study of this cluster using FORS1 and UT1 obtained with 12 hours of observations during Period 63. We emphasise those aspects of the

study that best illuminate the performance of this instrument combination for crowded field photometry that might be of interest to anyone contemplating doing this sort of work with the VLT in the future. Results from a preliminary study of this object using the VLT Test Camera during the UT1 Science Verification period were reported in De Marchi et al. (1999).

## 2. VLT Observations of NGC 6712

NGC 6712 (  $\alpha = 18^{\text{h}} 53^{\text{m}} 04.3$ ,  $\delta = -08^{\circ} 42' 21.5''$  ) is a relatively metal poor, small and sparse GC ( $[\text{Fe}/\text{H}] = -1.01$  and concentration ratio  $c = 0.9$ ; Harris 1996) located in the midst of a rich star field at the centre of the Scutum cloud (Sandage 1965), which

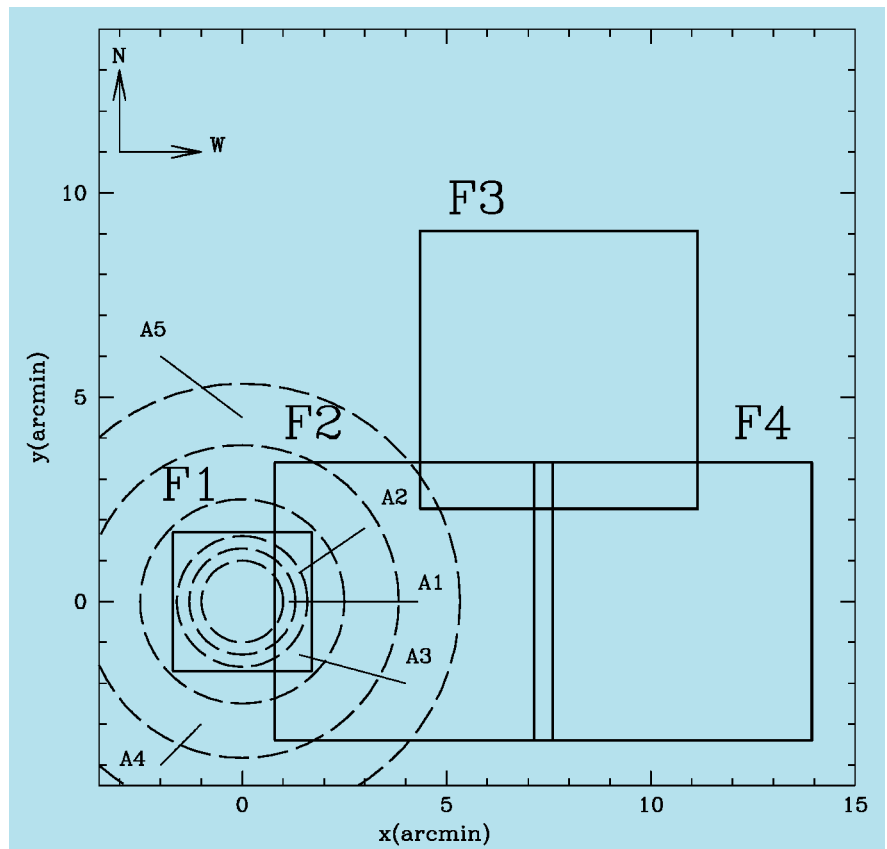


Figure 1: Locations of the four FORS1 fields on NGC 6712. The centre of the cluster is located at the origin of the co-ordinate system.



Figure 2: VLT-FORS1 high-resolution image (180s exposure) of the core of NGC6712 in the R band (field F1). The size of the image is  $3.4 \times 3.4$ . North is up and East to the left.

is one of the highest surface-brightness regions with high space-density gradients of the Milky Way (Karaali 1978). Its Galactic orbit forces it to penetrate deeply into the bulge. With a perigalactic distance smaller than 300 pc, this cluster ventures so frequently and so deeply into the Galactic bulge (Dauphole et al. 1996) that it is likely to have undergone severe tidal shocking during the numerous encounters with both the disk and the bulge during its lifetime. The latest Galactic plane crossing could have happened as late as  $4 \cdot 10^6$  year ago (Cudworth 1988), which is much less than its half-mass relaxation time of 1 Gyr (Harris 1996). It is precisely on this basis that Takahashi & Portegies Zwart (2000) have suggested that NGC 6712 may have lost

99% of its mass during its lifetime. If true, this implies that NGC 6712 was originally one of the most massive clusters in the Galaxy.

There are two peculiarities of this seemingly inconsequential cluster that point to its being now only a pale reflection of its former glory. The first is the presence in the core of the well-known high luminosity X-ray source (X1850-086) with an optical counterpart (Anderson et al. 1993). This is unexpected for such a loose cluster because most clusters with such sources tend to have a much higher central concentration. The second is a clear and continuous drop of its global mass function (MF) with decreasing mass starting already at the TO and continuing down to the observation limit at  $\sim 0.5 M_{\odot}$

(Vesperini & Heggie 1997). For all the other clusters surveyed so far with HST in this mass range, the global MF increases steadily with decreasing mass (Paresce & De Marchi 2000).

NGC 6712, therefore, could hold the key to a better understanding of the observable effects of tidal interactions, and especially to learning more about the mechanisms leading to the dissolution of GC in the Galaxy and about the possible variation of the cluster IMF with time. The specific objectives of our study were twofold: (1) to obtain a more precise LF of the MS below the TO at various distances from the centre, so as to evaluate the possible effects of mass segregation on the derived MF and to sample more of the cluster at or near the tidal radius to see whether or

not one could detect an excess of low-mass stars ejected from the interior and still lightly bound to the cluster; (2) to study the evolved population above the turn-off in greater detail than has been possible heretofore in order to determine more precisely the hot star population characteristics and the cluster age and distance.

For this, we obtained deep images of 5 fields in the V and R bands, four of which are located as shown in Figure 1. The fifth field, used as a control field (field F0), is located 42 N of the cluster centre and was imaged using the standard FORS1 resolution of 0.2 /pixel.

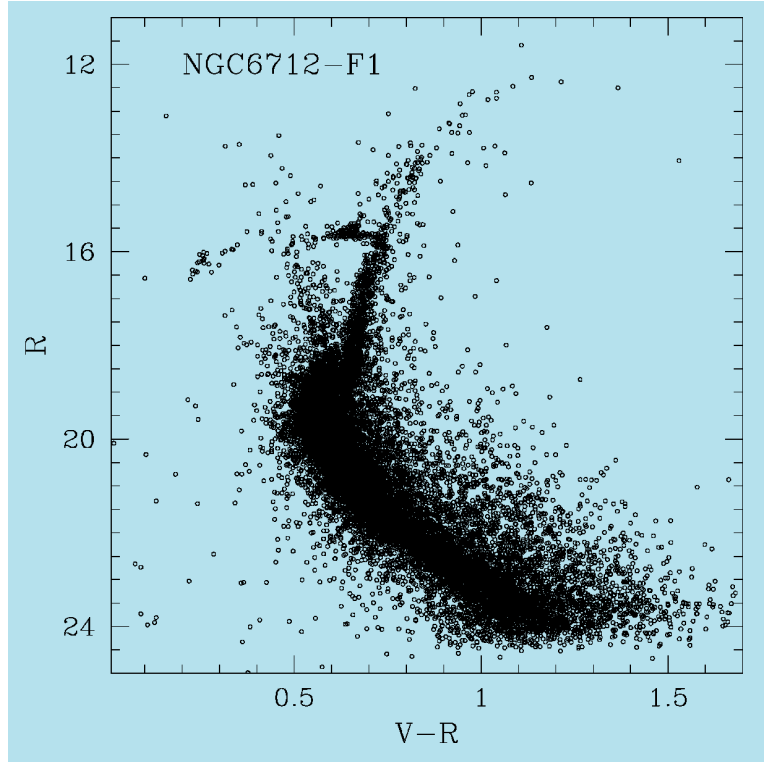
Because the level of crowding varies considerably from the core of the cluster out to its periphery, our observations were carried out according to the following strategy: the fields covering the external regions of the cluster were imaged at standard resolution (SR, plate-scale 0.2 /pixel) with 4 900-s exposures and cover an area of 46.2 arcmin square each ( $6.8 \times 6.8$ ); they are located respectively 5 W (field F2), 8 NW (field F3) and 11 W (field F4) of the centre of the cluster; to improve the photometry in the central regions, where the level of crowding is particularly high, we have covered it with images taken in the high resolution mode of FORS1 (HR, plate-scale 0.1 /pixel) with 4 180-s exposures, with a field  $3.4 \times 3.4$  in size (field F1). To ensure a homogeneous calibration and to transform the co-ordinates into a common local system from the centre of the cluster out to the more external regions, each field has been selected so as to overlap with at least a neighbouring one.

In order to study the evolved part of the CMD above the turn-off where the effects of saturation in the bright stars would otherwise seriously compromise the photometric accuracy, five 10-s B-, V-, R-band exposures, five 120-s U-band exposures were taken for each field. An additional 700-s HO exposure was obtained only in the central field F1. The long exposure (180 s) R-band image of this latter field covering the core of the cluster obtained with 0.3 seeing is shown in Figure 2. This image gives a good idea of the level of crowding encountered in this situation. All the data were taken in good seeing conditions ranging from 0.3 to 0.7 in service mode. Images taken during the best seeing conditions in high resolution mode compare quite favourably with existing archive short exposure images taken with the WFPC2 camera on HST outside the core.

### 3. Data Reduction

Except for a small subset of the R-band images, we have adopted the reduced and calibrated (i.e. bias-subtracted and flat-fielded) data as provided by the standard ESO-VLT pipeline.

Figure 3: Colour-magnitude diagram of the stars in field F1 (core) of NGC 6712



Some of the raw R-band data, however, had not been processed through the automated pipeline, and for them we had to run standard IRAF routines following the same recipe employed in the ESO-VLT pipeline. Subsequent data reduction and analysis was done using standard IRAF photometry routines (*digiphot.daophot*).

Since our goal was to reliably detect the faintest object in these images, for each field and filter we first created a mean frame using all available applicable frames and then ran the standard *digiphot.daofind* routine on the average images so obtained to locate stars. Typical values of the PSF-FWHM are 0.3 and 0.7, respectively at high and low resolution. Although, in principle, we could have also averaged images in different filters, the presence of bad columns in the R-band frames (usually due to heavily saturated pixels and spikes of the bright stars) suggested not to follow this approach. With a detection threshold set in the V and R bands typically at 3–5 above the local average background level, we obtained two independent co-ordinate lists for each field (one per filter), which we then fed to the PSF-fitting routine *allstar* to measure the instrumental magnitude of each object in each filter. We found that a Moffat function gave the best representation of the shape of the PSF, both at high and low resolution.

The positions of the identified objects in each mean R and V-band image were matched to one another, so as to obtain a final catalogue containing only the positions and magnitudes of the stars common to both filters.

Objects lying in overlapping regions between two adjacent fields were used

to determine the transformations between instrumental magnitudes and to translate *local* frame co-ordinates to a *common* co-ordinate system, with origin at the cluster centre. Typically, about one hundred stars in each overlapping region were used to derive such transformations. Only linear transformations were used to match star measurements, with all magnitudes being referred to those of the high resolution field (F1). For stars in the overlapping region, multiple magnitude measurements were averaged using appropriate weights (which take into account the photometric quality of each field). At the end of this procedure, a homogeneous set of instrumental magnitudes, colour and positions (referred to field F1) were obtained for a total of 106,092 stars, in F1, F2, F3 and F4.

Instrumental (F1) magnitudes were finally transformed to the standard Johnson system, using the stars in common with the bright portion of the CMD which has been properly calibrated using ten photometric standard stars in selected areas PG1528, PG2213, PG2331 (Landolt 1992). Since we have repeated exposures in each filter, the internal accuracy of our photometry has been estimated from the rms frame-to-frame scatter of the instrumental magnitudes. The resulting mean photometric errors are very small ( $< 0.05$ ) over the whole bright magnitude range ( $R = 13$  to 21) covered by our short exposure observations in all the filters while they vary from 0.05 to 0.1 mag in the deep exposure observations of the MS below the TO. Figure 3 shows the total CMD of the central region of NGC 6712 (field F1). The figure is obtained by merging the deep (180-s long expo-

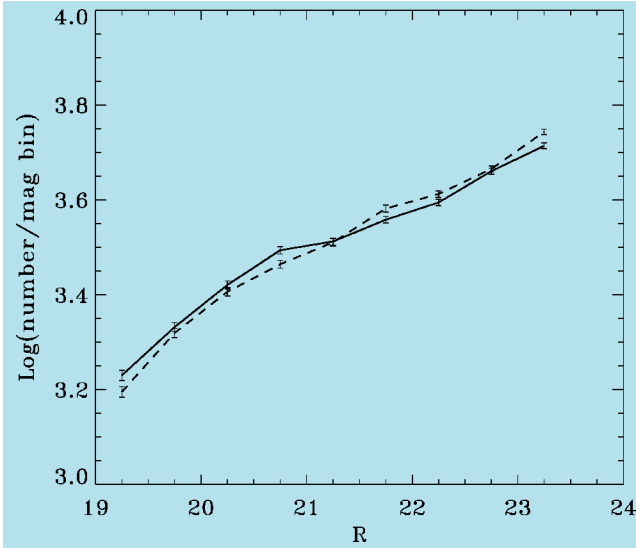


Figure 4: Luminosity functions measured in fields F0 (dashed line) and F3 (solid line).

sure) and the bright (10-s exposure) data covering the core of the cluster.

Especially for the deep images probing the faint end of the cluster MS, correction for incompleteness clearly becomes of critical importance. The correction depends on the level of crowding in the observed fields and, therefore, on their location with respect to the cluster centre. In particular, an insufficient or inappropriate correction for crowding will result in the distortion of the stellar LF with a preferential loss of fainter stars and a relative increase of bright and spurious objects. In our case, crowding is not the only source of incompleteness: the distribution in luminosity of the stars is also modified by the large number of hot pixels and bad columns affecting the original images.

To correct our photometry for incompleteness, we ran artificial star tests on both sets of frames (V and R) independently, so as to be able to estimate the overall completeness of our final CMD. First, we applied the artificial star test to the mean R-band images: artificial stars in each given 0.5 magnitude bin were added randomly to the frames, making sure not to exceed a few per cent (10%) of the total number of stars actually present in that bin so as to avoid a significant enhancement of image crowding. We then added an equal number of stars at the same positions in the V-band frames and with a magnitude such that they would fall on the cluster MS. It should be noted that we made the assumption that all artificial stars were to lie on the MS since our intent was to verify the photometric completeness of MS stars. This procedure was repeated for all the bins of each field's CMD in both filters. To obtain a robust result, we simulated more than 200,000 stars in 250 artificial images for each field.

All pairs of V and R frames obtained in this way were then subjected to

the same analysis used for the original frames, with the result being a catalogue of matching objects, each characterised by a position and a pair of V and R-band magnitudes. Each of these 250 catalogues (one per artificial pair of images) was compared with the catalogue of input artificial stars: an artificial star was considered detected only when its final position and magnitudes were found to coincide with the input catalogue within  $x, y$  1.5 pixel,  $\text{mag}$  0.3. This approach allowed us to build a map showing how photometric incompleteness varies with position in our frames. Completeness reaches the 50% level at  $V \approx R \approx 23$  at  $r = 70$  from the core, for example. Inside this point, the level of crowding and the large ensuing incompleteness would have resulted in a poor determination of the LF. Moreover, we did not include a region between  $r = 116$  and 150 because the level of crowding there is too high for the low resolution of the FORS1 camera at 0.2 /pixel and a standard seeing quality of  $\text{FWHM} \approx 0.6$ .

Finally, inspection of the CMD presented in Figure 3 shows that the field contamination is particularly severe in the region of NGC 6712. A reliable determination of the physical characteristics and especially of the LF of NGC 6712 requires that we account for the

contamination caused by field stars. We have dealt with this correction in a statistical way by using the comparison field FO, for which we have produced a CMD and assessed photometric incompleteness precisely as we did for all other fields. When it comes to measuring the LF – our final goal – we subtract from the stars found in a given magnitude on the cluster CMD the objects detected in the same magnitude bin in an area of equal size on the FO field. Clearly, both numbers are corrected for their respective photometric incompleteness before doing the subtraction.

#### 4. Data Analysis and Interpretation

By applying the statistical field star subtraction described above, we discovered that stars located in fields F3 and F4 can be considered as belonging to the field because all the objects in the CMD of these fields are statistically compatible with being field stars. We show this in Figure 4, where we plot the R-band LF, corrected for incompleteness, as measured in fields F3 and FO (respectively solid and dashed line). The absence of any significant trend or systematic departures of one function with respect to the other (within 2) confirms that there are no residual cluster stars at distances greater than  $\sim 5$  from the cluster centre.

A plot of the radial density profile determined from our sample of stars brighter than  $V \approx 20$  shown in Figure 5 confirms this result. The thick dashed line marks a typical King-type profile with core radius  $r_c = 55$  and tidal radius  $r_t = 5.1$ , superposed to a plateau of field stars. A tidal radius of  $\sim 5$  is fully consistent with our finding of a statistically null cluster in Fields F3 and F4 and implies that it will always be very difficult to detect an excess of cluster

low mass stars at or beyond the tidal radius ejected from the interior and still lightly bound to the cluster due to the very severe field contamination against which these faint stars have to be detected.

As a result of these findings, we considered all stars lying in F3 and F4 as field stars, thus improving the statistical sample of the field, and redefined the decontamination procedure above using as comparison field the whole catalogue

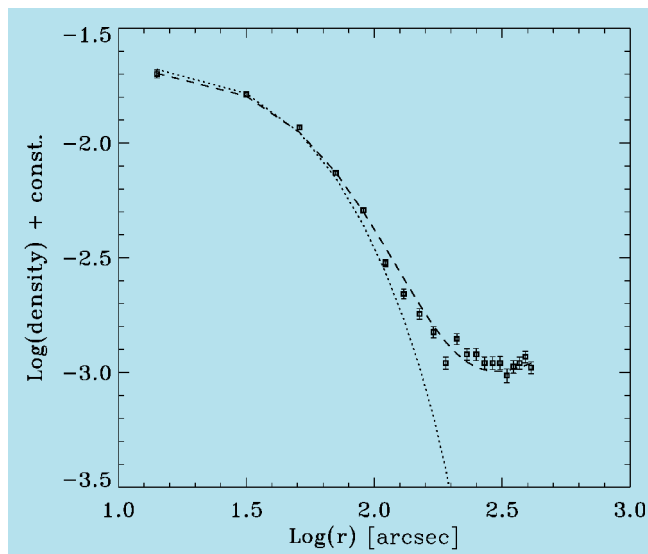


Figure 5: Surface density profile of  $\sim 0.75 M_{\odot}$  stars. The thin line shows a King-type profile with  $r_c = 60''$  and  $r_t = 300''$ , whereas the thick dashed line shows the superposition of the latter on a plateau of field stars of uniform surface density.

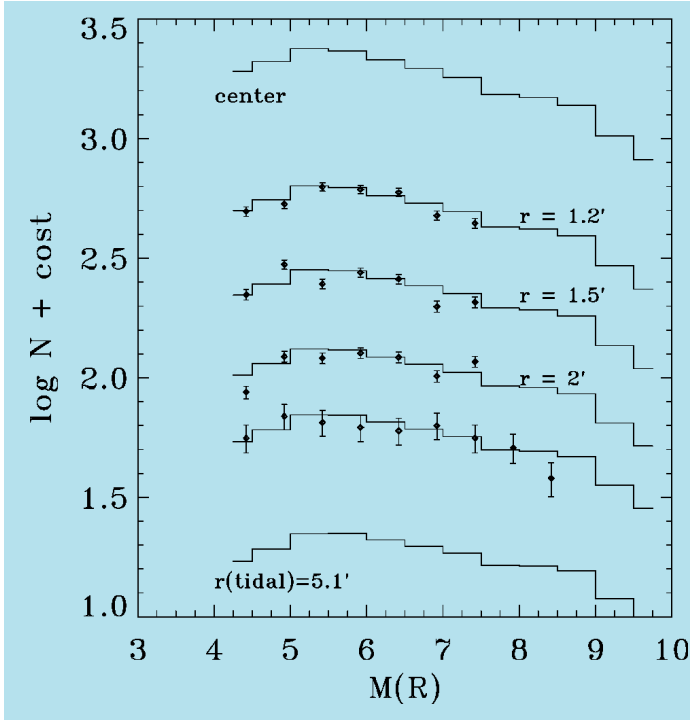


Figure 6: Theoretical LF as a function of distance as predicted by the multi-mass Michie-King model described in the text. Boxes represent the observed LF in annuli A1 – A3, and in the Test Camera field.

for F3, F4 and F0 ( $r \approx 5$ ). This result also strongly implies that the field around NGC 6712 is relatively uniform at our required level of accuracy thereby fully justifying our confidence that the field contamination at the position of the cluster is properly accounted for. We, therefore, regarded only the F1 and F2 fields as containing cluster stars. Because of the richness of our sample, we investigated the variation of the LF as a function of distance on a scale smaller than the typical size of a frame.

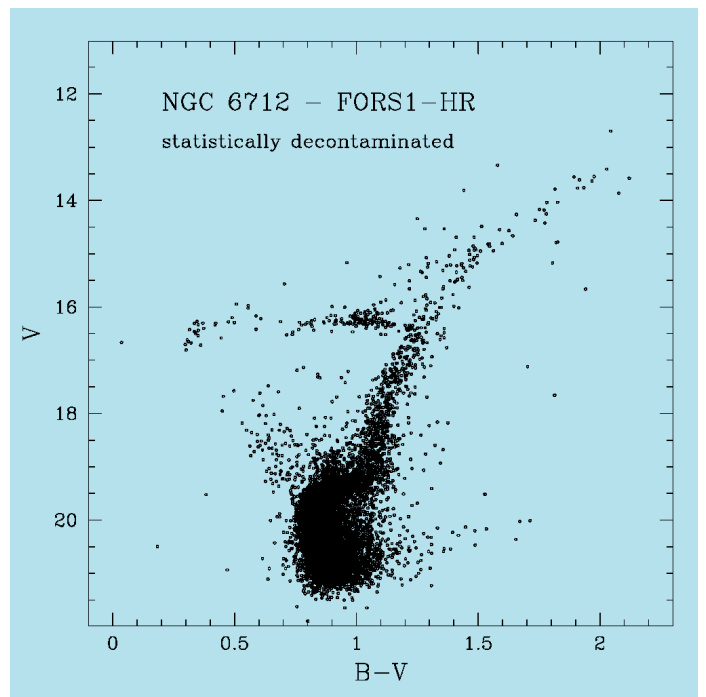
The LF determined in annuli centred at 1.2, 1.5, 2 and 2.25 from the centre and of average thickness  $\sim 0.1$  are shown in Figure 6 together with the theoretical expectations of a Michie-King multi-mass model at these distances and, for comparison, at the centre and at the tidal radius. The best fit is obtained with a power-law global MF with an index of  $\approx 0.9$ . The key result here, then, is that the global MF of NGC 6712 is indeed an inverted function, i.e. one that decreases with decreasing mass below  $\sim 0.8 M_{\odot}$ . Although all clusters whose LF has been studied in the core show an inverted local MF there (as a result of mass segregation: see e.g. Paresce, De Marchi & Jędrzejewski 1995; King, Sosin & Cool 1995; De Marchi & Paresce 1996), NGC 6712 is the only known cluster so far to feature an inverted MF on a global scale.

The field star decontamination procedure was also applied to each of the CMDs resulting from the brief exposures in the central Field 1. Figure 7 shows the  $(V, B - V)$  CMD statistically decontaminated for this field. Here the result is quite good as the statistical decontamination successfully removes

most of the field stars and the cluster sequences appear clearly well defined. In particular, the large population of blue straggler stars (BSS) is clearly visible together with a few blue objects present in the very central region of NGC 6712 and lying outside the main loci defined by the cluster stars. These include three faint and one bright blue stars. The peculiar blue colour of these stars is confirmed by the  $(U, U - B)$  CMD (Figure 8) where they are plotted as filled triangles.

The bright star (#9620) located roughly at the HB level but significantly bluer than the bluest HB stars is the most UV-bright object in the field. Its

Figure 7: The  $V, B - V$  CMD for stars observed in the high-resolution field after the statistical decontamination from field stars.



position in the CMD closely resembles that of the UV-bright post-AGB star found in M3 (vZ1128, see Buonanno et al. 1994). Such objects are indeed very rare in GC: only a few post-AGB stars have been found in GC due to their short evolutionary lifetime of  $\sim 10^5$  yr (only 0.5 Post-AGB stars are expected to be found in a typical  $\sim 10^5 L_{\odot}$  cluster). In order to check whether the position of this star is consistent with the hypothesis that it is a post-AGB star, we performed a qualitative comparison with theoretical models. A  $\sim 12.5$  Gyr isochrone with appropriate metallicity ( $Z = 0.004$ ) from Bertelli et al. 1994 has been over-plotted in the CMD of Figure 8 as a reference. It has been shifted to fit the main loci in order to show the location of the post-AGB track and the subsequent cooling sequence. As can be seen, the position of the UV-bright star in the CMD nicely agrees with that predicted by the theoretical cooling track.

Two out of the three faint UV-excess stars (namely #10261 and #9774) are located within the cluster core. Star #9774 is star S identified by Anderson et al. (1993) as the optical counterpart to the known luminous low-mass X-ray binary (LMXB). Its position is only  $\sim 1'$  away from the X-ray source, in agreement with Anderson et al. (1993). Our observations confirm that it is the bluest object within  $\sim 15'$  of the X-ray source's nominal position, and for this reason it remains the best candidate to be the optical counterpart to the LMXB. Star #10261 is the brightest object among the three faint UV sources in Figure 8. Moreover, it is the only object showing a clearcut H $\alpha$  emission in the core of NGC 6712. The other two UV-excess stars have normal colour  $((H\alpha - R) > -0.1)$ , and thus they are fully compatible,

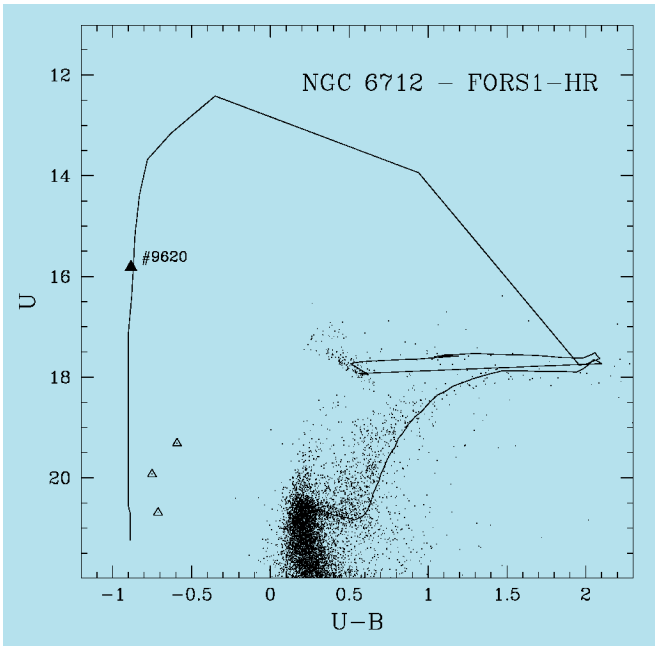


Figure 8:  $U, U - B$  CMD of NGC 6712 from FORS1-high-resolution images. The bright blue object #9620 is plotted as a large filled triangle. The three faint UV stars are plotted as open triangles. An isochrone from Bertelli et al. (1994) is also plotted for reference.

within the errors, with the  $(H\alpha - R)$  colour of *normal* cluster MS stars.

UV-excess and H emission together with X-ray emission are characteristic signatures of interacting binaries (IB). In fact, when a binary system contains a compact object (like a neutron star or a white dwarf) and a close enough secondary, mass transfer can take place: the streaming gas, its impact zone on the compact object and the presence of an accretion disk can give such systems observational signatures which make them stand out above ordinary cluster stars. These signatures include X-ray emission, significant radiation in the ultraviolet, H emission lines, X-ray emission, etc. In particular, Cool et al. (1995) have shown the efficiency of the H emission technique in pinpointing candidate IB among the *normal* GC population. For this reason, we can consider star #10261 as a very promising IB. Interestingly enough, the new IB discovered by us in the core of NGC 6712 is located only a few arcsec away from star #9774, the optical counterpart to the LMXB.

Thus NGC 6712 turns out to harbour in its core two unrelated IB systems a few arcsec apart. This fact, coupled with a large BSS population and an inverted mass function, indicates an unusual level of dynamical activity for a GC of such a moderate density, suggesting again that, at some early epoch, NGC 6712 was much more massive and concentrated than now, and its interaction with the Galaxy is driving it towards dissolution.

This result demonstrates the huge potential of the VLT for exploring the IB population in moderate-density GC. For

this reason, we intend to further exploit the sensitivity of FORS1 at UT1 to search for H- and UV-excess from IB in a set of GC with moderate central density. The project as a whole will finally shed light on the formation and evolution of IB (and their progeny) in GC.

## 5. Lessons Learned

Several lessons were learned from this exercise concerning the use of the VLT for crowded-field photometry. Some of them were already al-

luded to in the text but we summarise them here for clarity. The photometric accuracy and completeness level depend crucially on several factors: level of crowding especially of the bright stars, pixel size and seeing. Obviously, a delicate balance has to be found between these parameters which determines the exposure time to limit the effect of saturation and the ultimate limiting magnitude reached in each filter. In general, we found that:

1. because of the high density of bright objects, only very short exposures taken with the high-resolution (HR) mode of FORS1 and seeing better than 0.3 yields acceptable results in the core of a GC with more than  $\sim 1$  star/arcsec<sup>2</sup>. Consequently, only the evolved part of the CMD of the core of a cluster can be studied with the FORS1+UT combination. For deeper images in the core, HST and, possibly, the CONICA+NAOS combination for small fields would be preferred.

2. The FORS1+UT combination and seeing better than 0.5 (routinely obtained at Paranal) is the ideal combination to search for relatively faint objects ( $U > 20$ ) like the IB in the central region of moderate-density GC ( $\log \rho < 3$ ) with large core radius ( $r_c > 1$ ). Our observations show that the VLT can be used as a complementary instrument to HST in efficiently searching for peculiar objects in the relatively large cores of moderate density clusters. The HST/WFPC2 combination due to its peculiar shape and small field of view is not well adapted to image clusters with large core radii.

3. Outside the core beyond about twice the half mass radius where crowding is still high but less of an is-

sue, the Standard Resolution (SR) mode of FORS1 is useful only if the seeing is very good ( $< 0.5$ ) and exposures are kept short enough to prevent severe saturation of the brightest red giants (about 200 s for NGC 6712 in the *R* band). If this is not the case, the high-resolution (HR) mode yields the best results even for moderate seeing ( $< 0.8$ ).

4. In any kind of crowded field, if the seeing is good ( $< 0.6$ ), the SR mode should be avoided if field size is not an issue. The SR mode is really useful only for sparsely crowded fields like those in an open cluster or in the periphery of a GC.

5. Registering dithered images is very useful in correcting for hot pixels.

6. The data-quality flag that is activated at the level of 3% saturated pixels should be deactivated to allow the image to pass through the pipeline processing so as not to waste time re-analysing the image afterwards (the pipeline software is not available to users).

Notwithstanding these difficulties, our observations of NGC 6712 have clearly shown that the VLT can be quite competitive with HST even in the case of crowded fields provided the proper combination of camera resolution, seeing and exposure time is adopted. In this case, the large collecting area of the VLT allows good photometric accuracy associated with more efficient and flexible scheduling than possible with HST.

## References

- Anderson, S., Margon, B., Deutsch, E., Downes, R. 1993, *AJ* **106**, 1049.
- Bertelli, G., Bressan, A., Chiosi, C., Fagotto, F., Nasi, E. 1994, *A&AS*, **106**, 275.
- Buonanno, R., Corsi, C., Buzzoni, A., Cacciari, C., Ferraro, F., Fusi Pecci, F. 1994, *A&A*, **290**, 69.
- Cool, A., Grindlay, J., Cohn, H., Lugger, P., Slavin, S. 1995, *ApJ*, **439**, 695.
- Cudworth, K.M. 1988, *AJ* **96**, 105.
- Dauphole, B., Geffret, M., Colin, J., Ducourant, C., Odenkirchen, M., Tucholke, H. 1996, *A&A*, **313**, 119.
- De Marchi, G., Leibundgut, B., Paresce, F., Pulone, L. 1999, *AA* **343**, L9.
- De Marchi, G., Paresce, F. 1996, *ApJ*, **467**, 658.
- Harris W. 1996, *AJ*, **112**, 1487.
- Karaali, S. 1979, *AAS*, **35**, 241.
- King, I.R., Sosin, C., & Cool, A. 1995, *ApJ*, **452**, L33.
- Landolt, A. 1992, *AJ*, **104**, 372.
- Paresce, F., De Marchi G. 2000, *ApJ*, **543**, 870.
- Paresce, F., De Marchi G., Jedrzejewski, R. 1995, *ApJ*, **442**, L57.
- Sandage, A., Smith, L.L. 1966, *ApJ* **144**, 886.
- Takahashi, K., Portegies Zwart, S. 2000, *ApJ*, **535**, 759.
- Vesperini, E., Heggie, D. 1997 *MNRAS* **289**, 898.

# Revealing High-Redshift Galaxies: Results from a New Damped Lyman- $\alpha$ System Survey

S.L. ELLISON<sup>1</sup>, L. YAN<sup>2</sup>, I.M. HOOK<sup>3</sup>, M. PETTINI<sup>4</sup>, P. SHAVER<sup>5</sup>, J.V. WALL<sup>6</sup>

<sup>1</sup>European Southern Observatory, Santiago, Chile

<sup>2</sup>SIRTF Science Center, Pasadena, California, USA; <sup>3</sup>Royal Observatory Edinburgh, UK

<sup>4</sup>Institute of Astronomy, Cambridge, UK; <sup>5</sup>European Southern Observatory, Garching, Germany

<sup>6</sup>Dept. of Astrophysics, University of Oxford, UK

## 1. Probing High-Redshift Galaxies with Quasar Absorption Lines

Using quasar absorption lines as a tool to probe matter in the line of sight towards high-redshift quasars has proved to be a powerful technique for studying both galaxies and the intergalactic medium (IGM) alike. High-resolution echelle spectrographs such as UVES on the VLT can now deliver exquisite data which probe the structure and chemical enrichment of the high-redshift universe with unparalleled accuracy. At somewhat lower resolution, instruments such as FORS can provide an efficient means with which to identify the high column density systems that are associated with distant galaxies. Within the menagerie of systems that make up the quasar absorption line 'zoo', Damped Lyman Alpha systems (DLAs) have the highest column densities and are traditionally defined as systems with neutral hydrogen column densities  $N(\text{H I}) \geq 2 \times 10^{20}$  atoms  $\text{cm}^{-2}$ . Although DLAs are thought to be the progenitors of present-day galaxies, the precise nature of these absorbers at high redshift is still unclear. At low redshift, however, there is mounting evidence that DLAs are likely to represent a mixed morphological bag (Le Brun et al 1997), including a significant population of LSBs (Bowen et al. 2000).

The power law distribution of H I column densities that extends from the low  $N(\text{H I})$  Ly forest clouds that constitute the IGM up to DLAs implies that these high  $z$  galaxies seen in absorption are relatively rare. Indeed, it has taken a considerable investment over many years to establish the current database of known DLAs (e.g. Wolfe et al. 1986; Lanzetta et al. 1991; Lanzetta, Wolfe and Turnshek 1995). However, one of the important consequences of this power law distribution,  $f(N) \sim N^{-1.5}$ , is that although Ly forest clouds are far more numerous, DLAs contain the bulk of the H I gas by mass. A measure often used to quantify the amount of neutral gas in DLAs is  $\tau_{\text{DLA}}$ , basically defined as the mass of H I expressed as a fraction of the closure density of the universe. Since this quantity does not depend on the geometry or covering factor of the absorbers, it

represents an unbiased census of the neutral gas in the universe. Many of the early DLA surveys have measured the redshift evolution of  $\tau_{\text{DLA}}$  and found that it decreases steadily from  $z \sim 3$  to  $z < 1$  (Lanzetta et al. 1991; Lanzetta, Wolfe and Turnshek 1995; Wolfe et al. 1995). Extending this work to higher redshifts, Storrie-Lombardi, McMahon and Irwin (1996) found evidence for a turnover in  $\tau_{\text{DLA}}$  beyond a  $z \sim 3$  and also noted that there is an agreement between the lowest  $\tau_{\text{DLA}}$  point and the measurement by Rao and Briggs (1993) of the local H I mass density inferred from 21-cm measurements (which is dominated by spirals). In addition, it has been pointed out (e.g. Lanzetta et al. 1999) that the mass of H I in DLAs at  $z \sim 3$  is approximately equal to that of luminous matter observed at the present time, i.e.  $\tau_{\text{DLA}}(z \sim 3) \sim \tau_{\text{stars}}(z = 0)$ . Together, these lines of evidence led to the interpretation that DLAs were the basic galactic building blocks assembling the major gas reservoirs for star formation at high redshift.

This rather simple picture has been queried recently by work which has extended the search for DLAs to lower redshifts. Using the HST, Rao and Turnshek (2000) have found evidence that  $\tau_{\text{DLA}}$  remains approximately constant from  $0.5 < z_{\text{abs}} < 3.5$ , evidence that the situation is probably more complex than once thought. However, it is important to realise that the interpretation of this work is pivotal upon the assumption that DLA surveys afford a fair representation of H I absorption systems over a range of redshifts. Our view of the universe could be severely blinkered if previous samples were shown to be biased due to a selection effect that preferentially identifies a particular breed of absorber.

One factor that could cause such a bias is the presence of dust in the intervening galaxy population, which would cause dimming of the background QSOs. Since almost all known DLAs at this time have been identified from optically-selected samples of quasars, they are susceptible to such a dust bias. It has been shown by Fall and Pei (1993) that, based on the dust-to-gas ratios inferred by reddening of background QSOs, up to 70% of bright quasars at  $z \sim 3$  could be miss-

ing from current samples. Moreover, Pei and Fall (1995) have shown that dust is *required* in order for the models to reproduce many of the observed properties of DLAs, such as their mean metallicity. The presence of dust in metal-rich systems could also explain the paucity of DLAs with high Zn abundances (Pettini et al. 1999) and the apparent anti-correlation between metallicity and  $N(\text{H I})$  (Prantzos and Boissier 2000).

## 2. A New DLA Survey Sample – Seeing Through the Dust

The strategy of this new survey for DLAs, which will indicate whether previous work has suffered from a dust bias, is to search for DLAs in a complete sample of *radio-selected* quasars. All of these targets will be followed up with optical spectroscopy, regardless of their optical magnitudes.

The survey described here is based on a complete sample of flat-spectrum radio sources from the Parkes Catalogue with flux densities at 2.7 GHz (11 cm)  $> 0.25$  Jy (Shaver et al. 1996). The sample consists of all flat-spectrum ( $> -0.4$ , measured at 2.7 and 5.0 GHz) sources with declinations between  $+2.5^\circ$  and  $-80^\circ$ , excluding low galactic latitudes ( $|b| < 10^\circ$ ) and regions around the Magellanic Clouds. Accurate radio source positions for these 878 sources were taken from the Parkes Catalogue where available and a combination of VLA and Australia Telescope measurements otherwise. Source identification and B-band magnitudes were determined by cross-correlation with images obtained from either the COSMOS Southern Sky Catalogue or taken at the ESO 3.6-m telescope at La Silla. Low-resolution spectra (FWHM = 12–14 Å) were obtained for the 442 stellar identifications (QSOs and BL Lacs) with the EFOSC on the ESO 3.6-m to determine redshifts.

For this survey, we have selected the 66 QSOs with emission redshifts  $z_{\text{em}} > 2.2$ . Optical spectroscopy is used to identify DLAs with  $1.8 < z_{\text{abs}} < z_{\text{em}}$  in all of these targets, the faintest of which has a  $B = 24.0$ . Our strategy has been to divide the sample into a 4-m sample ( $B < 20$ ) and an 8-m sample ( $B > 20$ ). The former have been observed with

the ESO 3.6-m on La Silla at a typical resolution of  $7 \text{ \AA}$  FWHM and at the AAT with a typical resolution of  $3 \text{ \AA}$  FWHM (see Ellison 2000 for more details), whilst the latter will be observed with FORS1 on the VLT.

### 3. Preliminary Results

Observations for the 4-m sample have now been completed and resulted in the identification of 10 DLAs towards 48 QSOs. Figure 1 shows an example of a DLA found towards one of our targets (left panel) and the DSS finding chart for the QSO with overlaid radio contours (right panel). The remaining 18 targets which constitute the 8-m sample will be observed this semester (Period 66) with FORS1 on the VLT. Clearly, these faint targets represent the important sight lines which will determine whether previous magnitude limited surveys suffer from a dust bias.

With the termination of 4-m observations, the survey is currently complete down to  $B = 20$  and therefore does not represent a major improvement over previous samples. In fact, somewhat encouragingly, we determine that  $\Omega_{DLA}$  for our 4-m sample is consistent with previous estimates from surveys with similar magnitude limits,  $\Omega_{DLA} h_{100} = 1.8 \times 10^{-3}$  ( $q_0 = 0.5$ ). In addition, we find that the number of DLAs per unit redshift also agrees with previous work,  $n(z) = 0.25$  for  $z_{abs} = 2.32$ . However, an interesting departure emerges when the 4-m sample (hereafter S1) is split by magnitude into S2 ( $B = 19.0$ ) and S3 ( $B < 19.0$ ). As can be seen in Figure 2, although the error bars are still large due to limited statistics (7 DLAs in S2 and 3 in S3), there appears to be more HI in systems found towards faint

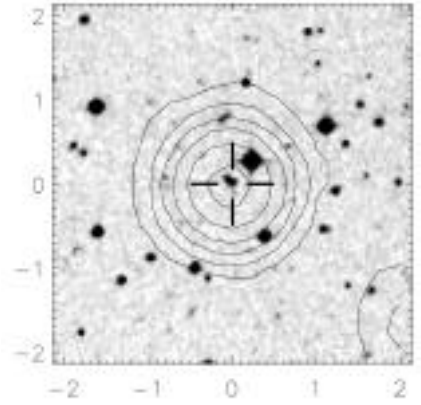
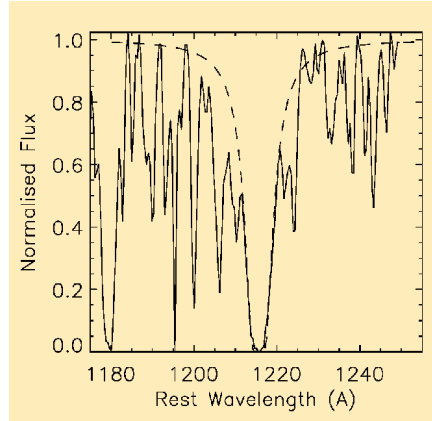


Figure 1: An example of one of the survey targets, B1354-107. In the left panel, a section of the AAT spectrum is shown, the broad absorption trough that is the signature of a DLA is clearly visible. The dashed line shows a fit to the DLA profile, with  $\log N(\text{H I}) = 20.4$ . In the right panel is a DSS image of the QSO overlaid with NVSS radio contours.

QSOs. Since we can discount the possibility that this is merely a colour effect caused by redshift (the S1 sample shows no trend of B magnitude versus  $z_{em}$ ), we conclude that this result is consistent with the presence of a dust bias. In order to improve the statistics, S3 has been supplemented with DLAs found in the LBQS (Wolfe et al 1995) which also has a limiting magnitude of approximately  $B = 19$ . The LBQS+S3 point in Figure 2 remains significantly lower than S2.

This is still just a tantalising hint that a dust bias may be affecting the selection of high redshift DLAs, but one which has far-reaching possibilities. DLAs play a key role in our understanding of chemical evolution and structure formation at high redshifts, work which assumes that we can sample high- $z$  galaxies in an unbiased way. For example, Pettini et al. (1997, 1999) have used the Zn abundance to trace the chemical enrichment of DLAs as a function of redshift but have failed to find a significant increase in metallicity with time. This surprising result may be an indication that metal-rich, and therefore dusty, DLAs are under-represented in current DLA sam-

ples, which would then give only a partial view of metal enrichment in high-redshift galaxies. As tracers of large matter overdensities, the space density of DLAs reflects the fraction of matter that has collapsed into bound structures at a given redshift. This fact has been used by Peacock et al. (1998) to constrain the initial spectrum of density fluctuations on small scales ( $< 1 \text{ Mpc}$ ) and has been shown to be a sensitive test of current theories of structure formation (Gardner et al. 1997).

However, proof will come with the execution of the 8-m VLT sample due to be completed with FORS1 in March 2001. Only with an 8-m-class telescope can intermediate resolution spectroscopy of such faint targets be realised. The VLT/FORS is poised to resolve this crucial issue and determine once and for all the extent to which our view of high-redshift DLAs is biased by dust.

### References

- Bowen, D., Tripp, T., Jenkins, E., 2000, astro-ph/0011134.  
 Ellison, S., 2000, PhD thesis, <http://sc6.sc.eso.org/sellison/astro.html>  
 Gardner, J., et al., 1997, *ApJ*, **486**, 42.  
 Fall, S.M., Pei, Y.C., 1993, *ApJ*, **402**, 479.  
 Lanzetta, K., et al., 1991, *ApJS*, **77**, 1.  
 Lanzetta, K., Wolfe, A., Turnshek, D., 1995, *ApJ*, **440**, 435.  
 Le Brun, V., et al., 1997, *ABA*, **321**, 733.  
 Peacock, J., et al., 1998, *MNRAS*, **296**, 1089.  
 Pei, Y.C., Fall, S.M., 1995, *ApJ*, **454**, 69.  
 Pettini, M., et al., 1997, *ApJ*, **486**, 665.  
 Pettini, M., et al., 1999, *ApJ*, **510**, 576.  
 Prantzos, N., Boissier, S., 2000, *MNRAS*, **315**, 82.  
 Rao, S., Briggs, F., 1993, *ApJ*, **419**, 515.  
 Rao, S., Turnshek, D., 2000, *ApJS*, **130**, 1.  
 Shaver, P., et al., 1996, *Nature*, **384**, 439.  
 Storrie-Lombardi, L., McMahon, R., Irwin, M., 1996, *MNRAS*, **283**, 79.  
 Wolfe, A., et al., 1986, *ApJS*, **61**, 249.  
 Wolfe, A., et al., 1995, *ApJ*, **454**, 698.

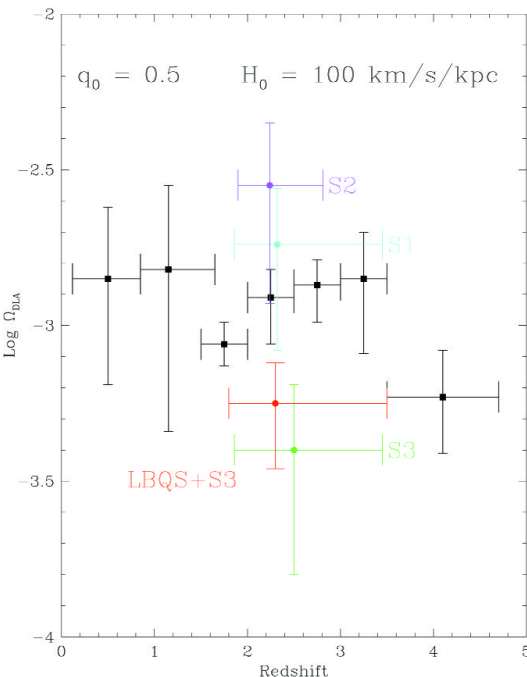


Figure 2: Possible evidence for a dust bias in DLA surveys. Coloured circles show the value of  $\Omega_{DLA}$  for the 3 sub-samples defined for the new survey described here. The cyan point represents the results for our full 4-m sample (S1), complete down to  $B = 20$  and is consistent with previous determinations from magnitude limited samples (black squares, Rao and Turnshek 2000). Comparison of sub-samples S2 and S3 (supplemented with the LBQS to improve statistics) is consistent with a dust bias and indicative of more HI towards fainter QSOs.

# 3D Structure and Dynamics of the Homunculus of Eta Carinae: an Application of the Fabry Perot, ADONIS and AO Software

## II. SPIKES AND BULLETS

D. CURRIE<sup>a</sup>, D. LE MIGNANT<sup>b</sup>, B. SVENSSON<sup>a</sup>, S. TORDO<sup>c</sup>, D. BONACCINI<sup>a</sup>

<sup>a</sup>European Southern Observatory, Garching, Germany

<sup>b</sup>Università di Bologna, Dipartimento di Astronomia, Bologna, Italy

<sup>c</sup>Osservatorio Astronomico di Bologna, Italy

### 1. Summary

Eta Carinae is an extremely massive and highly evolved member of the Carinae starburst region. It has undergone numerous eruptions over the past millennium. In 1841, a giant eruption ejected several solar masses or more of material. Most of this material is currently in the dusty nebula denoted as the “Homunculus”.

In an initial article (*The Messenger* No. 101, September 2000, p. 24), we presented results on the 3-dimensional structure and dynamics of the nebula. In addition to the smoothly distributed light from the nebula, there are sharp spikes or “jets” extending far beyond the Homunculus and very small condensations or “bullets”.

This second article presents new results on these features obtained as an application of two new software packages developed in the frame of the PAPA0 programme (*The Messenger* No. 100, June 2000, p. 12).

The first is STARFINDER (*The Messenger* No. 100, June 2000, p. 23) that has been developed for use with AO data (as well as other types of data) by ESO and Emiliano Diolaiti of the University of Bologna<sup>3</sup>. The second is LINEPHOT developed at ESO by B. Svensson<sup>5</sup> and S. Tordo. In order to test the performance of these software packages for astrometric applications, we require observations in which there is significant and known relative motion of the objects in the field. In the short life of the PAPA0<sup>2</sup> programme, the collection of such data has not been feasible. Therefore, we have conducted these tests on observations of eta Carinae obtained by WFPC2 IDT on the Hubble Space Telescope<sup>1</sup>. We also present results of observations obtained by D. Currie with VLT FORS1.

### 2. Spike (or “Jets”) and Bullets

David Malin obtained colour images of eta Carinae and the surrounding nebula using the Anglo-Australian Telescope<sup>4</sup>. John Meaburn<sup>6</sup> noticed a peculiar red Spike in this image, and performed a series of spectroscopic

measurements on this “Spike”. The Doppler velocities or red shifts of the clumps in this “Spike” indicated very high velocities. Later Weis et al.<sup>7</sup> again observed the Spike and other similar features about eta Carinae. The motions along the spikes have the remarkable and unique property that the velocities increase towards larger distances from the star<sup>7</sup>. At the time that we measured the astrometric motion of the Homunculus in the WFPC2 images<sup>1</sup>, it was difficult to measure the astrometric motion of Spike. However, a later review of the images following some special processing techniques found that there were two very faint, barely resolved objects at the head of the Spike<sup>1</sup>. The astrometric measurements on these two “Bullets” could be performed and they were found to be moving at almost 1% the speed of light (i.e. 3000 km/sec. This led to the application of the special capabilities of the STARFINDER programme, that has been developed in a joint programme between University of Bologna and ESO<sup>2,3</sup>. The STARFINDER programme is especially adapted to perform astrometric and photometric measurements on adaptive optics observations of target fields in which there is a large contamination with background radiation. Using this programme, we were able to re-determine the earlier measurement of

the astrometric motion of the two Bullets, as well as measure the astrometric or Plane-of-the-Sky (PoS) motion of the individual knots or clumps within Spikes. In addition, it was possible to measure the motion of the components of the other Spikes and many other such Bullets were discovered that were moving at a velocity that implied that they, like the original Bullets and the clumps within the original Spike, were emitted in 1841, at the same time as the clumps that compose the Homunculus. Most of the results presented here address the Spike #1 with the 2 bullets at its tip (Fig. 1). Very detailed results have also been obtained on spike #2. As we shall discuss, the diameters of these Bullets and the Spikes are unresolved in the Planetary Camera images, so they have a diameter of less than the extended solar system. Comparison with the diameter of stellar images indicates that these diameters (FWHM) are 100 AU or less in the direction perpendicular to the long axis of the Spike. By comparing the plane-of-the-sky (PoS) velocity component (i.e. the astrometric velocity) with the line-of-sight (LoS) velocity compo-

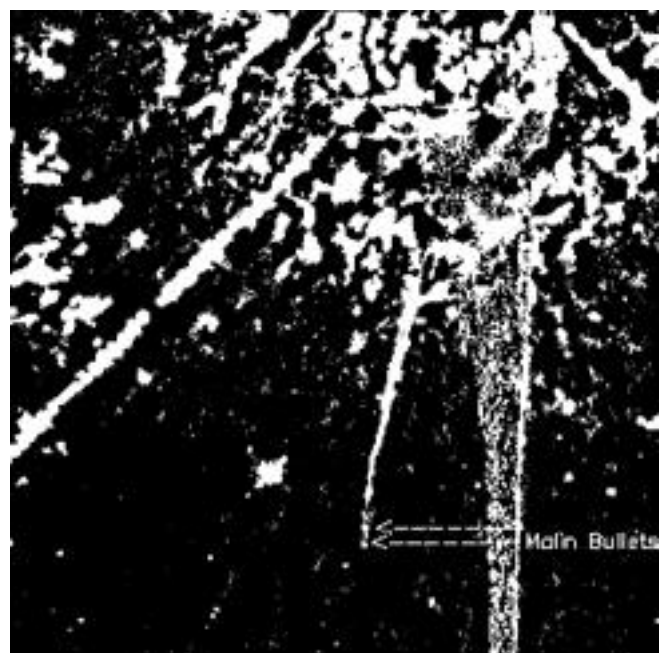


Figure 1: HST image of the southern edge of the nebula of Eta Carinae, the Homunculus, with Malin Spike #1 and its 2 bullets at the end. The 2 brighter spikes are diffraction effects.

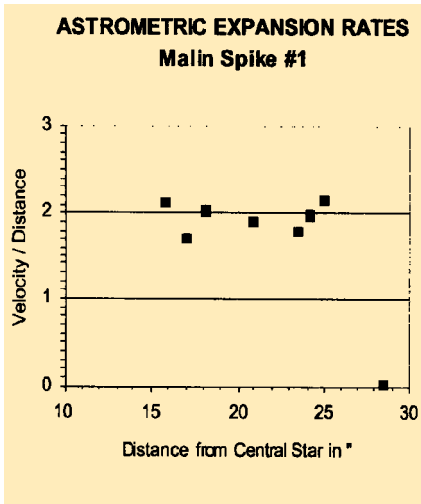


Figure 2: Astrometric motions (on the plane of the sky) of knots and clumps which compose spike #1. Abscissa: distance from central star in arcsec. Ordinates: velocity, in pixel per year, divided by radial distance in arcsec. By combining the astrometric and spectroscopic data, one obtains a consistent picture in which all the clumps in the spike left the star about 165 years ago, that is in 1841. The point at 28.4" is a (stationary) background star.

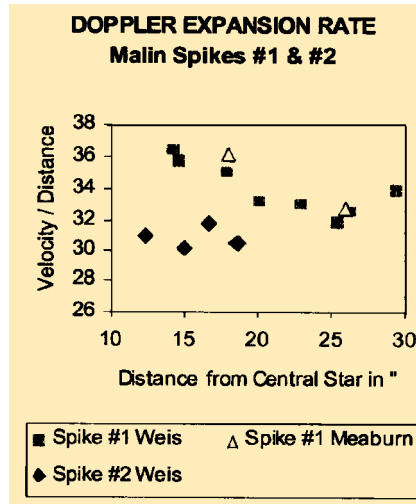


Figure 3: Line-of-sight velocity of the clumps divided by the distance from the star plotted as a function of the distance from the star. The velocity increases with distance from the star<sup>6, 7</sup>.

ment (i.e. the Doppler velocity) we can determine that the angle from the line of sight is about 65 degrees from the line of sight.

The PoS motion was detected by using pairs of images of eta Carinae that were recorded using the WFPC2 on the HST in 1990, 1991, 1994, 1995 and 1997. Positional measurements of the clumps or knots in these images, using STARFINDER, have been used to derive the astrometric velocities of the bullets and of the clumps that compose the Spikes. In Figure 2, the astrometric velocity (PoS) measurements for Spike #1 are plotted as a function of the distance to the central star (in the PoS). In Figure 3, the Doppler velocities (i.e. LoS) of Spikes #1 and #2, determined by spectroscopic measurements of the Spikes<sup>7, 8</sup>, are plotted as a function of the PoS distance from the central star. The relatively uniform values of the linear expansion rates (i.e. the velocities/distances) imply a relatively smooth linear increase in the velocity with distance. In addition, there is very little spreading of the ejecta. The mechanics of the generation and propagation of such features is unknown. Finally, this in turn implies that each of the clumps was ejected from the central star at the same time in different directions, again a phenomenon for which the physics is not understood.

In the past, the direct analysis of properties of width and straightness for the Spikes have been confused by the changes in brightness along the Spikes and the existence of non-uniform nebulosity surrounding the Spike. To allow the extraction of this information, we

have developed a programme, LINEPHOT, to fit the peak intensity, the width and central position of the Spike with a Gaussian function along a line that is orthogonal to the long dimension of the Spike. We have separately estimated the various parameters describing the background nebulosity, in order to reduce their influence on the parameters of the Spike<sup>4</sup>. The results of such an analysis applied to our WFPC2 image (HST Proposals 1138, 2887, 5239, 7253 by Westphal, and the IDT) is shown in Figure 4. A similar analysis of the FORS1 data from the VLT (VLT Proposal 63.I-0619(A) by Currie, et. al.) is shown in Figure 5. In both of these figures, the uppermost plot shows the total brightness of the Spike (peak intensity times twice the Gaussian width). The second plot shows the position of the centroid of the Gaussian, more precisely, the component of the position that is orthogonal to the Spike, illustrating the deviations from straight-line motion. Finally the last curve shows the width of the Spike, where the width of a stellar image in the same frame, obtained with the same fitting programme, is shown by the dashed line.

The HST and the FORS1 observations were conducted in narrow-band filters at the wavelength of the H emission or slightly longward. In this region, we are seeing primarily the 6583 locally emitted, blue-shifted [NII]6583 radiation, with a small component (i.e. at the edge of the filter band pass) of locally emitted, blue-shifted H emission. In addition, there would be expected to be some components of the H radiation emitted by the central star and scattered by the dust contained in the Spike. Recent observations on the FORS1 instrument on the VLT at Paranal, taken at the wavelength selected for maximum sensitivity show that the Bullets are indeed the leading

elements of the Spikes, with no component beyond the Bullets. This starts to give us information to address the physics of the generation and dynamics of these remarkable objects.

The similarly detected results obtained for Spike #2 illustrate the contrast in the apparent and physical properties of the different Spikes that surround eta Carinae. The lengths differ by almost a factor of two. Spike #1 is rather "knotty" while Spike #2 is relatively smooth. Spike #1 shows a number of small bends, while Spike #2 shows a single large bend, and the rest of the motion is straight. Spike #1 has a leading bullet, while Spike #2 does not. In both cases, the width of the Spike is beyond the resolving power of the telescope/camera/atmosphere at the time.

Finally we wish to address the width of the original Spike (Spike #1) and Spike #2. Discussion in the literature either states or implies that these features were well resolved. However, the LINEPHOT programme allows a much more quantitative consideration of this issue. The major portions of the Spikes are essentially unresolved by FORS1 and by the WF camera. In order to obtain a better estimate for the width (or at least a better upper limit), we apply the LINEPHOT procedures to the images obtained in the Planetary Camera of HST. The result is that the Spikes are essentially unresolved, with the resolution of the telescope empirically determined by the measurement of stellar images, i.e., about 100 milli-arc-seconds (mas). This value was determined using a nearby star from the same frame, and using our same LINEPHOT programme. (Spike #2 is especially smooth). That indicates a width of less than 50 mas, or less than 120 AU. In particular, the widths of the Spikes are essentially unresolved from their emergence out of the glare of the central star to their tip. Thus the Spikes are very thin features that have a (length)/(width) ratio of over 600.

Analysis of the FORS1 images have also resulted in the discovery of several new Spikes that have a very high redshift, such that neither the locally emitted nor the locally reflected radiation was admitted by the H or the [NII] filters on HST. The FORS1 images also allow a rough red shift determination and thus a classification of the Spikes, as well as a guide for interpreting the spectroscopic measurements. Data reduction and analysis is continuing on the other Spikes, as well as the many Bullets that have been found in the outer regions beyond the Homunculus.

### 3. Conclusions: Adaptive Optics Operation and Data Reduction Techniques

In conclusion, we have demonstrated that the very large velocities of the Spikes and Bullets indeed represent

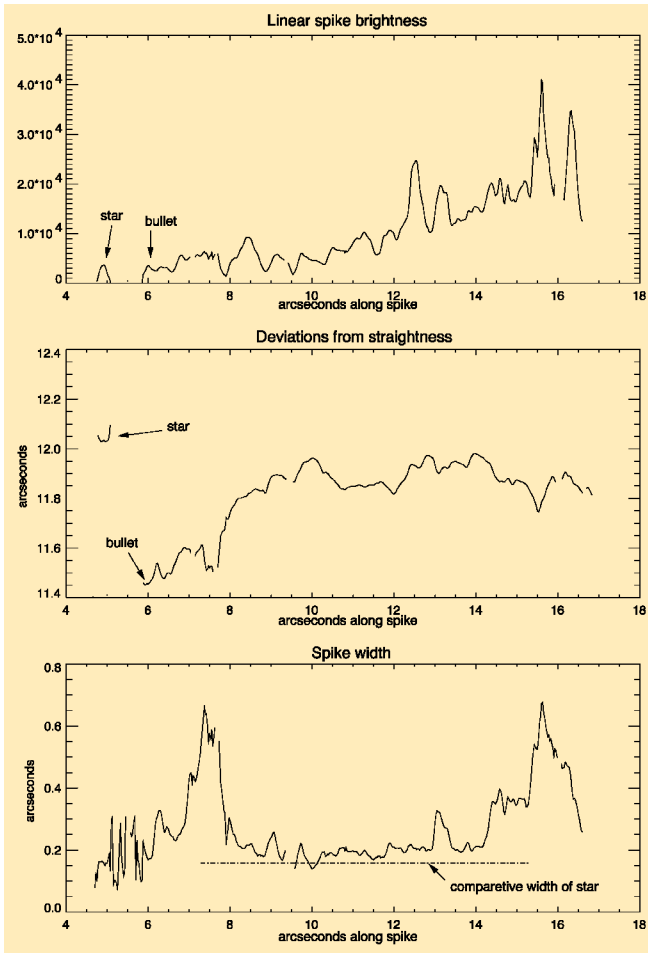


Figure 4: Intensity, position and width of Spike #1 as obtained with LINEPHOT applied to HST/WFPC2 images taken through an  $H\alpha$  filter, and all plotted as a function of distance from centre. Upper plot: intensity (i.e. peak values times width); middle plot: position of the centroid as compared to a straight line, i.e. deviation from straightness; lower plot: width (dashed line: width of a star). Date of the observations: 1997.

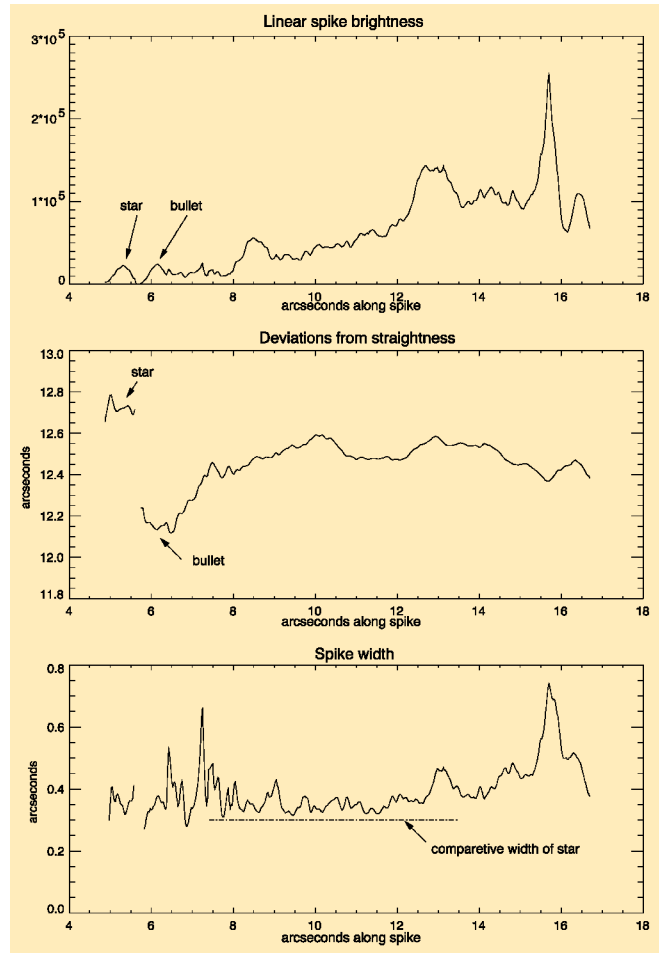


Figure 5: Same as Figure 4, but from LINEPHOT applied to  $H\alpha$  images taken with VLTFORS1. Date of the observations: 1999. The small differences with Figure 4 are mostly due to the difference in angular resolution and filter band-pass.

actual physical motions of clumps of material. The individual clumps, both in terms of the astrometric and spectroscopic velocities, move in a manner to indicate that all of the elements of the Spikes were emitted in 1841. We have also shown that the Bullets are the leading elements of these strange structures, that is, there is no fainter extension of the Spike that lies beyond the bullets. The width of the Spikes and the diameter of the Bullets are less than 120 AU.

The astrophysical results presented here and in article I have been made possible by the combination of the unique capabilities of ADONIS, the WFPC2 of the Hubble Space Telescope and the FORS1 instrument on the VLT. This programme also shows the importance of the auxiliary instrumentation on an AO system, specifically the Fabry-Perot Interferometer and the Coronagraphic Occulting Spot.

The final point concerns the data reduction and analysis methods that are used, and that are discussed in considerably more detail in *The Messenger* No. 100, p. 12, and in other papers<sup>2,3</sup>, and references therein. Present methods of data reduction and analysis for

adaptive optics data have intrinsic photometric errors that are significantly larger than the basic limitations imposed by the photon noise in the target, the skirts or wings of nearby objects, and the sky and the read noise. An unknown portion of this is due to errors in the flat fielding. Addressing and solving these issues can either greatly improve the science that can be obtained from AO data, or can result in a significant reduction in the telescope time required to achieve a given science goal. As we proceed with the AO systems on the 8–10-metre-class telescopes, this will become an even more critical issue.

We wish to thank the 3.6-metre team at La Silla for support in the ADONIS observations, the FORS1 team at Paranal, and NASA and the Space Telescope Institute for the HST Observations. We also wish to thank David Malin for a high-resolution image of his discovery image of the spikes and bullets in eta Carinae.

## References

<sup>1</sup>Currie, D.G. and D.M. Dowling. (1999) "Astrometric Motion and Doppler

Velocity". Eta Carinae at the Millennium, ASP Conference Series, Vol. 179. 1999 J.A. Morse, R. M. Humphries, and A. Damineli, eds.

<sup>2</sup>Currie, D.G.; E. Diolaiti; S. Tordo; K. Naesgarde; J. Liwing; O. Bendinelli; G. Parmeggiani; L. Close; D. Bonaccini. (1999) "ESO Photometric and Astrometric Analysis Program for Adaptive Optics" Astronomical Data Analysis Software and Systems - IX 3–6 October 1999.

<sup>3</sup>Diolaiti, E.; D.G. Currie; S. Tordo; K. Naesgarde; J. Liwing; O. Bendinelli; G. Parmeggiani; L. Close; D. Bonaccini. "ESO Photometric and Astrometric Analysis Program for Adaptive Optics", Astronomical Data Analysis Software and Systems - IX 3–6 October 1999.

<sup>4</sup><http://www.aao.gov.au/AAO/local/www/dfm/aa032.html> (David Malin Image Showing Spike).

<sup>5</sup>Svensson, B. (2000) "3-D Structure of the eta Carinae Nebula and the Configuration of the Hyper-Velocity Jets", Masters Thesis, Lulea University of Technology, Sweden.

<sup>6</sup>Meaburn, J; P. Boumis, J.R. Walsh et al. 1966 *MNRAS* **282**, 1313.

<sup>7</sup>Weis, K.; W. Duschl and Y-H. Chu (1999) *A&A* **349**, 467.

## The Second NEON Observing Euroschool

The Network of European Observatories in the North (NEON) is pleased to announce its second observing school, sponsored by the European Community, which will take place at

### Observatoire de Haute-Provence (France) from July 9 to 21, 2001

The school is organised jointly and alternately by Asiago Observatory (Italy), Calar Alto Observatory (Germany-Spain) and Haute-Provence Observatory (France), with additional tutorial assistance from ESO.

The purpose of the school is to provide opportunity to gain practical observational experience at the telescope, in observatories with state-of-the-art instrumentation. To this end, the school proposes tutorial observations in small groups of 3 students, under the guidance of an experienced observer, centred around a small research project and going through all steps of a standard observing programme. Some complementary lectures will be given by experts in the field.

The school is open to students working on a PhD thesis in Astronomy and which are nationals of a Member State or an Associated State of the European Union. The working language is English. Up to fifteen participants will be selected by the Organising Committee and will have their travel and living expenses paid, if they satisfy the EC rules (age limit of 35 years at the time of the Euro Summer School).

Applicants are expected to fill in an application form (available on the Web site), with a CV and description of previous observational experience, and to provide a letter of recommendation from a senior scientist familiar with the work of the applicant. **The application deadline is March 31, 2001.**

**Secretary of the school:**  
**Mrs. Brigitte RABAN at IAP 98bis,**  
**Bd Arago, F-75014 PARIS raban@iap.fr**

Further instructions and practical details will be found on the school Web site, which is hosted by the European Astronomical Society at: <http://www.iap.fr/eas/schools.html>

You will also find on this site a description of the activities in the previous school, hosted in 2000 by the Calar Alto Observatory. Over 60 applications were received for this first edition of the NEON school, almost all of high quality, and it was a difficult (and painful) task for the Selection Committee to extract the "happy few"! The others are really encouraged to apply again for the next edition!

The school was a success, thanks to the enthusiasm of the participants, to the dedication of the tutors and lecturers, and to the efforts of the local staff (the Director, R. Gredel, even provided good weather!).

After some lectures on basics of observations (Telescope Optics and Imaging by C. Barbieri; Photometry by H. Röser; Spectroscopy by M. Dennefeld), the very diverse scientific topics selected for the observations, all at the forefront of research, brought the students into the hard reality!

A. Pizzella (Padova) guided his group into "Tracing the dark matter in spiral galaxies", by measuring rotation curves and deriving photometric profiles in galaxies of various spiral types. S. Pedraz (Calar Alto) looked with his students into the radial variation of the stellar content in dwarf galaxies and compared it with model predictions. P. Prada (Calar Alto) searched for substructures in the halo of nearby galaxies, using on-off interference-filter imaging in prominent emission lines to detect PNe or regions of star formation. A. Pasquali (ST-ECF) and F. Comerón (ESO) joined their forces (and their groups) to investigate a star-forming region in Cygnus OB2, making a systematic IR map, discovering new clusters and following the most interesting objects in spectroscopy. And P. Leisy (ESO) helped many of the students to survive within the intricacies of MIDAS.

But the unforeseen, scientific actuality added other required observations and boosted the general interest: during the first night, the 2.2-m was requisitioned to follow spectroscopically the transit of an extrasolar planet in front of HD209459. Several tens of spectra were obtained and accumulated, in the hope to show a change in spectral shape of the parent star. During several nights also, Asteroid 140 SIWA was monitored photometrically to add points to the light curve and try to figure out what was the rotation period of this asteroid, target of the Rosetta mission. And, finally, the last night, the discovery of SN2000cw by the Lick SN search group gave an opportunity to the Neon school to observe spectroscopically this target of opportunity and to announce in an IAU Circular that it was a SNIa close to maximum.

Therefore, many important aspects of observations were covered by the school and gave hopefully a good incentive to the students to continue on that track. Indeed, several of the projects started there will continue in collaboration and lead to publications, and fellowship applications have also been written! No doubt this is partly due also to the nice atmosphere surrounding the school: cheerful tutors, helpful staff and a joyful director, Spanish food, proximity of the sea... and excitement to see beautiful objects in a clear sky. Despite the hard work, the life of an observer may after all be a good choice...

*M. DENNEFELD*  
*Co-ordinator of the NEON School*

# Success for “Physics on Stage” Festival in Geneva

C. MADSEN and R. WEST (ESO EPR Dept.)

Can you imagine how much physics is in a simple match of ping-pong, in throwing a boomerang, or in a musical concert? Physics is all around us and governs our lives. But who is going to maintain these technologies and develop new ones in the future? Recent surveys show a frightening decline of interest in physics and technology among Europe's citizens, especially school children. Fewer and fewer young people enrol in physics courses at Europe's universities while scepticism towards science and technology is spreading and causing great concern among governments and educators.

This is the background for several current initiatives that aim at raising the public awareness of science in Europe. With the European Science and Technology Week, the European Commission has become an increasingly active partner in this important process, supporting a range of projects to stimulate public interest in science. The flagship project of this year was the “Physics on Stage” Science Teaching Festival, the final, high point of the year-long programme of that name (cf. *The Messenger* No. 99, p. 46, March 2000).

This unique project was organised jointly by CERN, ESA and ESO, in collaboration with the European Physics Society (EPS) and the European Association for Astronomy Education (EAAE) and was supported by the EC. It took place at CERN during the week of November 6–10, when about 550 physics educators, government officials and media representatives from more than 25 European countries came together to show how fascinating and entertaining physics can be. There were also overseas visitors, including Chilean representation at ESO's initiative.

Each of the delegates to the festival had been selected in the course of the year by “Physics on Stage” National Committees in each of the countries. Mostly through national competitions, these committees had identified the most outstanding projects for promoting science in their area which were then presented at the Geneva Festival.

The colourful centrepiece of this week was the Physics Fair. Like in a real marketplace, each country had its own stand where delegates could show their projects, programmes or experiments and at the same time gain inspiration from the exhibits of other countries.

Other important elements of the meeting were plenary presentations and ten most impressive, staged performances. Here art and science came together to offer strong and persuasive communication about physical concepts as well as scientific controversies.



CERN photographer Laurent Guiraud caught this symbolic act at the “Physics on Stage” Festival in Geneva. In the front row: Commissioner Philippe Busquin, Member of European Parliament Christian Rovsing, CERN Director General Prof. Luciano Maiani.

But “Physics on Stage” was more than stunning experiments and pure fun. In 13 workshops around carefully selected, central themes related to the current problems, the many delegates were confronted with a wide spectrum of issues, ranging from science teaching in primary and secondary schools, the delicate balance between addressing the topics of the day versus teaching basic concepts, woman and physics, the role of the European organisations in the context of science teaching and, not least, a dedicated attempt to describe in quantitative terms the magnitude and effect of the current disenchantment with science, and physics in particular.

The resulting reports, including a series of well-defined recommendations, will be made publicly available as soon as possible. With input from all corners of Europe and representing the outcome of intensive discussions among participants with a broad range of backgrounds, this will be useful and interesting reading for all related parties, including the makers of European educational policies.

Already in the preparation phase, “Physics on Stage” had attracted the vivid interest of the teaching community. By the time of the festival, “Physics on Stage” had also caught the attention of European decision-makers. High-ranking politicians from several countries (including Spain and the UK) visited the meeting in its early phases. On November 9, Philippe Busquin, European Commissioner for Research, spent a full day at the event, together with Prof. Luciano Maiani, Director-

General of CERN, Dr. Catherine Cesarsky, Director-General of ESO, and Mr. Christian Rovsing, member of the European Parliament and of its Committee on Industry, External Trade, Research and Energy. The distinguished guests moved around within the fair area, witnessing experiments, discussing many different issues with the participants, speaking to school children in remote areas of the continent via webcam and obviously enjoying the exciting and cordial atmosphere. In addition to the current member countries of the European Union, the participation of several candidate countries provided welcome opportunities for information and contacts.

“Physics on Stage” was clearly a unique event. Nothing like it has ever happened in terms of international exchange, collaboration and presentation of state-of-the-art science and technology education methods and means. It is therefore not surprising that Europe's leading intergovernmental science organisations, ESA, CERN and ESO, as organisers of this very successful project, are looking for ways to maintain the momentum now gained, through new joint projects in the field of public understanding of science.

ESO is producing an 18-min video about the Festival that will become available in early January 2001. Full information about the outcome, including the complete workshop reports and recommendations, etc., will be placed at the “Physics on Stage” Festival website at:

<http://CERN.web.cern.ch/CERN/Announcements/2000/PhysicsOnStage/>

# UK Announces Intention to Join ESO

(Taken from ESO Press Release 23/00 – 22 November 2000)

## Summary

On November 22, the Particle Physics and Astronomy Research Council (PPARC), the UK's strategic science investment agency, announced that the government of the United Kingdom is making funds available that provide a baseline for this country to join the European Southern Observatory (ESO).

The ESO Director General, Dr. Catherine Cesarsky, and the ESO Community warmly welcome this move towards fuller integration in European astronomy. "With the UK as a potential member country of ESO, our joint opportunities for front-line research and technology will grow significantly", she said. "This announcement is a clear sign of confidence in ESO's abilities, most recently demonstrated with the construction and operation of the unique Very Large Telescope (VLT) on Paranal. Together we will look forward with confidence towards new, exciting projects in ground-based astronomy."

It was decided earlier this year to place the 4-m UK Visible and Infrared Survey Telescope (VISTA) at Paranal.

Following negotiations between ESO and PPARC, a detailed proposal for the associated UK/ESO Agreement with the various entry modalities will now be presented to the ESO Council for approval. Before this Agreement can enter into force, the ESO Convention and associated protocols must also be ratified by the UK Parliament.

## Research and Key Technologies

According to the PPARC press release, increased funding for science,

announced by the UK government today, will enable UK astronomers to prepare for the next generation of telescopes and expand their current telescope portfolio through membership of the European Southern Observatory (ESO).

The uplift to its baseline budget will enable PPARC to enter into final negotiations for UK membership of ESO. This will ensure that UK astronomers, together with their colleagues in the ESO member states, are actively involved in global scale preparations for the next generation of astronomy facilities. Among these are ALMA (Atacama Large Millimeter Array) in Chile and the very large optical/infrared telescopes now undergoing conceptual studies.

ESO membership will give UK astronomers access to the suite of four world-class 8.2-metre VLT Unit Telescopes at the Paranal Observatory, as well as other state-of-the-art facilities at ESO's other observatory at La Silla. Through PPARC the UK already participates in joint collaborative European science programmes such as CERN and the European Space Agency (ESA), which have already proved their value on the world scale. Joining ESO will consolidate this policy, strengthen ESO and enhance the future vigour of European astronomy.

## Statements

Commenting on the funding announcement, Prof. Ian Halliday, PPARC's Chief Executive Officer, said that "this new funding will ensure our physicists and astronomers remain at the forefront of international research – leading

in discoveries that push back the frontiers of knowledge – and the UK economy will also benefit through the provision of highly trained people and the resulting advances in IT and commercial spin-offs".

Prof. Mike Edmunds, UCW Cardiff, and Chairman of the UK Astronomy Review Panel which recently set out a programme of opportunities and priorities for the next 10 to 20 years added that "this is excellent news for UK science and lays the foundation for cutting-edge research over the next ten years. British astronomers will be delighted by the Government's rapid and positive response to their case".

Speaking on behalf of the ESO Organisation and the community of more than 2500 astronomers in the ESO member states, the ESO Director General, Dr. Catherine Cesarsky, declared: "When ESO was created in 1962, the UK decided not to join, because of access to other facilities in the Southern Hemisphere. But now ESO has developed into one of the world's main astronomical organisations, with top technology and operating the VLT at Paranal, the largest and most efficient optical/infrared telescope facility in the world. We look forward to receiving our UK colleagues in our midst and work together on the realization of future cutting-edge projects."

Joining ESO was considered a top priority for UK astronomy following a community report to the UK Long Term Science Review, which set out a programme of opportunities and priorities for PPARC science over the next 10 to 20 years. The report is available on the web at URL: [www.pparc.ac.uk/ltsr](http://www.pparc.ac.uk/ltsr).

# The VLT Weighs the Invisible Matter in the Universe

## SHAPES AND ORIENTATIONS OF 76,000 DISTANT GALAXIES

(Taken from ESO Press Release 24/00 – 1 December 2000)

## Summary

An international team of astronomers<sup>1</sup> has succeeded in mapping the

"dark" (invisible) matter in the Universe, as seen in 50 different directions from the Earth. They find that, within the uncertainty, it is unlikely that mass alone

would stop the current expansion of the Universe.

This fundamental result is based on the powerful, but challenging method of "cosmic shear". It depends on very accurate measurements of the apparent, weak distortion and preferential orientation of images of distant galaxies. This effect is caused by deflection of the light from those galaxies by the

<sup>1</sup> The team consists of Yannick Mellier (Principal Investigator [PI], Institut d'Astrophysique de Paris [IAP] and Observatoire de Paris/DEMIRM [OP-DEMIRM], France); Ludovic van Waerbeke (co-PI, IAP); Roberto Maoli (IAP, OP-DEMIRM and University La Sapienza, Rome, Italy); Peter Schneider

(University of Bonn, Germany); Bhuvnesh Jain (John Hopkins University, Baltimore, USA); Francis Bernardeau (Service de Physique Theorique, C.E. de Saclay, France); Thomas Erben (Max-Planck-Institut für Astrophysik, Garching, Germany, IAP and OP-DEMIRM), and Bernard Fort (IAP).

large mass concentrations in the Universe it encounters on its way to us. The larger these masses are, the larger are the apparent image distortions and the more pronounced are the alignments of neighbouring galaxy images.

The new analysis was made possible by means of unique observational data, obtained under excellent conditions with the the ESO 8.2-m VLT ANTU telescope and the multi-mode FORS1 instrument at the Paranal Observatory.

## The VLT Observations

An international team led by astronomers at the Institut d'Astrophysique de Paris used for the first time the VLT to probe the mass density of dark matter in the Universe, by means of weak gravitational lensing effects. The team selected 50 different sky fields which were then observed in service mode by the ESO staff at the Paranal Observatory.

Long exposures of these fields were made with the FORS1 instrument (in its imaging mode) on the VLT 8.2-m ANTU telescope and only during nights with the very best observing conditions. In fact, 90% of the fields have image quality better than 0.65 arcsec, guaranteeing a superb basis for the subsequent study.

## Clumps of Dark Matter

The unprecedented quality of these data enabled the astronomers to measure the shapes and orientations of the images of more than 70,000 galaxies with very high precision. After a careful statistical analysis, they were able to demonstrate that the distant galaxies are not randomly oriented on the sky – they show a certain degree of alignment over substantial sky areas (to distances of several arcmin). The astronomers refer to this as a coherent orientation. It can only be explained by gravitational lensing effects produced by clumps of dark matter in space, distributed along huge “filaments”. Figure 1 demonstrates this, by means of the VLT exposure (left) and the deduced mass distribution in the same direction, based on these measurements (right).

## The Weak Lensing Effect

The gravitational lensing effect was predicted by Einstein's theory of general relativity at the beginning of the 20th century. When the light of a distant galaxy passes close to a concentration of matter in space, it will be (more or less) deflected, due to the effect of the field of gravity of this matter. The observed image of the galaxy is therefore distorted. Very strong gravitational lensing effects (by very heavy objects) pro-

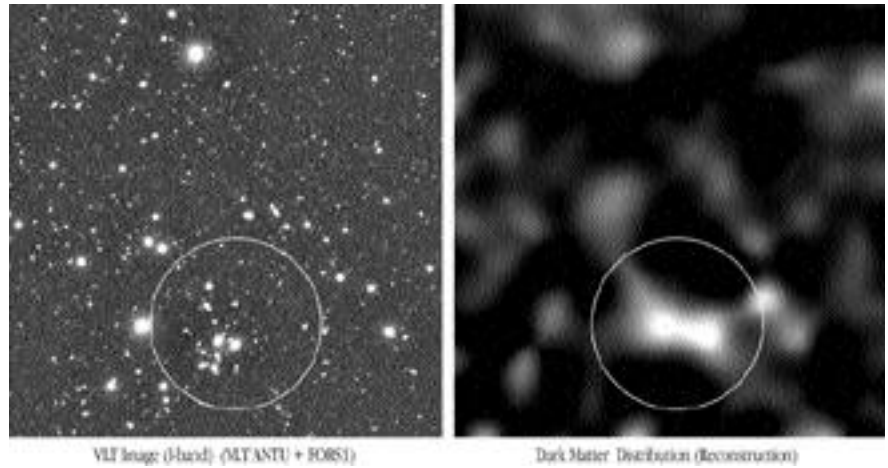


Figure 1: The figure shows an example of the mapping of the dark mass distribution in one of the 50 sky fields observed with the VLT and FORS1. To the left is the original image, a 36-min exposure in a near-infrared wavelength band. To the right is the reconstructed map of the mass (a “mass photo”) in this direction, based on an analysis of the weak shear effect seen in the field; that is, on the measured elongations and directions of the axes of the galaxy images in this field. The brighter areas indicate the directions in which there is most mass along the line of sight. The circle in the left photo surrounds the images of a distant cluster (or group) of galaxies, seen in this direction. Note that there is a corresponding concentration of mass in the “mass photo”; this is obviously the mass of that cluster. The mass reconstruction map shows the (mostly) dark matter responsible for the cosmic shear found on the small scales, now measured with the VLT.

duce spectacular gravitational arcs observed in some rare clusters of galaxies, cf. the VLT images of CL2244-0 (<http://www.eso.org/outreach/press-rel/pr-1998/phot-46d-98-preview.jpg>) and Abell 370 (<http://www.eso.org/outreach/press-rel/pr-1998/phot-47c-98-preview.jpg>).

Much weaker lensing effects (by less massive objects) are in fact present everywhere in the Universe, but they are not easy to detect. This was the effect the astronomers searched for. It manifests itself as a small stretching in a particular direction of the images of all galaxies that are located behind the gravitational lens. This phenomenon may then be observed as an alignment of galaxies in that particular sky area. The existence of the lens and its overall mass and extension can then be determined, albeit with some uncertainty only.

## An Important Contribution to the Map of the Universe

Thanks to the large light collecting power of the VLT and the superb quality of the present images, the team succeeded in detecting large-scale, weak lensing effects in the Universe, in a large number of different (and thus independent) directions. Moreover, the analysis of this large data sample enabled the astronomers, for the first time, to set limits to the overall mass density of the universe, by means of the gravitational lensing by large-scale structures. It turns out that their results are in remarkable agreement with the current constraints obtained by other cosmological considerations.

This kind of investigation is rather difficult and cannot be based on individual

sky fields alone. The final result, in terms of the inferred mass density of the Universe, only emerges when “adding” all of the 50 observed fields. Making the reasonable assumption that the distribution of galaxies and dark matter in space is similar, the new investigation shows that the total matter density is less than half of what is needed to stop the current cosmic expansion. The new result also supports the existence of a non-zero “cosmological constant” (vacuum energy), already indicated by supernova observations.

In the ongoing quest for establishing the first true mass map of the Universe from the gravitational lensing effects caused by this mass, the VLT has now demonstrated its great potential with bravura. The light collecting power and, not least, its excellent image quality provides what is likely to be the best observing configuration for this very challenging research programme. It was also made possible because of the opportunity to use the VLT Service Mode during which ESO staff astronomers at Paranal are responsible for carrying out the actual observations, at the moment of the very best atmospheric conditions.

## More Information

The research described in this Press Release is reported in a research article (“Cosmic Shear Analysis in 50 Uncorrelated VLT Fields. Implications for Omega-0 and sigma-8.”), submitted by the team to the European journal “Astronomy and Astrophysics”. Note also the related article in the *The Messenger* No. 101, p. 10–14, September 2000).



*A Challenge for*

# **Astronomers, Software Engineers Electrical/Mechanical Engineers**

If you have a degree related to one of these professional fields, and if you are ready to work in areas of front-line technology - together with highly qualified scientists and engineers, then please send us your application.

For further information about currently available positions, please consult the ESO homepage: <http://www.eso.org/> or contact Ms. Angelika Beller (e-mail: [abeller@eso.org](mailto:abeller@eso.org)).

We offer an attractive remuneration package, including a competitive salary (tax-free), comprehensive social benefits and professional training opportunities.

ESO, Karl-Schwarzschild-Str. 2,  
D-85748 Garching near Munich,  
Germany;  
Tel.: +49 89 320 06 553  
Fax: +49 89 320 06 490

**ESO. Astronomy made in Europe**

# PERSONNEL MOVEMENTS

## International Staff

(October – December 2000)

### ARRIVALS

#### EUROPE

ALMAGRO GARCIA, Susana (E), Secretary/Adm. Employee  
ARSENAULT, Robin (CDN), Optical Engineer/Physicist  
BONNET, Henri (F), Optical Engineer/Physicist  
DI FOLCO, Emmanuel (F), Coopérant  
HUMMEL, Wolfgang (D), Astronomical Data Quality Control Scientist  
JERAM, Bogdan (Slovenian), Software Engineer  
KASPER, Markus (D), Optical Engineer/Physicist  
PANCINO, Elena (I), Student  
PRIMAS, Francesca (I), User Support Astronomer  
RAHMER, Gustavo (RCH), CCD System Engineer  
ROMANIELLO, Martino (I), User Support Astronomer

#### CHILE

BILLERES, Malvina (F), Fellow  
CABANAC, Rémi (F), Fellow  
DELSANTI, Audrey (F), Student  
DOUBLIER, Vanessa (F), Operations Staff Astronomer  
FAURE, Cécile (F), Student  
GALLIANO, Emmanuel (F), Coopérant

### DEPARTURES

#### EUROPE

BENOIST, Christophe (F), EIS Associate  
CLOSE, Laird (CDN), Adaptive Optics Instrument Scientist

KEMP, Robert (UK), Application Software Designer  
MEYLAN, Georges (CH), Astronomer  
MICHEL, Alain (F), Optical Engineer  
RITE, Charles (Brazilian), EIS Associate  
SCHIRMER, Michael (D), EIS Associate  
TOKOVININE, Andrei (Russian), Associate  
VAN BEMMEL, Ilse (NL), Student  
VAN ECK, Sophie (B), Fellow  
VIARD, Elise (F), Student  
VIEZZER, Rodolfo (I), Associate

#### CHILE

HÖÖG, Torbjörn (S), Mechanical/Electrical Engineer

## Local Staff

(October – November 2000)

### ARRIVALS

ROBINSON, William, Mechanical Engineer, Santiago  
RIQUELME, Miguel, Instrumentation Technician, Paranal

### DEPARTURES

RAHMER BASS, Gustavo, Optical Detector Engineer, Paranal  
ROJAS, Roberto, Ing. Ejec. en Computación, Paranal  
URRUTIA, Cristian, Human Interface Programmer, La Silla

## Scientific Preprints

(October – December 2000)

1393. V.D. Ivanov, J. Borissova, L. Vanzi: Deep Infrared Photometry of New Galactic Globular Clusters. *A&A*.
1394. L. Vanzi, L.K. Hunt, T.X. Thuan, Y.I. Izotov: The Near-Infrared View of SBS 0335-052. *A&A*.
1395. F. Primas, M. Asplund, P.E. Nissen, V. Hill: The Beryllium Abundance in the Very Metal-Poor Halo Star G 64-12 from VLT/UVES Observations. *A&A*.
1396. E. Scannapieco and T. Broadhurst: The Role of Heating and Enrichment in Galaxy Formation. *ApJ*.
1397. S. Mei, D. Silva, P.J. Quinn: VLT Deep I-Band Surface Brightness Fluctuations of IC 4296. *A&A*.
1398. D.A. Erasmus and M. Sarazin: Forecasting Precipitable Water Vapour and Cirrus Cloud Cover for Astronomical Observations: Satellite Image Processing Guided by Synoptic Model Dissemination Data. *SPIE* 4168 - Barcelona - 25-29 September 2000, p. 1.
1399. R. Tüllmann, R.-J. Dettmar, M. Soida, M. Urbanik, J. Rossa: The Thermal and Non-Thermal Gaseous Halo of NGC 5775. *A&A*.
1400. C. Lidman, F. Courbin, J.-P. Kneib, G. Golse, F. Castander, G. Soucail: Exploring the Gravitationally Lensed System HE 1104-1805: VLT Spectroscopy of the Lens at  $z = 0.729$ . *A&A*.
1401. F. Comerón: A Gould-Belt-like Structure in M 83. *A&A*.
1402. R. Siebenmorgen and E. Krügel: The Protostellar System HH108MMS. *A&A*.
1403. J. Vernet et al.: Radio Galaxies at  $z \sim 2.5$ : Results from Keck Spectropolarimetry. *A&A*.
1404. F. Comerón, J. Torra, R.A. Méndez, A.E. Gómez: Possible Star Formation in the Halo of NGC 253. *A&A*.
1405. P. Petitjean, R. Srianand, C. Ledoux: Molecular Hydrogen and the Nature of Damped Lyman- Systems. *A&A*.
1406. H.W.W. Spoon et al.: The Obscured Mid-Infrared Continuum of NGC 4418: a Dust- and Ice-Enshrouded AGN. *A&A*.
1407. D. Hutsemékers and H. Lamy: Confirmation of the Existence of Coherent Orientations of Quasar Polarization Vectors on Cosmological Scales. *A&A*.

## ESO Workshop Proceedings Still Available

Most ESO Conference and Workshop Proceedings are still available and may be ordered at the European Southern Observatory. Some of the more recent ones are listed below.

No.	Title	Price
50	Handling & Archiving Data from Ground-based Telescopes. Trieste, Italy, April 21-23, 1993. M. Albrecht & F. Pasian (eds.)	DM 35.-
51	Third CTIO/ESO Workshop on "The Local Group: Comparative and Global Properties". La Serena, Chile, 25-28 January 1994. M. Albrecht and F. Pasian (eds.)	DM 35.-
52	European SL-9 Jupiter Workshop. February 13-15, 1995, Garching, Germany. R. West and H. Bönnhardt (eds.)	DM 80.-
53	ESO/ST-ECF Workshop on "Calibrating and understanding HST and ESO instruments", Garching, Germany. P. Benvenuti (ed.)	DM 60.-
54	Topical Meeting on "Adaptive Optics", October 2-6, 1995, Garching, Germany. M. Cullum (ed.)	DM 80.-
55	NICMOS and the VLT. A New Era of High Resolution Near Infrared Imaging and Spectroscopy. Pula, Sardinia, Italy, May 26-27, 1998	DM 20.-
56	ESO/OSA Topical Meeting on "Astronomy with Adaptive Optics - Present Results and Future Programs". Sonthofen, Germany, September 7-11, 1999. D. Bonaccini (ed.)	DM 100.-
57	Bäckaskog Workshop on "Extremely Large Telescopes". Bäckaskog, Sweden, June 1-2, 1999. T. Andersen, A. Ardeberg, R. Gilmozzi (eds.)	DM 60.-

## SUBJECT INDEX

### TELESCOPES AND INSTRUMENTATION

- Successful Commissioning of UVES at Kueyen **99**, 1
- S. D'Odorico: UVES at Kueyen: Bright Prospects for High-Resolution Spectroscopy at the VLT **99**, 2
- R. Hanuschik and P. Amico: VLT Pipeline Operation and Quality Control: FORS1 and ISAAC **99**, 6
- B. Leibundgut, B. Pirenne, M. Albrecht, A. Wicenec and K. Gorski: Access to VLT Data in the ESO Archive **99**, 12
- M. Sarazin: Chile Astroclimate, a Biannual Update **99**, 13
- R. Heald and R. Karban: ESO Demonstration Project with the NRAO 12-m Antenna **99**, 14
- O. Hainaut and the NTT Team: News from the NTT **99**, 15
- New Pictures from Paranal Observatory **99**, 15
- R. Gilmozzi and P. Dierickx: OWL Concept Study **100**, 1
- D. Currie, D. Bonaccini, E. Diolaiti, S. Tordo, K. Naesgarde, J. Liwing, O. Bendinelli, G. Parmeggiani, L. Close: The ESO Photometric and Astrometric Analysis Programme for Adaptive Optics **100**, 12
- E. Diolaiti, O. Bendinelli, D. Bonaccini, L. Close, D. Currie, G. Parmeggiani: Star-Finder: a Code to Analyse Isoplanatic High-Resolution Stellar Fields **100**, 23
- D. Bonaccini, W. Hackenberg, R.I. Davies, S. Rabien, T. Ott: VLT Laser Guide Star Facility: First Successful Test of the Baseline Laser Scheme **100**, 27
- C. Cesarsky: Successful Completion of an Ambitious Project – A Midwinter Night's Dream **101**, 1
- J.G. Cuby, C. Lidman, C. Moutou: ISAAC: 18 Months of Paranal Science Operations **101**, 2
- Message to the ESO Community: Opening of the VLT Visitor Focus **101**, 8
- G. Avila, G. Conti, E. Mattaini, L. Chiappetti, D. Maccagni, E. Sant'Ambrogio, O. Le Fèvre, G. Vettolani, M. Saïsse: Successful installation of the VIMOS Laser Mask Manufacturing Unit (MMU) at Paranal **102**, 1
- H.U. Käufel, N. Ageorges, E. Dietzsch, J. Hron, H. Relke, D. Scholz, A. Silber, M. Sperl, M. Sterzik, R. Wagner, U. Weilenmann: First Astronomical Light with TIMM2, ESO's 2nd-Generation Thermal Infrared Multimode Instrument at the La Silla 3.6-m Telescope **102**, 4
- S. Cristiani, S. D'Odorico, T.-S. Kim: Exploring the Lyman forest at  $z = 2$  with UVES **102**, 8

### THE LA SILLA NEWS PAGE

- H. Jones: 2p2 Team News **100**, 29
- M. Sterzik, M. Kürster: News from the 3.6-m Telescope **100**, 30
- 2p2 Team News **101**, 9

- La Silla under the Milky Way **100**, 31
- H. Jones: 2p2 Team News **102**, 12

### DATA MANAGEMENT AND OPERATIONS

- N. Devillard: Astronomical Image Resampling **100**, 48
- P. Ballester, A. Modigliani, O. Boitquin, S. Cristiani, R. Hanuschik, A. Kaufer, S. Wolf: The UVES Data Reduction Pipeline **101**, 31

### REPORTS FROM OBSERVERS

- E. Tolstoy, J. Gallagher, L. Greggio, M. Tosi, G. De Marchi, M. Romaniello, D. Minniti and A. Zijlstra: Imaging With UT1/FORS1: The Fossil Record of Star-Formation in Nearby Dwarf Galaxies **99**, 16
- M. Franx, A. Moorwood, H.-W. Rix, K. Kuijken, H. Röttgering, P. van der Werf, P. van Dokkum, I. Labbe and G. Rudnick: FIRES at the VLT: the Faint InfraRed Extragalactic Survey **99**, 20
- R.P. Mignani, P.A. Caraveo and G.F. Bignami: Optical Observations of Pulsars: the ESO Contribution **99**, 22
- P. Rosati, C. Lidman, R. Della Ceca, S. Borgani, M. Lombardi, S.A. Stanford, P.R. Eisenhardt, G. Squires, R. Giacconi and C. Norman: The ROSAT Deep Cluster Survey: Probing the Galaxy Cluster Population out to  $z = 1.3$  **99**, 26
- P. Møller: Spectral PSF Subtraction I: The SPSF Look-Up-Table Method **99**, 31
- P. Møller, S.J. Warren, S.M. Fall, P. Jakobsen and J.U. Fynbo: SPSF Subtraction II: The Extended Ly Emission of a Radio Quiet QSO **99**, 33
- B. Leibundgut, J. Sollerman, C. Kozma, C. Fransson, P. Lundqvist, F. Ryde and P. Woudt: The Late Phase of SN 1998bw **99**, 36
- J.-M. Conan, T. Fusco, L. M. Mugnier and F. Marchis: MISTRAL: Myopic Deconvolution Method Applied to ADONIS and to Simulated VLT-NAOS Images **99**, 38
- A New Look at the Sombrero Galaxy **99**, 45
- H. Pedersen, J.-L. Atteia, M. Boer, K. Beuermann, A.J. Castro-Tirado, A. Fruchter, J. Greiner, R. Hessman, J. Hjorth, L. Kaper, C. Kouveliotou, N. Masetti, E. Palazzi, E. Pian, K. Reinsch, E. Rol, E. van den Heuvel, P. Vreeswijk, R. Wijkers: Gamma-Ray Bursts – Pushing Limits with the VLT **100**, 32
- D. Rigopoulou, A. Franceschini, H. Aussel, C.J. Cesarsky, D. Elbaz, R. Genzel, P. van der Werf, M. Dennefeld: ISAAC on the VLT Investigates the Nature of the High-Redshift Sources of the Cosmic Infrared Background **100**, 37
- R. Häfner: The Deep Eclipse of NN Ser **100**, 42
- I. Appenzeller, R. Bender, A. Böhm, N. Drory, K. Fricke, R. Häfner, J. Heidt, U.

- Hopp, K. Jäger, M. Kümmel, D. Mehler, C. Möllenhoff, A. Moorwood, H. Nicklas, S. Noll, R. Saglia, W. Seifert, S. Seitz, O. Stahl, E. Sutorius, T. Szeifert, S. Wagner, B. Ziegler: The FORS Deep Field **100**, 44

- R. Maoli, Y. Mellier, L. van Waerbeke, P. Schneider, B. Jain, T. Erben, F. Bernardau, B. Fort, E. Bertin, M. Dantel-Fort: Cosmic Shear with ANTU/ FORS1: An Optimal Use of Service Mode Observation **101**, 10
- R. Falomo, J. Kotilainen, A. Treves: VLT/ISAAC Images of Quasar Hosts at  $z \sim 1.5$  **101**, 15
- C. Lidman, A. Goobar, R. Pain: Type Ia Supernovae, Cosmology and the VLT **101**, 18
- F. Courbin, C. Lidman, I. Burud, J. Hjorth, P. Magain, G. Golse, F. Castander: Lensed Quasars: A Matter of Resolution **101**, 20
- D. Currie, D. Le Mignant, B. Svensson, S. Tordo, D. Bonaccini: 3D Structure and Dynamics of the Homunculus of Eta Carinae: an Application of the Fabry-Perot, ADONIS and AO Software. I. Motions in Homunculus **101**, 24
- F. Kerber, R. Palsa, J. Köppen, T. Blöcker, M. R. Rosa: Unlocking the past of Sakurai's Object Using FORS/VLT **101**, 27
- J. Setiawan, L. Pasquini, L. Da Silva, A. Hatzes, O. von der Lühe, A. Kaufer, L. Girardi, R. de la Reza, J.R. de Medeiros: A Study of the Activity of G and K Giants Through Their Precise Radial Velocity; Breaking the 10-m/sec Accuracy with Feros **102**, 13
- F. Paresce, G. de Marchi, G. Andreuzzi, R. Buonnanno, F. Ferraro, B. Paltrinieri, L. Pulone: Crowded Field Photometry with the VLT: the Case of the Peculiar Globular Cluster NGC 6712 **102**, 17
- S.L. Ellison, L. Yan, I.M. Hook, M. Pettini, P. Shaver, J.V. Wall: Revealing High-Redshift Galaxies: Results from a New Damped Lyman- System Survey **102**, 23
- D. Currie, D. Le Mignant, B. Svensson, S. Tordo, D. Bonaccini: 3D Structure and Dynamics of the Homunculus of Eta Carina: an Application of the Fabry Perot, ADONIS and AO Software. II. Spikes and Bullets **102**, 25

### OTHER ASTRONOMICAL NEWS

- Portugal to Accede to ESO **100**, 51
- C. Waelkens: The Observing Programmes Committee – an Evolving Process **101**, 37
- M. Dennefeld: The Second NEON Observing Euroschool **102**, 28
- R. West and C. Madsen: Physics on Stage **102**, 29
- C. Madsen and R. West: Success for "Physics on Stage" Festival in Geneva **102**, 29
- UK Announces Intention to Join ESO **102**, 30

The VLT Weighs the Invisible Matter in the Universe. Shapes and Orientations of 76,000 Distant Galaxies **102**, 30

## ANNOUNCEMENTS

CERN, ESA and ESO Launch "Physics On Stage" **99**, 46

ALMA Science Advisory Committee **99**, 46

## AUTHOR INDEX

### A

I. Appenzeller, R. Bender, A. Böhm, N. Drory, K. Fricke, R. Häfner, J. Heidt, U. Hopp, K. Jäger, M. Kümmel, D. Mehlert, C. Möllenhoff, A. Moorwood, H. Nicklas, S. Noll, R. Saglia, W. Seifert, S. Seitz, O. Stahl, E. Sutorius, T. Szeifert, S. Wagner, B. Ziegler: The FORS Deep Field **100**, 44

G. Avila, G. Conti, E. Mattaini, L. Chiappetti, D. Maccagni, E. Sant'Ambrogio, O. Le Fèvre, G. Vettolani, M. Saisse: Successful installation of the VIMOS Laser Mask Manufacturing Unit (MMU) at Paranal **102**, 1

### B

P. Ballester, A. Modigliani, O. Boitquin, S. Cristiani, R. Hanuschik, A. Kaufer, S. Wolf: The UVES Data Reduction Pipeline **101**, 31

D. Bonaccini, W. Hackenberg, R.I. Davies, S. Rabiën, T. Ott: VLT Laser Guide Star Facility: First Successful Test of the Baseline Laser Scheme **100**, 27

### C

C. Cesarsky: Successful Completion of an Ambitious Project – A Midwinter Night's Dream **101**, 1

J.-M. Conan, T. Fusco, L. M. Mugnier and F. Marchis: MISTRAL: Myopic Deconvolution Method Applied to ADONIS and to Simulated VLT-NAOS Images **99**, 38

F. Courbin, C. Lidman, I. Burud, J. Hjorth, P. Magain, G. Golse, F. Castander: Lensed Quasars: A Matter of Resolution **101**, 20

J.G. Cuby, C. Lidman, C. Moutou: ISAAC: 18 Months of Paranal Science Operations **101**, 2

D. Currie, D. Bonaccini, E. Diolaiti, S. Tordo, K. Naesgarde, J. Liwing, O. Bendinelli, G. Parmeggiani, L. Close: The ESO Photometric and Astrometric Analysis Programme for Adaptive Optics **100**, 12

D. Currie, D. Le Mignant, B. Svensson, S. Tordo, D. Bonaccini: 3D Structure and Dynamics of the Homunculus of Eta Carinae: an Application of the Fabry-Perot, ADONIS and AO Software. I. Motions in Homunculus **101**, 24

S. Cristiani, S. D'Odorico, T.-S. Kim: Exploring the Lyman forest at  $z = 2$  with UVES **102**, 8

D. Currie, D. Le Mignant, B. Svensson, S. Tordo, D. Bonaccini: 3D Structure and Dynamics of the Homunculus of Eta Carina: an Application of the Fabry

ESO Studentship Programme **99**, 47

Personnel Movements **99**, 47

Scientific Preprints **99**, 47

Scientific Preprints (March–June 2000) **100**, 52

K. Kjær: About The ESO Messenger **100**, 53

A Challenge for Engineers and Astronomers **100**, 54

ESO Fellowship Programme 2000/2001 **100**, 55

Perot, ADONIS and AO Software. II. Spikes and Bullets **102**, 25

### D

S. D'Odorico: UVES at Kueyen: Bright Prospects for High-Resolution Spectroscopy at the VLT **99**, 2

N. Devillard: Astronomical Image Resampling **100**, 48

M. Dennefeld: The Second NEON Observing Euroschool **102**, 28

E. Diolaiti, O. Bendinelli, D. Bonaccini, L. Close, D. Currie, G. Parmeggiani: Star-Finder: a Code to Analyse Isoplanatic High-Resolution Stellar Fields **100**, 23

### E

S.L. Ellison, L. Yan, I.M. Hook, M. Pettini, P. Shaver, J.V. Wall: Revealing High-Redshift Galaxies: Results from a New Damped Lyman-System Survey **102**, 23

### F

R. Falomo, J. Kotilainen, A. Treves: VLT/ISAAC Images of Quasar Hosts at  $z \sim 1.5$  **101**, 15

M. Franx, A. Moorwood, H.-W. Rix, K. Kijken, H. Röttgering, P. van der Werft, P. van Dokkum, I. Labbe and G. Rudnick: FIRES at the VLT: the Faint InfraRed Extragalactic Survey **99**, 20

### G

R. Gilmozzi and P. Dierickx: OWL Concept Study **100**, 1

### H

R. Häfner: The Deep Eclipse of NN Ser **100**, 42

O. Hainaut and the NTT Team: News from the NTT **99**, 15

R. Hanuschik and P. Amico: VLT Pipeline Operation and Quality Control: FORS1 and ISAAC **99**, 6

R. Heald and R. Karban: ESO Demonstration Project with the NRAO 12-m Antenna **99**, 14

### J

H. Jones: 2p2 Team News **100**, 29

H. Jones: 2p2 Team News **102**, 12

### K

F. Kerber, R. Palsa, J. Köppen, T. Blöcker, M.R. Rosa: Unlocking the past of Sakurai's Object Using FORS/VLT **101**, 27

H.U. Käuffel, N. Ageorges, E. Dietzsch, J. Hron, H. Relke, D. Scholz, A. Silber, M. Sperl, M. Sterzik, R. Wagner, U. Weilenmann: First Astronomical Light with

Personnel Movements **100**, 55

Tragic Car Accident Involves ESO Employees **100**, 56

Scientific Preprints (July–September 2000) **101**, 39

Personnel Movements **101**, 40

Advertisement **102**, 29

Staff Movements **102**, 29

Scientific Preprints (October – December 2000) **102**, 30

TIMM2, ESO's 2nd-Generation Thermal Infrared Multimode Instrument at the La Silla 3.6-m Telescope **102**, 4

K. Kjær: About The ESO Messenger **100**, 53

### L

B. Leibundgut, B. Pirenne, M. Albrecht, A. Wicenec and K. Gorski: Access to VLT Data in the ESO Archive **99**, 12

B. Leibundgut, J. Sollerman, C. Kozma, C. Fransson, P. Lundqvist, F. Ryde and P. Woudt: The Late Phase of SN 1998bw **99**, 36

C. Lidman, A. Goobar, R. Pain: Type Ia Supernovae, Cosmology and the VLT **101**, 18

### M

C. Madsen and R. West: Success for "Physics on Stage" Festival in Geneva **102**, 29

R. Maoli, Y. Mellier, L. van Waerbeke, P. Schneider, B. Jain, T. Erben, F. Bernardau, B. Fort, E. Bertin, M. Dantel-Fort: Cosmic Shear with ANTU/ FORS1: An Optimal Use of Service Mode Observation **101**, 10

R.P. Mignani, P.A. Caraveo and G.F. Bignami: Optical Observations of Pulsars: the ESO Contribution **99**, 22

P. Møller: Spectral PSF Subtraction I: The SPSF Look-Up-Table Method **99**, 31

P. Møller, S.J. Warren, S.M. Fall, P. Jakobsen and J.U. Fynbo: SPSF Subtraction II: The Extended Ly Emission of a Radio Quiet QSO **99**, 33

### P

F. Paresce, G. de Marchi, G. Andreuzzi, R. Buonanno, F. Ferraro, B. Paltrinieri, L. Pulone: Crowded Field Photometry with the VLT: the Case of the Peculiar Globular Cluster NGC 6712 **102**, 17

H. Pedersen, J.-L. Atteia, M. Boer, K. Beuermann, A.J. Castro-Tirado, A. Fruchter, J. Greiner, R. Hessman, J. Hjorth, L. Kaper, C. Kouveliotou, N. Masetti, E. Palazzi, E. Pian, K. Reinsch, E. Rol, E. van den Heuvel, P. Vreeswijk, R. Wijkers: Gamma-Ray Bursts – Pushing Limits with the VLT **100**, 32

### R

D. Rigopoulou, A. Franceschini, H. Aussel, C.J. Cesarsky, D. Elbaz, R. Genzel, P. van der Werf, M. Dennefeld: ISAAC on the VLT Investigates the Nature of the High-Redshift Sources of the Cosmic Infrared Background **100**, 37

P. Rosati, C. Lidman, R. Della Ceca, S. Borgani, M. Lombardi, S.A. Stanford,

ESO, the European Southern Observatory, was created in 1962 to "... establish and operate an astronomical observatory in the southern hemisphere, equipped with powerful instruments, with the aim of furthering and organising collaboration in astronomy ...". It is supported by eight countries: Belgium, Denmark, France, Germany, Italy, the Netherlands, Sweden and Switzerland. ESO operates at two sites. It operates the La Silla observatory in the Atacama desert, 600 km north of Santiago de Chile, at 2,400 m altitude, where several optical telescopes with diameters up to 3.6 m and a 15-m submillimetre radio telescope (SEST) are now in operation. In addition, ESO is in the process of building the Very Large Telescope (VLT) on Paranal, a 2,600 m high mountain approximately 130 km south of Antofagasta, in the driest part of the Atacama desert. The VLT consists of four 8.2-metre and three 1.8-metre telescopes. These telescopes can also be used in combination as a giant interferometer (VLTI). The first and the second 8.2-metre telescopes (called ANTU and KUEYEN) are already in regular operation, and the third and the fourth telescopes (called MELIPAL and YEPUN) have already delivered pictures of excellent quality. Over 1200 proposals are made each year for the use of the ESO telescopes. The ESO Headquarters are located in Garching, near Munich, Germany. This is the scientific, technical and administrative centre of ESO where technical development programmes are carried out to provide the La Silla and Paranal observatories with the most advanced instruments. There are also extensive astronomical data facilities. In Europe ESO employs about 200 international staff members, Fellows and Associates; in Chile about 70 and, in addition, about 130 local staff members.

The ESO MESSENGER is published four times a year: normally in March, June, September and December. ESO also publishes Conference Proceedings, Preprints, Technical Notes and other material connected to its activities. Press Releases inform the media about particular events. For further information, contact the ESO Education and Public Relations Department at the following address:

EUROPEAN  
SOUTHERN OBSERVATORY  
Karl-Schwarzschild-Str. 2  
D-85748 Garching bei München  
Germany  
Tel. (089) 320 06-0  
Telefax (089) 3202362  
ips@eso.org (internet)  
URL: <http://www.eso.org>  
<http://www.eso.org/gen-fac/pubs/messenger/>

The ESO Messenger:  
Editor: Marie-Hélène Demoulin  
Technical editor: Kurt Kjær

Printed by  
J. Gotteswinter GmbH  
Buch- und Offsetdruck  
Joseph-Dollinger-Bogen 22  
D-80807 München  
Germany

ISSN 0722-6691

P.R. Eisenhardt, G. Squires, R. Giacconi and C. Norman: The ROSAT Deep Cluster Survey: Probing the Galaxy Cluster Population out to  $z = 1.3$  **99**, 26

## S

M. Sarazin: Chile Astroclimate, a Biannual Update **99**, 13

J. Setiawan, L. Pasquini, L. Da Silva, A. Hatzes, O. von der Lühe, A. Kaufer, L. Girardi, R. de la Reza, J.R. de Medeiros: A Study of the Activity of G and K Giants Through Their Precise Radial Velocity; Breaking the 10-m/sec Accuracy with Feros **102**, 13

M. Sterzik, M. Kürster: News from the 3.6-m Telescope **100**, 30

## T

E. Tolstoy, J. Gallagher, L. Greggio, M. Tosi, G. De Marchi, M. Romaniello, D. Minniti and A. Zijlstra: Imaging With UT1/FORS1: The Fossil Record of Star-Formation in Nearby Dwarf Galaxies **99**, 16

## W

C. Waelkens: The Observing Programmes Committee – an Evolving Process **101**, 37

# Contents

## TELESCOPES AND INSTRUMENTATION

- G. Avila, G. Conti, E. Mattaini, L. Chiappetti, D. Maccagni, E. Sant'Ambrogio, O. Le Fèvre, G. Vettolani, M. Saisse: Successful installation of the VIMOS Laser Mask Manufacturing Unit (MMU) at Paranal . . . . . 1
- H.U. Käufel, N. Ageorges, E. Dietzsch, J. Hron, H. Relke, D. Scholz, A. Silber, M. Sperl, M. Sterzik, R. Wagner, U. Weilenmann: First Astronomical Light with TIMM12, ESO's 2nd-Generation Thermal Infrared Multimode Instrument at the La Silla 3.6-m Telescope . . . 4
- S. Cristiani, S. D'Odorico, T.-S. Kim: Exploring the Lyman forest at  $z = 2$  with UVES . . . . . 8

## THE LA SILLA NEWS PAGE

- H. Jones: 2p2 Team News . . . . . 12

## REPORTS FROM OBSERVERS

- J. Setiawan, L. Pasquini, L. Da Silva, A. Hatzes, O. von der Lühe, A. Kaufer, L. Girardi, R. de la Reza, J.R. de Medeiros: A Study of the Activity of G and K Giants Through Their Precise Radial Velocity; Breaking the 10-m/sec Accuracy with Feros . . . . . 13
- F. Paresce, G. de Marchi, G. Andreuzzi, R. Buonnanno, F. Ferraro, B. Paltrinieri, L. Pulone: Crowded Field Photometry with the VLT: the Case of the Peculiar Globular Cluster NGC 6712 . . . . . 17
- S.L. Ellison, L. Yan, I.M. Hook, M. Pettini, P. Shaver, J.V. Wall: Revealing High-Redshift Galaxies: Results from a New Damped Lyman- System Survey . . . . . 23
- D. Currie, D. Le Mignant, B. Svensson, S. Tordo, D. Bonaccini: 3D Structure and Dynamics of the Homunculus of Eta Carina: an Application of the Fabry Perot, ADONIS and AO Software. II. Spikes and Bullets . . . . . 25

## OTHER ASTRONOMICAL NEWS

- M. Dennefeld: The Second NEON Observing Euroschool . . . . . 28
- C. Madsen and R. West: Success for "Physics on Stage" Festival in Geneva . . . . . 29
- UK Announces Intention to Join ESO . . . . . 30
- The VLT Weighs the Invisible Matter in the Universe. Shapes and Orientations of 76,000 Distant Galaxies . . . . . 30

## ANNOUNCEMENTS

- A Challenge for Astronomers, Software Engineers, Electrical/Mechanical Engineers . . . . . 32
- Personnel Movements . . . . . 29
- Scientific Preprints (October – December 2000) . . . . . 30
- ESO Workshop Proceedings Still Available . . . . . 33

- MESSENGER INDEX 2000 (Nos. 99–102) . . . . . 34